THREE DIMENSIONAL FRACTURE ANALYSIS
OF FGM COATINGS

A THESIS SUBMITTED TO

THE GRADUATE SCHOOL OF NATURAL AND APPLIED SCIENCES

OF

MIDDLE EAST TECHNICAL UNIVERSITY

BY

ÖZGÜR İNAN

IN PARTIAL FULFILLMENT OF THE REQUIREMENTS

FOR

THE DEGREE OF MASTER OF SCIENCE

IN

MECHANICAL ENGINEERING

SEPTEMBER 2004

Approval of the Graduate School of Natural and Applied Sciences.

_____

Prof. Dr. Canan ÖZGEN

Director

I certify that this thesis satisfies all the requirements as a thesis for the degree of Master of Science.

_____

Prof. Dr. S. Kemal İDER

Head of the Department

This is to certify that we have read this thesis and that in our opinion it is fully adequate, in scope and quality, as a thesis for the degree of Master of Science.

_____

Asst.Prof.Dr. Serkan DAĞ

Supervisor

Examining Committee Members

Prof. Dr. Y. Samim ÜNLÜSOY   (METU, ME)_____

Asst.Prof.Dr. Serkan DAĞ   (METU, ME)_____

Prof. Dr. Mehmet ÇALIŞKAN   (METU, ME)_____

Assoc.Prof.Dr. F. Suat KADIOĞLU   (METU, ME)_____

Prof. Dr. Mehmet AKGÜN   (METU, AEE)_____

I hereby declare that all information in this document has been obtained and presented in accordance with academic rules and ethical conduct. I also declare that, as required by these rules and conduct, I have fully cited and referenced all material and results that are not original to this work.

Name, Last name : Özgür İNAN

Signature   :

ABSTRACT

**THREE DIMENSIONAL FRACTURE ANALYSIS
OF FGM COATINGS**

İNAN, Özgür

M.S., Department of Mechanical Engineering

Supervisor: Asst. Prof. Dr. Serkan Dağ

September 2004, 93 pages

The main objective of this study is to model the three dimensional surface cracking problem in Functionally Graded Material (FGM) coatings bonded to homogeneous substrates. The FGM coating is assumed to be a (ZrO_2) – (Ti-6Al-4V) layer. Homogeneous ceramic, metal – rich, ceramic – rich and linear variation material compositions are considered in the analyses. The surface crack is assumed to have a semi – circular crack front profile. The surface crack problem in the FGM coating – substrate system is examined under mechanical and transient thermal loading. Structural and thermal problems are modeled using three dimensional finite elements. Strain singularity around the crack front is simulated using collapsed 20 – node quarter – point brick elements. Three - dimensional displacement correlation technique is utilized to extract the stress intensity factors. The main results of the study are the stress intensity factors around the crack front for FGM coating - substrate structures subjected to uniform tension, bending, fixed – grip tension, three point bending and transient thermal loading.

Keywords: FGM coatings, fracture mechanics, semi – circular surface crack, displacement correlation technique, stress intensity factors.

ÖZ

FONKSİYONEL DERECELENMİŞ KAPLAMALARIN ÜÇ BOYUTLU KIRILMA ANALİZİ

İNAN, Özgür

Yüksek Lisans, Makina Mühendisliği Bölümü

Tez Yöneticisi: Y. Doç. Dr. Serkan Dağ

Eylül 2004, 93 sayfa

Bu çalışmanın başlıca amacı, homojen taban tabakaya bağlı fonksiyonel olarak derecelenmiş malzeme (FDM) kaplamalarda üç boyutlu yüzey çatlak problemlerinin modellenmesidir. FDM kaplamanın bir (ZrO_2) – (Ti-6Al-4V) tabakası olduğu varsayılmıştır. Analizlerde homojen seramik, zengin metal, zengin seramik ve lineer değişimli malzeme bileşimleri dikkate alınmıştır. Yüzey çatlağının yarı dairesel bir çatlak yüzü profiline sahip olduğu varsayılmıştır. FDM kaplama – taban tabaka sistemindeki yüzey çatlağı problemi mekanik ve zamana bağlı ısıl yükleme altında incelenmiştir. Yapısal ve ısıl problemler üç boyutlu sonlu elemanlar kullanılarak modellenmiştir. Çatlak yüzündeki gerinim tekilliği çökertilmiş 20 düğümlü çeyrek noktalı elemanlar kullanılarak benzetilmiştir. Gerilme şiddeti faktörlerinin hesaplanmasında, üç boyutlu yerdeğiştirme korelasyon tekniği kullanılmıştır. Çalışmanın başlıca sonuçları; düzgün dağılımlı gerilme, eğilme, düzgün dağılımlı yerdeğiştirme, üç nokta eğme veya zamana bağlı ısıl yüklemeye maruz kalmış FDM kaplama modeli için çatlak yüzü etrafındaki gerilme şiddeti faktörleridir.

Anahtar Kelimeler: FDM kaplamalar, kırılma mekaniği, yarı dairesel yüzey çatlağı, yerdeğiştirme korelasyon tekniği, gerilme şiddeti faktörleri.

ACKNOWLEDGMENTS

I want to thank, first and foremost, to my advisor Asst. Prof. Dr. Serkan Dağ, for his help and support during this study.

Thanks are also to Asst. Prof. Dr. Bora Yıldırım for his valuable help in finite element modelling and to Prof. Dr. Müfit Gülgeç for his support during this study. I would also like to thank Prof. Dr. Fazıl Erdoğan for his valuable comments and suggestions.

Finally, I want to thank to my parents Mr. Mustafa Reşit İnan and Mrs. Munire İnan, to my sister Mrs. Evrim İnan and to my brother Mr. Mert İnan for their support throughtout the course of my studies.

TABLE OF CONTENTS

LIST OF TABLES

TABLES

LIST OF FIGURES

FIGURES

LIST OF SYMBOLS

a	Radius of the Circular Surface Crack
ϕ	Parametric Angle
h_1	Thickness of the Substrate
h_2	Thickness of the FGM Coating
b	Half - Width of the Cracked Plate
l	Half - Length of the Cracked Plate
p	Material Nonhomogeneity Parameter for the FGM Layers
T	Temperature
E_c	Elastic Modulus of the Ceramic Component (ZrO$_2$)
υ_c	Poisson's Ratio of the Ceramic Component
k_c	Thermal Conductivity of the Ceramic Component
c_c	Specific Heat of the Ceramic Component
ρ_c	Density of the Ceramic Component
α_c	Thermal Expansion Coefficient of the Ceramic Component
E_s	Elastic Modulus of the Metal Component (Ti-6Al-4V)
υ_s	Poisson's Ratio of the Metal Component
k_s	Thermal Conductivity of the Metal Component
c_s	Specific Heat of the Metal Component
ρ_s	Density of the Metal Component
α_s	Thermal Expansion Coefficient of the Metal Component

K_I Mode I Stress Intensity Factor

K_{In} Normalized Mode I Stress Intensity Factor

Q Shape Factor for a Semi - Elliptical Crack

σ_t Uniform Tension Stress

σ_b Normal Stress on the Outer Fiber for Bending Load

v_0 Uniform Normal Displacement for Fixed – Grip Tension

σ Uniform Compressive Traction for Three Point Bending

δ Half – Length of the Rectangular Region where Uniform Compressive Traction is applied for Three Point Bending

P The Resultant Force due to Loading in Three Point Bending

T_0 Environment Temperature

h Convection Coefficient

T_m Average of the Environment and Processing Temperatures

S Normalization Stress

D Thermal Diffusivity Coefficient

t Time

τ Normalized Time

u_b Normal Displacement Component on the Crack Front

σ_{bb} Normal Stress Component on the Crack Front

r Distance from the Crack Tip

θ Angle from the Crack Plane

σ_{ij} The Components of Stresses

u_i The Components of Displacements

K_{II} Mode II Stress Intensity Factor

K_{III} Mode III Stress Intensity Factor

μ Shear Modulus

CHAPTER 1

INTRODUCTION

1.1 Introduction

Back in the Middle Ages (and even earlier in China), weapons and tools were made of iron; either wrought iron, which was fairly soft and wouldn't hold an edge for long, or cast iron, which was extremely hard, unable to deform, and would break quite easily. Introducing a precise amount of carbon in the smelting process produced steel, which combined the useful qualities of wrought and cast iron, making it infinitely more useful and much more valuable.

Materials science has come a long way since the Middle Ages, but one thing remains the same—as our technology improves we increase our demands on structural materials, subjecting them to greater loads and more severe environments. In the same way that steel was a big improvement over iron, today's metal alloys are giving way to advanced materials that can perform better under a variety of demanding conditions, from outer space to thousand-degree jet engines.

An ideal material combines the best properties of metals and ceramics—the toughness, electrical conductivity, and machinability of metals, and the low density, high strength, high stiffness, and temperature resistance of ceramics. Take away some of the brittleness of ceramics and make strong metals lighter and stiffer, and the material becomes really useful. You've got a material that is hard but won't break; one that will conduct electricity but can withstand high temperatures. These materials, known as Functionally Graded Materials (FGMs) have incredible promise in many engineering applications. Demand for such materials comes from the automotive industry (lightweight and strong materials would increase fuel

efficiency and last longer), electronics, telecommunications, and the aerospace and defense industries.

FGMs are "functionally graded" to provide the exact combination of characteristics desired, and in these materials or structures the material properties vary with location in such a way as to optimize some function of the overall FGM. The metal, the ceramic, the volume, shape, and location of the ceramic, and the fabrication method can all be tailored to achieve particular desired properties. The design of FGMs requires an explicit understanding of the material behavior at each location and over all these length scales. There has been quite considerable work on the manufacturing methods of metal/ceramic FGMs. Advanced manufacturing techniques are used to process FGMs, among which we may mention spark plasma sintering (SPS), 3D-printing, electrophoretic deposition and high – temperature infiltration [1]. Due to the brittle nature of the ceramic components in ceramic/metal FGMs, fracture mechanics of graded materials is also studied quite extensively. A detailed literature review of the fracture mechanics of graded materials is given by Dağ [2].

Surface coatings of homogeneous substrates are among the most important technological applications of FGMs. Usually the substrate is the main structural component and is a metal or a metal alloy and the coating is a metal/ceramic FGM. Typical applications include coatings to protect the substrate against adverse thermal and chemical environments and preparation of surfaces for impact, penetration and wear resistance. In most of these applications the FGM coating is designed in such a way that its composition continuously varies from 100% metal at the interface to 100% ceramic at the surface along the thickness direction. Thus, from the stand point of fracture initiation and propagation the necessary impact, penetration and wear resistance is provided by ceramic and ceramic – rich part of the coating and the toughness is provided by the metal substrate and metal-rich part of the coating. Considering the fact that generally ceramics are brittle materials, in FGM coatings fracture initiation would invariably take place in the form of part –

2

through surface cracks. The surface cracking of FGM layers can be due to mechanical or thermal loading. An example for the thermal fracture problem is the formation of the part – through cracks at the graded surface under high transient tensile residual stresses, as the coating – substrate system cools from an initially high processing temperature. The part – through nature of the crack initiation necessitates a three dimensional analysis of the surface crack problems in FGMs in order to develop a better understanding of the fracture mechanisms.

In this study, three dimensional surface cracking problem in FGM coatings is examined using a three dimensional finite element technique. The behavior of the surface cracks is investigated under both mechanical and thermal loading. A brief summary of the work done in this thesis can also be found in the paper by İnan et al. [3].

1.2 Literature Survey

The main objective of this study is to model three dimensional semi–circular surface cracks in FGM coatings and to compute the mode I stress intensity factors around the crack front under mechanical or transient thermal loading using the finite element method. Surface crack problems in functionally graded coatings are considered by various researchers in the past. However, in most of the previous studies in the literature, the crack problems studied are confined to either planar or axisymmetric geometries. The present study can be considered as one of the first in the literature dealing with three dimensional cracks in FGMs.

An important study on FGMs was published in 1997 by F. Erdoğan and B. H. Wu [4]. In this study the plane elasticity problem for a nonhomogeneous layer containing an internal or an edge crack perpendicular to the boundaries is considered. Three different mechanical loading types, namely fixed grip, membrane loading, and bending, which are perpendicular to the plane of the crack, are applied to the layer away from the crack region. In this research, it is assumed that the

Young's modulus of the medium varies continously in the thickness direction. The influence of the Poisson's ratio on the stress intensity factors is not very significant. Therefore, to make the analysis tractable, it is further assumed that the Poisson's ratio of the graded medium is constant. In this paper, mode I stress intensity factors are presented for embedded as well as edge cracks for various values of dimensionless parameters representing the size and the location of the crack and the material nonhomogeneity. Moreover, some crack-opening displacement and stress distribution results are also presented.

In the paper by Kadıoğlu, Dağ and Yahşi [5] in 1998, internal and edge crack problems for an FGM layer attached to an elastic foundation are considered. It is assumed that the Young's modulus of the layer varies in thickness direction exponentially. Because of its insignificant effect on stress intensity factors, Poisson's ratio is assumed to be constant. Mode I stress intensity factors are calculated for various values of the nonhomogeneity parameter.

In the study by Jin and Paulino [6], an edge crack in a strip of a functionally graded material is studied under transient thermal loading conditions. The material is assumed to be elastically homogeneous but thermally nonhomogeneous. A multi-layered material model is used to solve the temperature field. The strip is initially at a constant temperature. And then, the surfaces in the thickness direction of the strip are suddenly cooled down to different temperatures. By using the Laplace transform and an asymptotic analysis, an analytical first order temperature solution for short times is obtained. In this paper thermal stresses and thermal stress intensity factors are calculated for a TiC/SiC FGM with various volume fraction profiles of the constituent materials, and the effect of the material composition on thermal stresses and thermal stress intensity factors is discussed.

Dağ et al. [7] considered both internal and edge cracks in a thin walled cylinder under transient thermal loading. The cylinder is assumed to be a functionally graded material and modelled as a layer on an elastic foundation to

make the problem analytically tractable. Hence, a plane strain crack problem is obtained. The material properties of this layer are assumed to be exponential functions of the thickness coordinate except the Poisson's ratio. In this study, first temperature and thermal stress distributions for a crack free layer are determined. And then using these solutions, the crack problem is reduced to a local perturbation problem where the only nonzero loads are the crack surface tractions. Stress intensity factors are computed as functions of crack geometry, material properties and time.

Again contributing Dağ with Erdoğan in 2002 [8], a surface crack problem is considered in a semi-infinite elastic graded medium under general mixed-mode loading conditions. The elastic properties of the medium are assumed to be exponential functions of the depth coordinate. In this study, first the problem is solved in the absence of a crack in order to reduce it to a local perturbation problem with arbitrary self-equilibrating crack surface tractions. Then, the local problem is solved by approximating the normal and shear tractions on the crack surfaces by polynomials and the normalized modes I and II stress intensity factors are given. The main results of this study are the variation of the stress intensity factors as functions of the material nonhomogeneity. Also, some sample results on crack opening displacements are presented.

In another paper by Dağ and Erdoğan [9], the coupled problem of crack/contact mechanics in a nonhomogeneous medium is considered, and the behavior of a surface crack in a functionally graded medium loaded by a sliding rigid stamp in the presence of friction is investigated. The dimensions of the graded medium are assumed to be very large in comparison with the local length parameters of the crack/contact region. Thus in formulating the problem the graded medium is assumed to be semi-infinite. In the formulating the problem it is further assumed that the shear modulus of the graded medium may be approximated by a two-parameter exponential function. In this study, contact stresses, the in-plane component of the surface stress and modes I and II stress intensity factors at the

crack tip are determined and presented for various combinations of friction coefficient, material nonhomogeneity constant and crack/contact length parameters.

In the study by Wang et al. [10], a functionally graded material strip containing an embedded or a surface crack perpendicular to its boundaries is considered. The graded medium is divided into a large number of layers in the thickness direction, with each layer being a homogeneous material. Surface crack in the functionally graded material is considered for arbitrarily distrubuted material properties in the thickness direction. In the numerical examples, the graded medium is subjected to two different loading types, a uniform mechanical pressure on the crack surfaces and a non-uniform thermal stress distribution. Using these loads, the mode I stress intensity factors are computed for different crack lengths and property distributions.

Wang et al. [11] provides an analysis method for the mode II in plane and mode III anti-plane problems for an FGM strip containing a crack along the gradient direction. The FGM strip is divided into homogeneous sub-layers along the thickness direction. In the numerical analyses, stress intensity factors for an FGM layer under uniform shear load (mode II and III) on the crack surfaces are obtained. Using the models developed in this paper and in [10], the fracture problems of FGMs under general loading conditions can be investigated to optimize the property distributions of FGMs.

Guo et al. [12] investigated a mode I crack problem for a functionally graded orthotropic strip. The crack which is perpendicular to the boundaries may be an internal or an edge crack. The elastic properties of the material are assumed to vary continuously along the thickness direction. The principal directions of orthotropy are parallel and perpendicular to the boundaries of the strip. In this study, a singular integral equation is derived to solve the problem. In the numerical calculations, the mode I stress intensity factors are computed for three different mechanical loading conditions, namely crack surface pressure, fixed-grip loading and bending. Using

6

these loading conditions, the influences of parameters such as the material constants on the stress intensity factors are investigated.

Again in Guo et al. [13], the static crack problem of a functionally graded coating-substrate structure with an internal or edge crack perpendicular to the interface is investigated under in-plane loading. The crack is located in the functionally graded coating. The material properties are assumed to vary continuously from the coating to the substrate. Integral transform techniques are used to reduce the boundary value problem to a singular integral equation. In the numerical calculations, the effects of the nonhomogeneity constant, crack length and thicknesses of the FGM and substrate structures on the stress intensity factors are investigated for an internal and edge cracks under uniform tension.

The transient response of a functionally graded coating-substrate system with an internal or an edge crack is considered under in-plane impact in the paper by Guo et al. [14]. The crack in the functionally graded coating is perpendicular to the interface and parallel to the variation direction of the material properties. These properties are assumed to vary continuously from the coating to the substrate. Fourier transform and Laplace transform techniques are used to reduce the boundary value problem to an integral equation. The solution in the time domain is obtained via numerical inverse of the Laplace transform. The dynamic stress intensity factors are calculated for a crack (an internal or an edge crack) subjected to normal impact load.

In the paper by Chi and Chung [15], stress intensity factors for cracked multi-layered and FGM coatings are calculated using the finite element method. The substrate is assumed to be a homogeneous material, while the coating consists of multi-layered media or Sigmoid FGMs (S-FGMs). For the multi-layered coatings, one, two, and four-layered homogeneous coatings are considered. Thirty-two layers are used in the thickness direction to establish the meshes in the S-FGM coating and to simulate the variation of the material properties. Each layer has different constant

material properties. In this research, MARC software is used in finite element analysis. In order to test the convergence of the finite element model, several different mesh sizes and shapes are used to calculate the stress intensity factors at the crack-tip. In the numerical examples, the normalized mode I stress intensity factors are computed and presented with respect to various crack lengths for one-, two- and four-layered coatings, and S-FGM coating.

Jin [16] investigated the effect of the thermal property gradients on edge cracking in an FGM coating bonded to a homogeneous substrate subjected to a thermal shock. The edge crack is parallel to the thickness direction. To simplify the analysis, this work focuses on the thermal property gradient effect and thus assumes that the FGM coating/substrate system has constant Young's modulus and Poisson's ratio, but graded thermal properties along the thickness direction of the coating. The strip is initially assumed to be at a constant temperature, and its surfaces perpendicular to the thickness direction are suddenly cooled down. Due to this thermal shock, the thermal stress intensity factors are induced at the crack tip. In this study, a closed-form, short time asymptotic solution of the temperature field in the FGM coating/substrate strip is obtained using Laplace transform and its asymptotic properties. Thermal stress intensity factor calculations are based on this asymptotic temperature distribution. In the numerical analyses, the stress intensity factors are computed with respect to time for various volume fraction profiles and crack lengths.

In the study of Lee and Erdoğan [17], the plane strain thermal stress problem for an interface crack in a homogeneous substrate with a graded coating is considered. The specimen contains two symmetrically oriented edge cracks along the interface. The substrate is a superalloy and the constituents of the graded coating are metals and ceramics. The volume fraction of ceramic in FGM coating is varied continuously from zero at the interface to 100% on the surface. The coating is exposed to a high temperature convective environment, the substrate on the bottom surface is forced cooled and the ends of the specimen are under natural

convection. The surfaces of the crack are assumed to be partially insulated. Thus, the mechanically unconstrained inhomogeneous medium is under steady-state heat conduction with convective boundary conditions. In the numerical examples, the temperature distribution on the surfaces of the substrate and coating, along the interface and on the crack surfaces are presented for various crack lengths for a sample FGM coating and heat conductivity index (this parameter describes the insulation condition on the crack surface). Also in this paper, the total heat flow across the substrate surface, modes I and II stress intensity factors, the strain energy release rate and normal component of the crack opening displacement are presented for various FGM coatings.

1.3 Scope of the Study

The aim of this study is to model semi-circular surface cracks in a ceramic (ZrO_2) – titanium alloy (Ti-6Al-4V) FGM coating bonded to a homogeneous titanium alloy substrate under mode I mechanical or thermal loading conditions. A three dimensional finite element model containing a semi-circular surface crack is generated using the general purpose finite element software ANSYS [18]. In this model quarter point three dimensional finite elements are used to simulate the crack tip singularity around the crack front and displacement correlation technique is used to extract the mode I stress intensity factors. Note that in the implementation of the displacement correlation technique, standard stress intensity factor computation functions given in the Ansys Parametric Design Language (APDL) library can not be utilized. This is due to the fact that, the material parameters in the asymptotic displacement expressions are functions of the spatial coordinates in FGMs. As a result, new APDL subroutines are developed in order to compute the stress intensity factors under mode I thermomechanical loading. In order to examine the accuracy of the model, calculated stress intensity factors are compared with those given by Newman and Raju [19] for various crack dimensions under tension or bending loads. A homogeneous aluminum alloy (2014-T651Al) is used in the comparisons.

In the investigation of the semi-circular surface crack in FGM coatings, material property variations are modeled by specifying the thermomechanical properties of each finite element at its centroid. The stress intensity factors are calculated for FGM coating – substrate systems subjected to uniform tension, bending, fixed-grip tension, three point bending and temperature gradients. Four different coating types are considered in the parametric analyses namely, a homogeneous ceramic coating (H), a ceramic – rich FGM (CR), a metal – rich FGM (MR) and an FGM coating with linear variation (LN) in the thermomechnical parameters. Numerical results are provided for the mode I stress intensity factors around the crack front to assess the performance of the mentioned coating types with regard to fracture failure.

This thesis contains five chapters. An introduction, literature survey and the scope of the study are given in the present chapter. Three dimensional fracture analysis techniques and problem definition are given in Chapter 2. The details of the finite element modeling and the displacement correlation technique (DCT) are given in Chapter 3. The computed results and comparisons are presented in Chapter 4. Finally, a discussion of the results and concluding remarks are given in Chapter 5.

CHAPTER 2

PROBLEM DEFINITION

2.1 Three Dimensional Fracture Analysis

Stress intensity factor is used in fracture mechanics to more accurately predict the stress state ("stress intensity") near the tip of a crack caused by a remote load or residual stresses. When this stress state becomes critical the crack grows ("extends") and the material fails. Under idealized conditions, the load at which this failure occurs is referred to as the fracture strength. The experimental fracture strength of solid materials is 10 to 1000 times below the theoretical strength values, where tiny internal and external surface cracks create higher stresses near these cracks, hence lowering the theoretical value of strength. Stress intensity factor is a measure of the strength of the singular fields at the crack tip under different loading modes. These load types are categorized as Mode I, II, or III. The Mode I stress intensity factor is the most often used engineering design parameter in fracture mechanics and hence must be calculated if we are to design fracture tolerant materials used in bridges, buildings, aircraft, or even bells. Polishing just won't do if we detect a crack. Typically for most materials if a crack can be seen it is very close to the critical stress state predicted by the "Stress Intensity Factor".

As the stress intensity factor reaches a critical value, unstable fracture occurs. This critical value of the stress intensity factor is known as the fracture toughness of the material. The fracture toughness can be considered as the limiting value of the stress intensity just as the yield stress might be considered as the limiting value of the applied stress. The fracture toughness depends on both temperature and the specimen thickness. Mode I plane strain fracture toughness is denoted as K_{IC}. K_C which is the plane stress fracture toughness, is used to measure a material's fracture

toughness in a sample that has a thickness that is less than some critical value, *B*. When the material's thickness is less than *B*, and stress is applied, the material is in a state called plane stress. A material's thickness is related to its fracture toughness graphically in Figure 2.1. If a stress is applied to a sample with a thickness greater than *B*, it is in a state called plane strain.
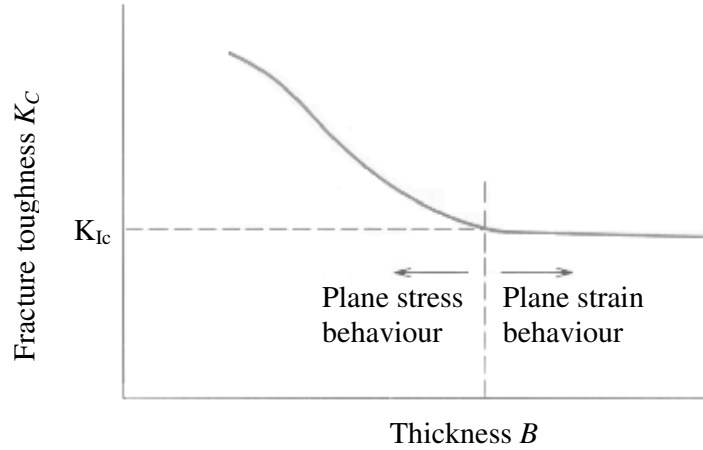
Figure 2.1 Fracture Toughness as a function of material thickness.

Generally there are three modes to describe different crack surface displacements as shown in Figure 2.2. Mode I is opening or tensile mode where the crack surfaces move directly apart. Mode II is sliding or in-plane shear mode where the crack surfaces slide over one another in a direction perpendicular to the leading edge of the crack. Mode III is the tearing or antiplane shear mode where the crack surfaces move relative to one another and parallel to the leading edge of the crack. Combinations of these modes are also possible. Mode I is the most common loading type encountered in engineering design and all computations in this study are related to this type.

The value of the stress intensity factor is a function of the applied stress, the size and the position of the crack as well as the geometry of the solid piece where

the cracks are detected. Figure 2.3 and 2.4 depict the stress field and polar coordinate system for a two dimensional crack. Two and three dimensional linear elastic crack tip fields (stress and displacement relations) and the stress intensity factor definitions are expressed below for each loading mode [20].
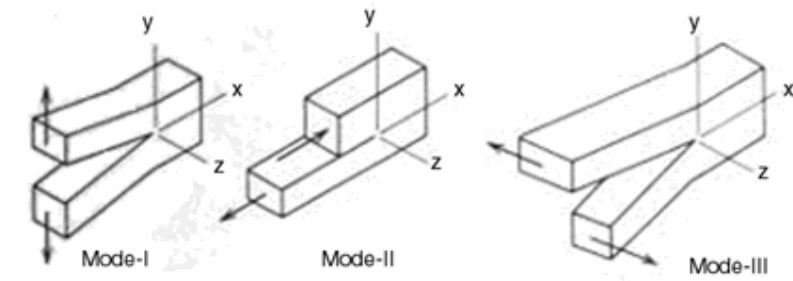
Figure 2.2 Basic modes of loading involving different crack surface displacements.
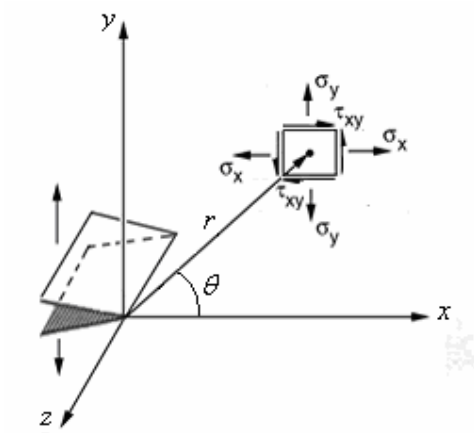
Figure 2.3 Distribution of stresses in vicinity of crack tip.
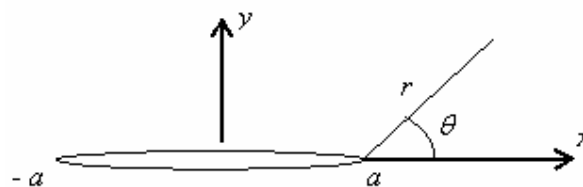
Figure 2.4 Two dimensional crack

Mode I crack:

$$\sigma_{yy}(r,\theta) = \frac{K_I}{\sqrt{2\pi r}} \cos\left(\frac{\theta}{2}\right)\left\{1 + \sin\left(\frac{\theta}{2}\right)\sin\left(\frac{3\theta}{2}\right)\right\} \tag{2.1a}$$

$$\sigma_{xx}(r,\theta) = \frac{K_I}{\sqrt{2\pi r}} \cos\left(\frac{\theta}{2}\right)\left\{1 - \sin\left(\frac{\theta}{2}\right)\sin\left(\frac{3\theta}{2}\right)\right\} \tag{2.1b}$$

$$\sigma_{xy}(r,\theta) = \frac{K_I}{\sqrt{2\pi r}} \cos\left(\frac{\theta}{2}\right)\sin\left(\frac{\theta}{2}\right)\cos\left(\frac{3\theta}{2}\right) \tag{2.1c}$$

$$u(r,\theta) = \frac{K_I}{2\mu}\sqrt{\frac{r}{2\pi}}\cos\left(\frac{\theta}{2}\right)\left\{\kappa - 1 + 2\sin^2\left(\frac{\theta}{2}\right)\right\} \tag{2.2a}$$

$$v(r,\theta) = \frac{K_I}{2\mu}\sqrt{\frac{r}{2\pi}}\sin\left(\frac{\theta}{2}\right)\left\{\kappa + 1 - 2\cos^2\left(\frac{\theta}{2}\right)\right\} \tag{2.2b}$$

where K_I is mode I stress intensity factor, σ_{xx}, σ_{yy} and σ_{xy} are the stress components (Figure 2.3) at a distance r from the crack tip and at an angle θ from the crack plane. In Equations 2.2, u and v are the displacement in x and y directions, respectively, μ is the shear modulus and κ is $(3-4\nu)$ for plane strain or $\left(\frac{3-\nu}{1+\nu}\right)$ for plane stress where ν is the Poisson's ratio. Relationship between the shear modulus and the Young's modulus E and Poisson's ratio ν is in the following form:

$$\mu = \frac{E}{2(1+\nu)} \tag{2.3}$$

Definition of the mode I stress intensity factors at the crack tips can be written as:

$$K_I(a) = \lim_{x \to a+} \sqrt{2\pi(x-a)}\,\sigma_{yy}(x,0) \tag{2.4a}$$

$$K_I(-a) = \lim_{x \to -a-} \sqrt{2\pi(-x-a)}\,\sigma_{yy}(x,0) \tag{2.4b}$$

where a is the half of the crack length.

Mode II crack:

$$\sigma_{yy}(r,\theta) = \frac{K_{II}}{\sqrt{2\pi r}}\sin\left(\frac{\theta}{2}\right)\cos\left(\frac{\theta}{2}\right)\cos\left(\frac{3\theta}{2}\right) \tag{2.5a}$$

$$\sigma_{xx}(r,\theta) = -\frac{K_{II}}{\sqrt{2\pi r}}\sin\left(\frac{\theta}{2}\right)\left\{2+\cos\left(\frac{\theta}{2}\right)\cos\left(\frac{3\theta}{2}\right)\right\} \tag{2.5b}$$

$$\sigma_{xy}(r,\theta) = \frac{K_{II}}{\sqrt{2\pi r}}\cos\left(\frac{\theta}{2}\right)\left\{1-\sin\left(\frac{\theta}{2}\right)\sin\left(\frac{3\theta}{2}\right)\right\} \tag{2.5c}$$

$$u(r,\theta) = \frac{K_{II}}{2\mu}\sqrt{\frac{r}{2\pi}}\sin\left(\frac{\theta}{2}\right)\left\{\kappa+1+2\cos^2\left(\frac{\theta}{2}\right)\right\} \tag{2.6a}$$

$$v(r,\theta) = -\frac{K_{II}}{2\mu}\sqrt{\frac{r}{2\pi}}\cos\left(\frac{\theta}{2}\right)\left\{\kappa-1-2\sin^2\left(\frac{\theta}{2}\right)\right\} \tag{2.6c}$$

where K_{II} is mode II stress intensity factor whose definition is given as:

$$K_{II}(a) = \lim_{x \to a+}\sqrt{2\pi(x-a)}\sigma_{xy}(x,0) \tag{2.7a}$$

$$K_{II}(-a) = \lim_{x \to -a-}\sqrt{2\pi(-x-a)}\sigma_{xy}(x,0) \tag{2.7b}$$

Mode III crack:

$$\sigma_{xz}(r,\theta) = -\frac{K_{III}}{\sqrt{2\pi r}}\sin\left(\frac{\theta}{2}\right) \tag{2.8a}$$

$$\sigma_{yz}(r,\theta) = \frac{K_{III}}{\sqrt{2\pi r}}\cos\left(\frac{\theta}{2}\right) \tag{2.8b}$$

$$\sigma_{xx}(r,\theta) = \sigma_{yy}(r,\theta) = \sigma_{zz}(r,\theta) = 0 \tag{2.8c}$$

$$w(r,\theta) = \frac{K_{III}}{\mu}\sqrt{\frac{r}{2\pi}}\sin\left(\frac{\theta}{2}\right) \tag{2.9a}$$

$$u(r,\theta) = v(r,\theta) = 0 \tag{2.9b}$$

where K_{III} is mode III stress intensity factor, w is the displacement in z direction and σ_{xz}, σ_{yz} and σ_{zz} are the stress components. Definition of the mode III stress intensity factor at the crack tip is given as:

$$K_{III}(a) = \lim_{x \to a+} \sqrt{2\pi(x-a)}\,\sigma_{yz}(x,0) \tag{2.10a}$$

$$K_{III}(-a) = \lim_{x \to -a-} \sqrt{2\pi(-x-a)}\,\sigma_{yz}(x,0) \tag{2.10b}$$

Figure 2.5 depicts a three dimensional crack front and a local coordinate system composed of the normal (n), tangential (t) and binormal (b) directions, n pointing into the material side. The asymptotic stress and displacement distribution in the local coordinate system is given below (Cisilino, [20]):
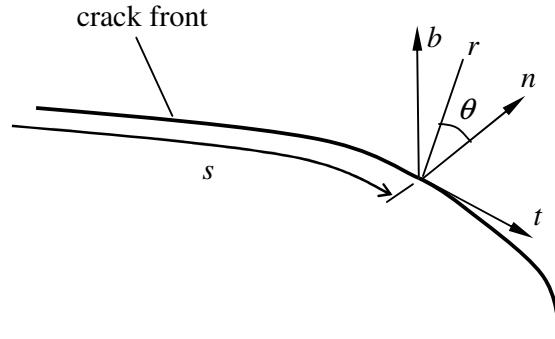
Figure 2.5 Three dimensional crack

$$\sigma_{nn} = \frac{K_I(s)}{\sqrt{2\pi r}}\cos\left(\frac{\theta}{2}\right)\left[1 - \sin\left(\frac{\theta}{2}\right)\sin\left(\frac{3\theta}{2}\right)\right]$$
$$- \frac{K_{II}(s)}{\sqrt{2\pi r}}\sin\left(\frac{\theta}{2}\right)\left[2 + \cos\left(\frac{\theta}{2}\right)\cos\left(\frac{3\theta}{2}\right)\right] \tag{2.11a}$$

16

$$\sigma_{bb} = \frac{K_I(s)}{\sqrt{2\pi r}} \cos\left(\frac{\theta}{2}\right)\left[1 + \sin\left(\frac{\theta}{2}\right)\sin\left(\frac{3\theta}{2}\right)\right]$$
$$+ \frac{K_{II}(s)}{\sqrt{2\pi r}} \sin\left(\frac{\theta}{2}\right)\cos\left(\frac{\theta}{2}\right)\cos\left(\frac{3\theta}{2}\right) \tag{2.11b}$$

$$\sigma_{tt} = 2\nu\left[\frac{K_I(s)}{\sqrt{2\pi r}} \cos\left(\frac{\theta}{2}\right) - \frac{K_{II}(s)}{\sqrt{2\pi r}} \sin\left(\frac{\theta}{2}\right)\right] \tag{2.11c}$$

$$\sigma_{nb} = \frac{K_I(s)}{\sqrt{2\pi r}} \sin\left(\frac{\theta}{2}\right)\cos\left(\frac{\theta}{2}\right)\cos\left(\frac{3\theta}{2}\right)$$
$$+ \frac{K_{II}(s)}{\sqrt{2\pi r}} \cos\left(\frac{\theta}{2}\right)\left[1 - \sin\left(\frac{\theta}{2}\right)\sin\left(\frac{3\theta}{2}\right)\right] \tag{2.11d}$$

$$\sigma_{nt} = -\frac{K_{III}(s)}{\sqrt{2\pi r}} \sin\left(\frac{\theta}{2}\right) \tag{2.11e}$$

$$\sigma_{bt} = \frac{K_{III}(s)}{\sqrt{2\pi r}} \cos\left(\frac{\theta}{2}\right) \tag{2.11f}$$

$$u_n = \frac{1+\nu}{E}\sqrt{\frac{2r}{\pi}}\left\{K_I(s)\cos\left(\frac{\theta}{2}\right)\left[(1-2\nu) + \sin^2\left(\frac{\theta}{2}\right)\right]\right.$$
$$\left. + K_{II}(s)\sin\left(\frac{\theta}{2}\right)\left[2(1-\nu) + \cos^2\left(\frac{\theta}{2}\right)\right]\right\} \tag{2.12a}$$

$$u_b = \frac{1+\nu}{E}\sqrt{\frac{2r}{\pi}}\left\{K_I(s)\sin\left(\frac{\theta}{2}\right)\left[2(1-\nu) - \cos^2\left(\frac{\theta}{2}\right)\right]\right.$$
$$\left. - K_{II}(s)\cos\left(\frac{\theta}{2}\right)\left[(1-2\nu) - \sin^2\left(\frac{\theta}{2}\right)\right]\right\} \tag{2.12b}$$

$$u_t = 2\frac{1+\nu}{E}\sqrt{\frac{2r}{\pi}}K_{III}(s)\sin\left(\frac{\theta}{2}\right) \tag{2.12c}$$

where the parameter s is the arc length of the crack front. In Equations 2.11, σ_{ij}, $(i, j = t, n, b)$ are the stress components and in Equations 2.12, u_i, $(i = t, n, b)$ are the displacement components. Definitions of the stress intensity factors for modes I, II and III loadings are given as:

$$K_I = \lim_{r \to 0} \sqrt{2\pi r}\, \sigma_{bb}(r,0) \qquad\qquad (2.13a)$$

$$K_{II} = \lim_{r \to 0} \sqrt{2\pi r}\, \sigma_{nb}(r,0) \qquad\qquad (2.13b)$$

$$K_{III} = \lim_{r \to 0} \sqrt{2\pi r}\, \sigma_{bt}(r,0) \qquad\qquad (2.13c)$$

In this study, we examine three dimensional semi – circular surface cracks in functionally graded material coatings. The cracks are assumed to be subjected to mode I thermomechanical loading. The asymptotic distributions of the stress and displacement components in functionally graded materials are previously shown to be the same as those for homogeneous materials (Eischen [24]) except the fact that the material parameters that are used in the displacement expressions (Equations 2.12a-c) have to be calculated at the point under consideration. Thus, in the implementation of the displacement correlation technique (DCT) for FGMs, aforementioned expressions can be used with appropriate modifications. Furthermore, due to mode I thermomechanical loading applied to the coating – substrate structure K_{II} and K_{III} are identically equal to zero.

2.2 Geometry of the Problem

The geometry of the semi – circular surface crack in an FGM coating bonded to a homogeneous substrate is shown by Figures 2.6 and 2.7. The thicknesses of the FGM coating and the substrate are taken as h_2 and h_1, respectively. There is a semi – circular "thumb – nail" crack of length $2a$ and depth a on the surface $x = h_1 + h_2$. A point P on the crack front can be located by using the parametric angle ϕ as shown in Figure 2.7. The specimen dimensions used in this study are given as $h_1 = 12.5$ mm, $h_2 = 2$ mm, $b = 20$ mm and $l = 20$ mm. The dimensions of the thicknesses are same as the dimensions given by Lee and Erdoğan [17].
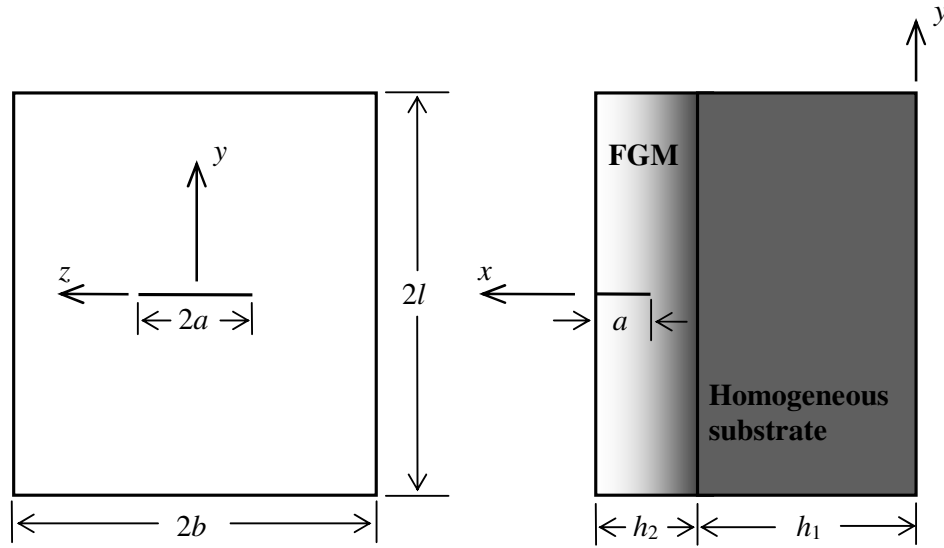
Figure 2.6 The geometry of the FGM coating bonded to a homogeneous substrate and the semi – circular surface crack.
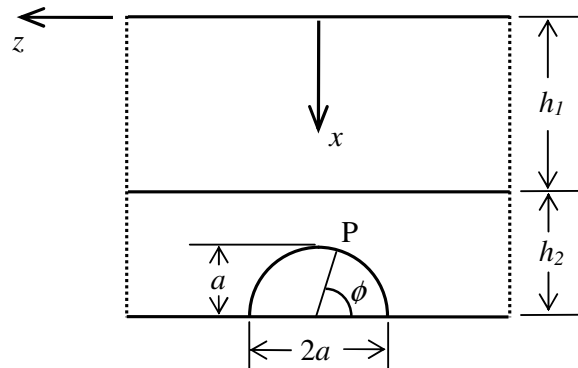
Figure 2.7 Parametric angle ϕ and the corresponding point P on the semi – circular crack front.

2.3 Material Property Variations and FGM Coating Types

The parametric analyses on FGMs in this study are based on a ZrO_2 (ceramic) – Ti-6Al-4V (Titanium alloy) FGM laid over a Ti-6Al-4V substrate. Assuming both the coating and the substrate to be isotropic, a total of six material parameters are

19

required to be known to carry out a transient thermal fracture analysis. These parameters are the elastic modulus (E), Poisson's ratio (ν), density (ρ), specific heat (c), thermal conductivity (k) and the thermal expansion coefficient (α). For mechanical loading only the elastic modulus and the Poisson's ratio are needed to be known. All the material parameters are assumed to be functions of the x – coordinate in the FGM coating and constant in the substrate. The material model used for the elastic modulus is expressed as

$$E(x) = \begin{cases} E_s, & 0 < x < h_1 \\ E_c + (E_s - E_c)\left(\dfrac{h_1 + h_2 - x}{h_2}\right)^p, & h_1 < x < h_1 + h_2 \end{cases} \tag{2.14}$$

where the subscripts s and c stand for the metallic alloy substrate (Ti-6Al-4V) and the ceramic coating surface (ZrO$_2$), respectively. This equation implies that elastic modulus is constant in the substrate. A power – law type variation is assumed to exist in the FGM coating. In Equation 2.14, p is a positive constant which may be adjusted to obtain a certain type of FGM coating. Exactly same type of variation is assumed to hold for the remaining five material parameters. The property variations for each of the material parameters are assumed to vary proportionally in the coating. Hence, the exponent p governs the variation of the material properties in the FGM coating for each of the six material parameters. In this study, four different types of material property variations are considered in the numerical examples. They correspond to homogeneous ceramic (H) and ceramic – rich (CR), linear variation (LN) and metal – rich (MR) FGM coatings. The particular values of the exponent p used in these examples are given in Table 2.1.

Table 2.1 The values of the exponent p for the FGM coating types.

FGM Coating Type	H	CR	LN	MR
p	∞	8	1	0.5

20

The material properties for the ceramic (ZrO$_2$) and metal (Ti-6Al-4V) components are given by Ootao et al. [21] as a function of the temperature T for the range $300\,\text{K} \leq T \leq 1300\,\text{K}$ as follows

$$E_c(T) = 132.2 - 50.3 \times 10^{-3}T - 8.1 \times 10^{-6}T^2 \quad \text{[GPa]} \tag{2.15a}$$

$$\upsilon_c = 0.333 \tag{2.15b}$$

$$k_c(T) = 1.71 + 0.21 \times 10^{-3}T + 0.116 \times 10^{-6}T^2 \quad \text{[W/(mK)]} \tag{2.15c}$$

$$c_c(T) = 2.74 \times 10^2 + 7.95 \times 10^{-1}T - 6.19 \times 10^{-4}T^2 + 1.71 \times 10^{-7}T^3 \quad \text{[J/(kgK)]} \tag{2.15d}$$

$$\rho_c(T) = 3657.0/\{1.0 + \alpha(T - 300.0)\}^3 \quad \text{[kg/m}^3\text{]} \tag{2.15e}$$

$$\alpha_c(T) = 13.3 \times 10^{-6} - 18.9 \times 10^{-9}T + 12.7 \times 10^{-12}T^2 \quad \text{[1/K]} \tag{2.15f}$$

$$E_s(T) = 122.7 - 0.0565T \quad \text{[GPa]} \tag{2.16a}$$

$$\upsilon_s(T) = 0.2888 + 32.0 \times 10^{-6}T \tag{2.16b}$$

$$k_s(T) = 1.1 + 0.017T \quad \text{[W/(mK)]} \tag{2.16c}$$

$$c_s(T) = 3.5 \times 10^2 + 8.78 \times 10^{-1}T - 9.74 \times 10^{-4}T^2 + 4.43 \times 10^{-7}T^3 \quad \text{[J/(kgK)]} \tag{2.16d}$$

$$\rho_s(T) = 4420.0/\{1.0 + \alpha(T - 300.0)\}^3 \quad \text{[kg/m}^3\text{]} \tag{2.16e}$$

$$\alpha_s(T) = 7.43 \times 10^{-6} + 5.56 \times 10^{-9}T - 2.69 \times 10^{-12}T^2 \quad \text{[1/K]} : 300\,\text{K} \leq T \leq 1100\,\text{K}$$

$$\alpha_s(T) = 10.291 \times 10^{-6} \quad \text{[1/K]} : 1100\,\text{K} \leq T \leq 1300\,\text{K} \tag{2.16f}$$

In the analyses carried out in this study, material properties calculated at $T = 300\,\text{K}$ and $T = 786.5\,\text{K}$ are used for mechanical and thermal loading problems, respectively. These properties are given in Table 2.2. The variations of the elastic moduli in the coating types considered are depicted in Figure 2.8 for $T = 300\,\text{K}$. Similar variations exist for the remaining five thermomechanical parameters.

In the calculations carried out to make comparisons to the results given by Newman and Raju [19], a homogeneous aluminum alloy (2014-T651Al) plate is used. The dimensions of this plate are same as the dimensions of the coating – substrate structure depicted in Figure 2.6. The elastic modulus and the Poisson's ratio of the aluminum plate are given as 73.1 GPa and 0.33, respectively.

Table 2.2 Material properties of the ceramic (ZrO_2) and metal (Ti-6Al-4V) components

	ZrO_2		Ti-6Al-4V	
	$T = 300$ K	$T = 786.5$ K	$T = 300$ K	$T = 786.5$ K
E [GPa]	116.4	87.6	105.8	78.3
ν	0.333	0.333	0.298	0.314
ρ [kg/m^3]	3657	3624	4420	4355
c [J/(kgK)]	461	600	538	654
k [W/(mK)]	1.78	1.95	6.20	14.47
$\alpha \times 10^{-7}$ [1/K]	88	63	89	101
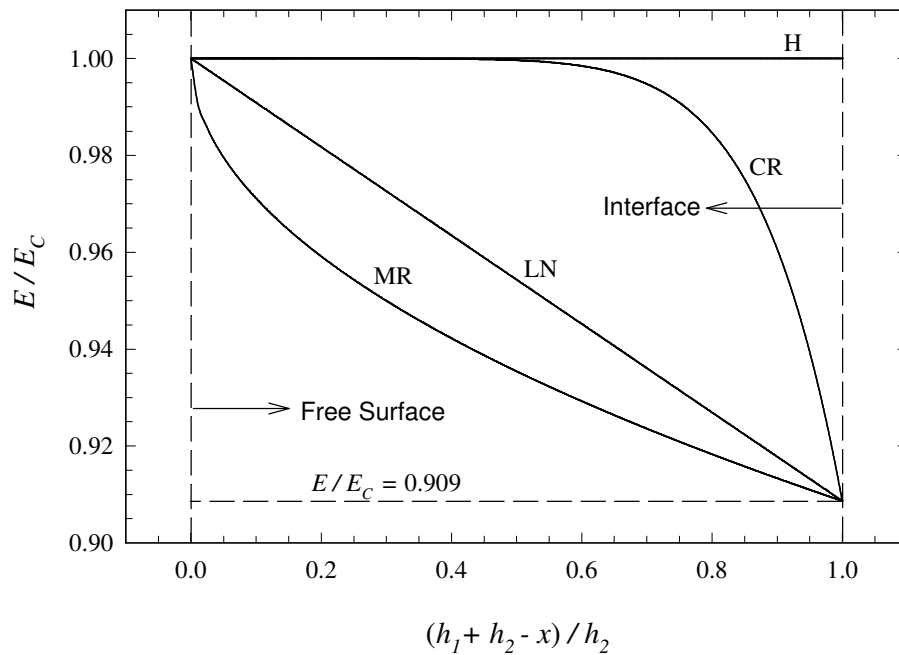
Figure 2.8 Variations of the elastic moduli in the coatings at $T = 300$ K.

2.4 Loading Types and Normalizations

The coating – substrate system is assumed to be subjected to mechanical or transient thermal loading conditions. The loading types are uniform tension, bending, fixed-grip tension, three point bending and transient thermal loading. Each

loading type and the corresponding normalized mode I stress intensity factors are given in this section.

2.4.1 Uniform Tension

In this loading condition, the FGM coating and substrate system is assumed to be subjected to uniform stress σ_t, at the ends $y = \pm l$. Finite element analyses are carried out using the material properties at $T = 300$ K which are given in Table 2.2. This loading type is also considered in the comparisons to the results given by Newman and Raju [19]. The FGM coating – substrate structure subjected to uniform tension is depicted in Figure 2.9.
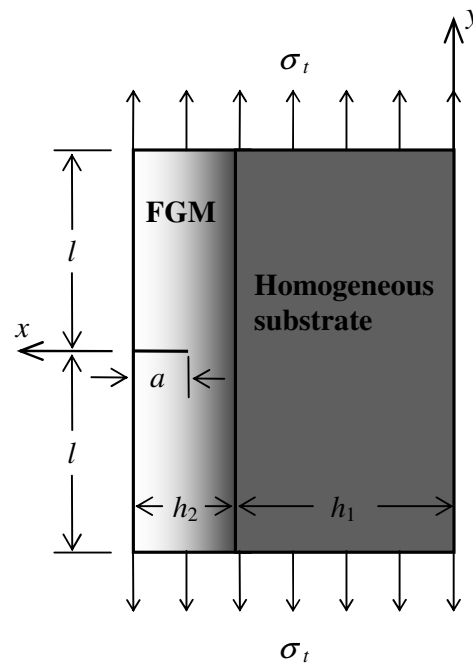
Figure 2.9 FGM coating – substrate structure subjected to uniform tension at the ends $y = \pm l$.

The normalized mode I stress intensity factor is given as

$$K_{In} = \frac{K_I}{\sigma_t \sqrt{\pi a/Q}} \tag{2.17}$$

23

where σ_t is the applied stress, a is the crack depth and Q is the shape factor for an elliptical crack. The value of Q is equal to 2.464 for the semi – circular crack considered in this study.

2.4.2 Bending

In this loading condition, the FGM coating – substrate system is subjected to a linearly varying normal stress at $y = \pm l$. The normal stress σ_{yy} is assumed to be equal to σ_b at $x = h_1 + h_2$ and $(-\sigma_b)$ at $x = 0$. There is a linear variation in between. Hence, on the loaded surface the normal stress is equal to 0 at $x = (h_1 + h_2)/2$ as can be seen in Figure 2.10. Finite element analyses are carried out using the material properties at $T = 300 \text{ K}$ which are given in Table 2.2. This loading condition is also used in the comparisons to the results given by Newman and Raju [19].
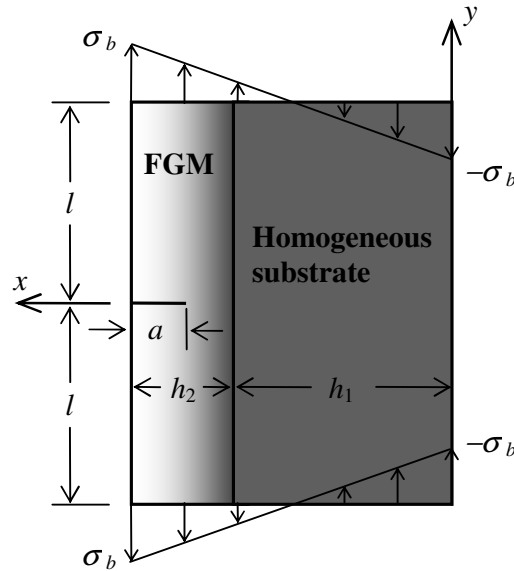
Figure 2.10 FGM coating – substrate structure subjected to bending at the ends $y = \pm l$.

The normalized mode I stress intensity factor is given as

$$K_{In} = \frac{K_I}{\sigma_b \sqrt{\pi a / Q}}$$

(2.18)

where σ_b is the normal stress at $x = h_1 + h_2$.

2.4.3   Fixed - Grip Tension

In this loading condition, the FGM coating and substrate system is assumed to be subjected to uniform normal displacement v_0 (displacement in y – direction), at the ends $y = \pm l$. Finite element analyses are carried out using the material properties at $T = 300\,\text{K}$ which are given in Table 2.2. Figure 2.11 depicts the fixed – grip tension case.
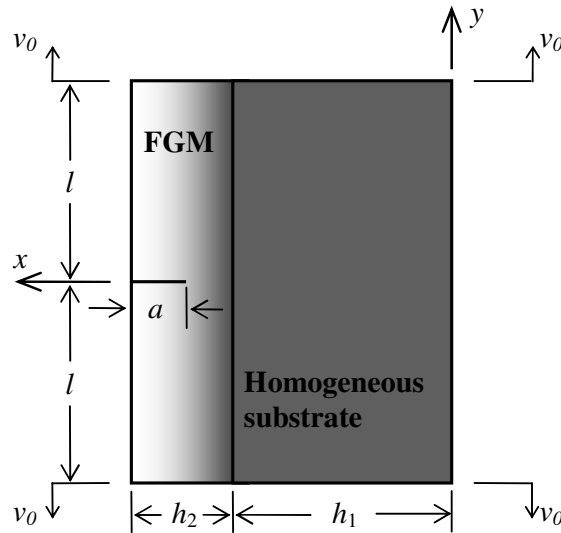
Figure 2.11 FGM coating – substrate structure subjected to uniform normal displacement v_0 at the ends $y = \pm l$.

The normalized mode I stress intensity factor is given as

$$K_{In} = \frac{K_I}{E_c(v_0/l)\sqrt{\dfrac{\pi a}{Q}}}$$

(2.19)

25

where l is the half-length of cracked plate, E_c is the elastic modulus of ZrO_2 at 300 K and v_0 is the applied displacement.

2.4.4   Three Point Bending
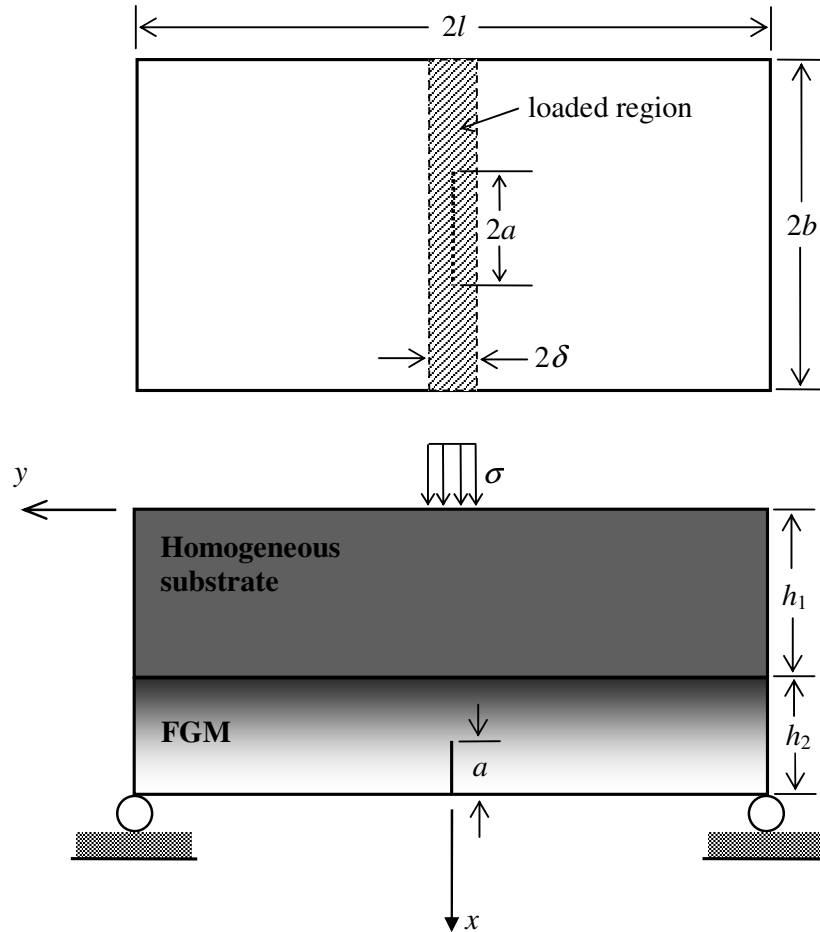
Figure 2.12 FGM coating – substrate structure subjected to three point bending.

In this loading case, the FGM coating-substrate system is loaded by applying a uniform compressive traction of magnitude σ to the surface, $x = 0$. The stress is applied to the rectangular region $-\delta < y < \delta$ and $-b < z < b$, $\delta \cong 2.11\,\text{mm}$. The structure is supported by rollers at $y = \pm l$, $x = h_1 + h_2$. Finite element analyses are carried out using the material properties at $T = 300\,\text{K}$ which are given in Table 2.2.

The FGM coating – substrate structure subjected to three point bending can be seen in Figure 2.12.

The normalized mode I stress intensity factor is given as

$$K_{In} = \frac{K_I}{\dfrac{P}{bl}\sqrt{\dfrac{\pi a}{Q}}} \tag{2.20}$$

where b is the half-width of cracked plate, l is the half-length of cracked plate and P is the resultant force. This force, P is defined as

$$P = 4b\delta\sigma \tag{2.21}$$

2.4.5 Transient Thermal Loading

In this loading case, the composite medium is initially assumed to be stress - free at a high processing temperature of 1273 K. Then, the coating – substrate system is placed in an environment whose temperature is $T_0 = 300\,\text{K}$. It is assumed that at all the surfaces except the surface at $x = h_1 + h_2$, there is free convection with a convection coefficient of $h = 5$ W/(m^2 K). At the surface, $x = h_1 + h_2$, there is forced convection and the convection coefficient is $h = 10000$ W/(m^2 K). In the analysis, the material properties computed at the mid temperature, $T_m = 786.5\,\text{K}$ are used. The thermomechanical properties are given in Table 2.2. In this problem, first, the transient temperature distribution in the composite medium is computed by considering the heat conduction in the nonhomogeneous medium. Then, this computed temperature distribution is used to solve the structural problem and to calculate transient thermal stress intensity factors around the crack front. In the analysis, the crack surfaces are assumed to be completely insulated and the medium is free of any mechanical constraints. The boundary conditions for this loading case are shown in Figure 2.13.
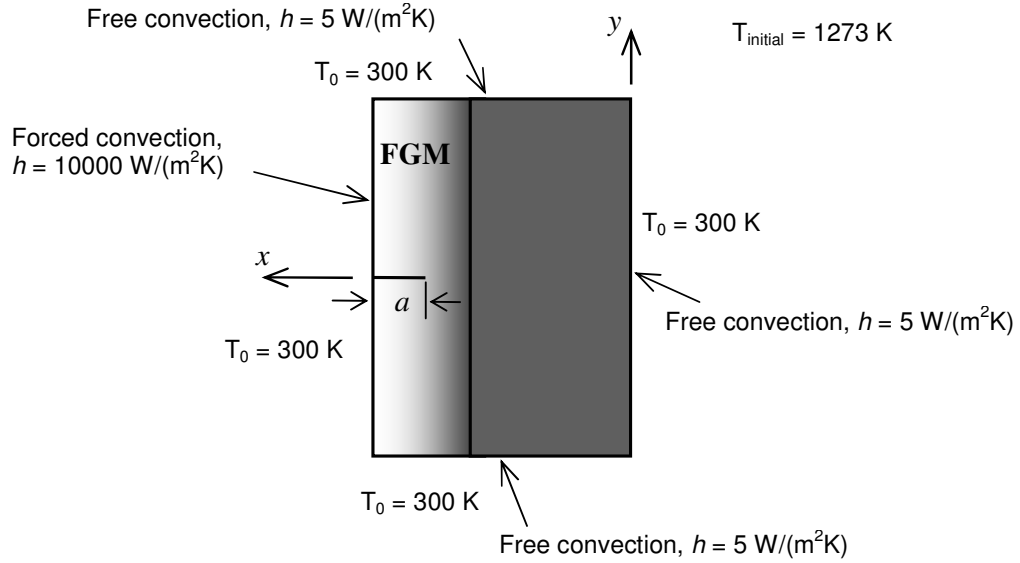
Figure 2.13 The boundary conditions for transient thermal loading.

The normalized mode I stress intensity factor is given as

$$K_{In} = \frac{K}{S\sqrt{\pi \dfrac{a}{Q}}} \qquad (2.22)$$

where S is the normalization stress and defined by

$$S = \alpha_c E_c T_m /(1 - v_c) \qquad (2.23)$$

where E_c, v_c and α_c are the elastic modulus, Poisson's ratio and thermal expansion coefficient of ZrO_2 at 786.5 K, respectively. In this problem, the normalized mode I stress intensity factors are computed with respect to normalized time which is defined by

$$\tau = \frac{D\,t}{h_2^2} \qquad (2.24)$$

where t is time, h_2 is the thickness of the coating and D is the thermal diffusivity coefficient of ZrO_2 which is expressed as

$$D = \frac{k_c}{\rho_c c_c} \qquad (2.25)$$

where k_c, ρ_c and c_c are the thermal conductivity, density and specific heat of ZrO_2 at 786.5 K, respectively.

CHAPTER 3

FINITE ELEMENT MODEL AND THE DISPLACEMENT CORRELATION TECHNIQUE (DCT)

3.1 The Finite Element Model

The finite element model of the specimen is shown in Figure 3.1. This model is created using the general purpose finite element analysis software ANSYS [18]. In all loading cases described in the previous chapter the crack plane is a plane of symmetry. Hence, it suffices to model only one – quarter of the composite medium to compute the mode I stress intensity factors.

In a standard finite element program, there are two ways of creating the models. First is solid modelling in which the boundaries of the model are created and then it is meshed automatically by the program itself. The other is the direct generation in which the elements are generated from the nodes directly. In this study, the finite element model is created by using the second method.

In the model totally, 29754 nodes and 6608 elements are used. These elements are SOLID95 for structural analysis and SOLID90 for thermal analysis in ANSYS. SOLID95 is defined by 20 nodes having three degrees of freedom per node: translations in x, y, and z directions. SOLID90 has also 20 nodes with a single degree of freedom, temperature, at each node. In the elements used around the crack front, in order to simulate the square – root strain singularity, one face of the 20 – node isoparametric three dimensional brick element is collapsed. In these elements, the mid – point nodes are moved to the quarter points to create the square – root singularity. The formulation of this element is given in [22]. The 20 – node brick element and the singular element are shown in Figures 3.2 and 3.3.
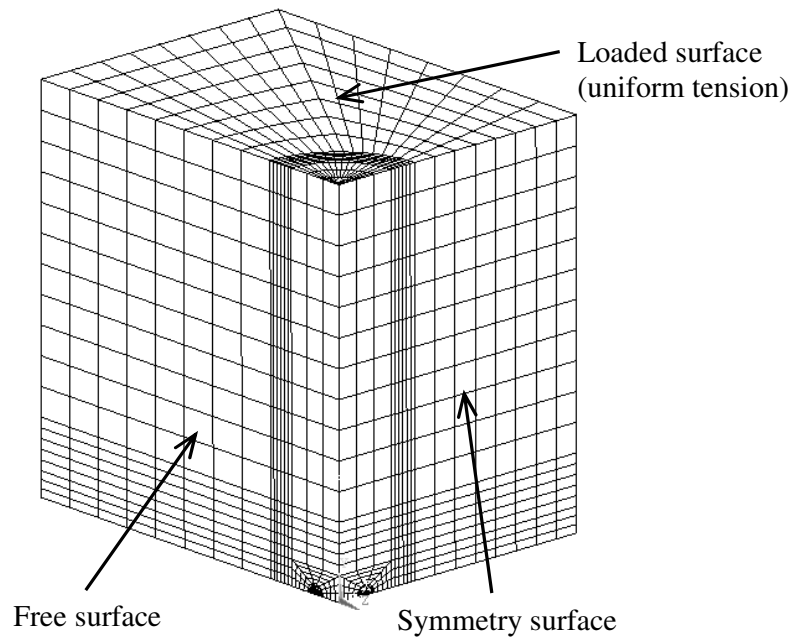
Figure 3.1 Finite element model.
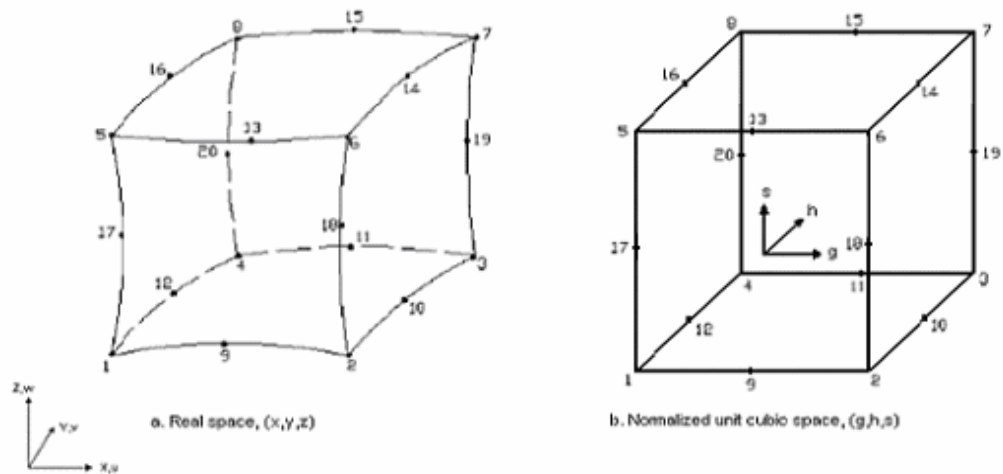
Figure 3.2 Node numbering of a 20 - node isoparametric brick element

The semi - circular surface crack and singular elements can be seen in Figures 3.4 and 3.5. The radius of the singular elements are taken as $a/25$. In addition, sixteen singular elements are used around the crack front. It is found out that the

31

combination of $a/25$ for the radius and 16 singular elements gives sufficiently convergent results.
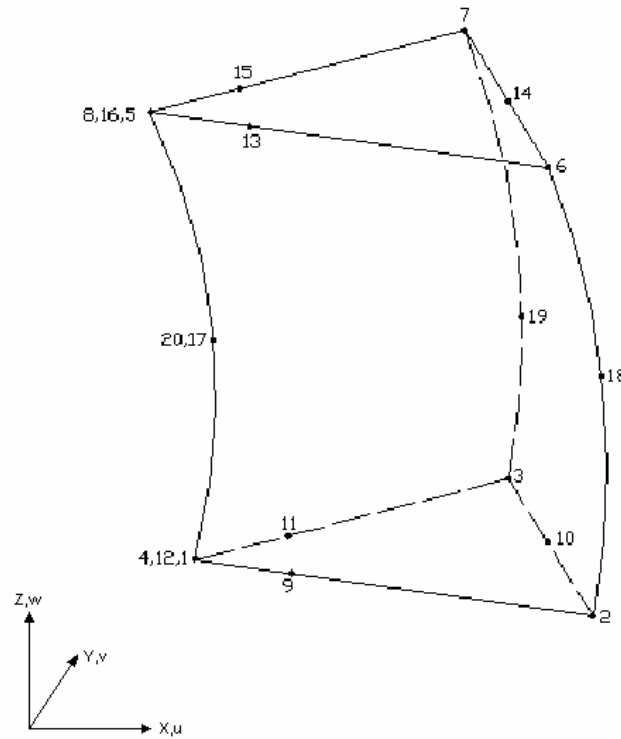
Figure 3.3 Collapsed 20-node isoparametric brick element.

Also, in order to avoid the creation of wedge shaped elements at the intersection of the free surface and the symmetry surface a small circular hole with a radius $0.1(h_1 + h_2)/250$ is used in the model, as shown in Figure 3.5.

In this study, the material properties vary continously in the FGM coatings as described in Chapter 2. This continuous variation of the thermomechanical properties in the graded coating is incorporated into the finite element model by specifying each thermomechanical property at the centroid of a finite element. An Ansys Parametric Design Language (APDL) source code is developed to be able to specify the thermomechanical properties of a finite element at its centroid. Since, a total of 6608 elements are used in the model, we can say that 6608 different

property values are calculated for each material parameter in the FGM coating.
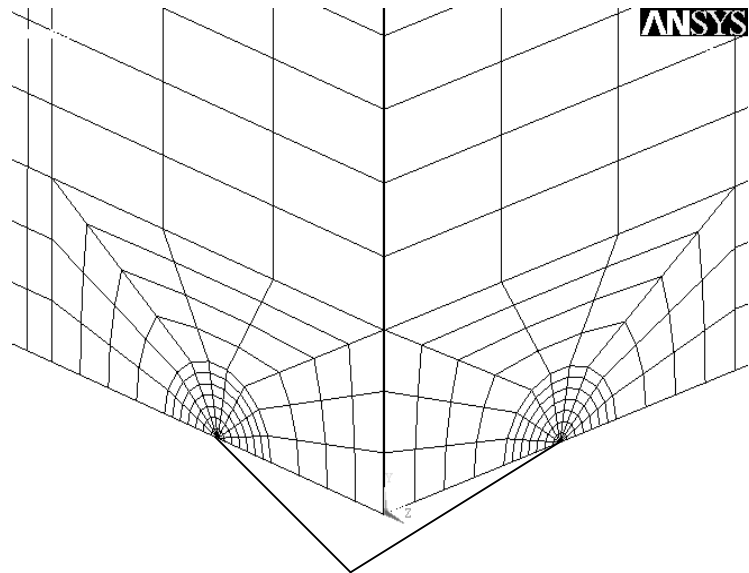
Singular elements around the crack front

Figure 3.4 Close – up view of the singular elements.
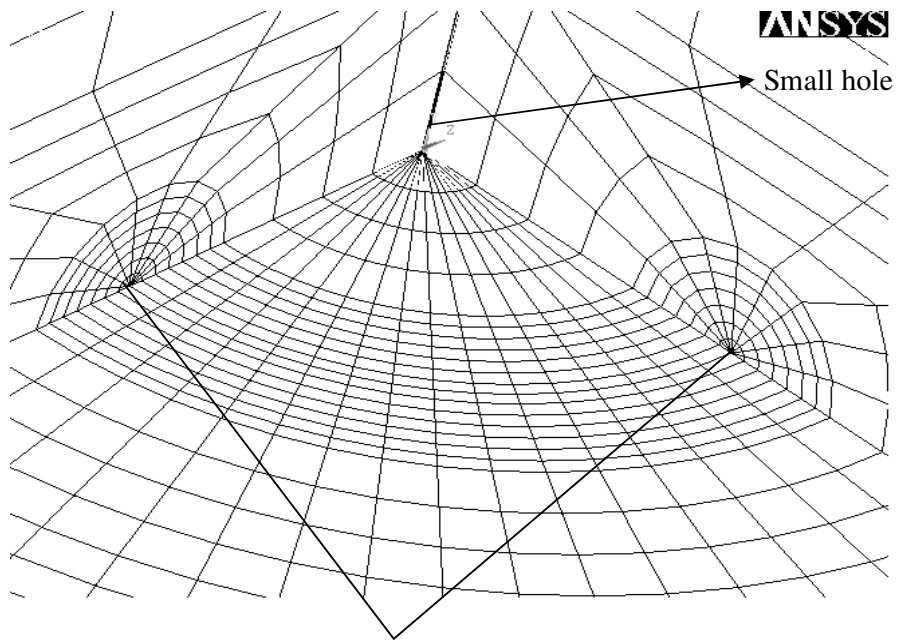
Singular elements

Figure 3.5 Singular elements around the crack front.

In the analyses, mechanical and transient thermal problems are investigated. In mechanical loading problems four different loading conditions, namely uniform tension, bending, fixed - grip and three point bending are considered. In fixed - grip tension all nodes on the top surface of the model are selected and uniform displacement values are entered. In the other mechanical loading conditions, the elements on which the normal stresses are applied are selected, and the stress values are entered for these selected elements. ANSYS automatically moves these loads to the nodes of the elements. In the bending problem, the normal stress acting at the top surface varies linearly. In 3-D analysis with ANSYS, this linearly varying load is specified using a slope command (SFGRAD). The slope of the linearly varying load is entered for a desired point using this command. After entering the normal stress value acting at this point, ANSYS calculates the stress values for the other loaded points automatically using the specified slope. The general procedure for the mechanical loading problems can be summarized as follows:

➢ Select static for analysis type,

➢ Choose 3-D 20-noded quadrilateral elements (SOLID95),

➢ Enter input parameters,

➢ Define nodes,

➢ Define elements by nodes,

➢ Merge the coincident nodes,

➢ Specify the material properties (Modulus of elasticity and Poisson's ratio) at the centroid of each element,

➢ Enter the symmetry boundary conditions (no symmetry boundary conditions are used on the crack surfaces),

➢ Enter the mechanical loading conditions (uniform tension, bending, fixed - grip or three point bending),

➢ Solve,

➢ Compute the stress intensity factors at the crack front nodes using the displacement correlation technique.

In the analysis of the thermal loading problem, transient coupled thermal – structural analysis is carried out. In this analysis, first transient heat conduction in the composite medium is considered and temperature distribution is computed. Then, this temperature distribution is used as an input to the structural problem. The crack surfaces are assumed to be completely insulated and the medium is free of any mechanical constraints. The inertia effects are not taken into account and coupling of the thermal and structural problems are assumed to be through the calculated temperature distribution only. In the thermal part of the problem, the environmental temperature and thermal convection coefficients given in Chapter 2 are entered as surface loads at the free surfaces. In the solution, minimum and maximum time step sizes are entered. In order to overcome oscillations in the temperature distribution, minimum time step size is chosen as a very small number, and maximum time step size is chosen as not too large. In the subsequent structural analysis all thermal loads are deleted and thermal 20 - noded isoparametric elements (SOLID90) are changed to SOLID95. The computed temperature results are read from the thermal results file for a given time and are applied as the load. The procedure for the coupled thermal - structural analysis is summarized as follows:

- In the thermal analysis:

  - Choose transient for the analysis type,
  - Choose 3-D 20 - noded brick elements. In thermal analysis SOLID90 is used with temperature as the DOF,
  - Enter input parameters,
  - Define nodes,
  - Define elements by nodes,
  - Merge the coincident nodes,
  - Specify the thermomechanical properties at the centroid of each element,
  - Enter the initial temperature,

➢ Enter the environmental temperature and thermal convection coefficients (free and forced). Then, use them on the free surfaces of the model,

➢ Enter time and min/max time step sizes. Also, activate the automatic time-stepping option,

➢ Compute the temperatures at each node.

- In the structural analysis:

➢ Choose static for the analysis type,

➢ Delete finite-element loads,

➢ Change thermal element type SOLID90 to SOLID95 whose DOFs are UX, UY and UZ,

➢ Enter the reference temperature,

➢ Enter the symmetry boundary conditions (on the crack face no symmetry boundary conditions are used),

➢ Read the results from the thermal results file for a given time and apply them as the loads,

➢ Solve,

➢ Compute the thermal stress intensity factors at each crack front node using the displacement correlation technique,

➢ Repeat last three steps for each required time.

In order to calculate the stress intensity factors the displacement correlation technique is used. Details of this method is given in Section 3.2. An APDL code using this method is generated for the computational analysis. In this code, the computed displacements of the nodes at the edge of a collapsed 20 – node brick element are used. To compute the stress intensity factors along the crack front, the material properties (Modulus of elasticity and Poisson's ratio) on the crack front nodes have to be calculated. The stress intensity factors are calculated automatically for each crack front node, using the APDL source code developed to implement the

displacement correlation technique.

3.2 The Displacement Correlation Technique (DCT)

Once the displacement field of the FGM coating – substrate structure is computed using the finite element method, the displacement correlation technique (DCT) can be used to calculate the mode I stress intensity factors. Consider a three dimensional crack front under mode I loading as shown in Figure 3.6. The crack front is assumed to be embedded in an FGM. The parameter s in this figure is the arc length of the crack front and (t, n, b) is a local coordinate system located at point P composed of the tangential (t), normal (n) and binormal (b) directions, n pointing into the material side. (r, θ) are the polar coordinates in the normal plane (n, b). Because of the reasons outlined in Section 2.1, the mode I asymptotic distribution of the normal stress and displacement components at point P can be expressed as
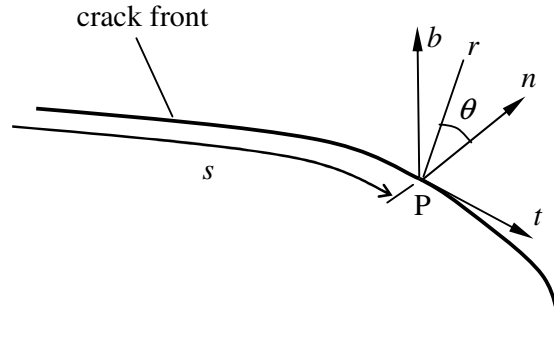
Figure 3.6 Crack front and the local coordinate system

$$\sigma_{bb}(r, \theta) = \frac{K_I(s)}{\sqrt{2\pi r}} \cos\left(\frac{\theta}{2}\right) \left[1 + \sin\left(\frac{\theta}{2}\right) \sin\left(\frac{3\theta}{2}\right)\right], \tag{3.1}$$

$$u_b(r, \theta) = \frac{1 + \nu^{\text{tip}}}{E^{\text{tip}}} \sqrt{\frac{2r}{\pi}} K_I(s) \sin\left(\frac{\theta}{2}\right) \left[2(1 - \nu^{\text{tip}}) - \cos^2\left(\frac{\theta}{2}\right)\right], \tag{3.2}$$

where the superscript (tip) refers to the material parameters that have to be

37

calculated at point P on the crack front and K_I is the mode I stress intensity factor. In order to calculate the mode I stress intensity factors we first take a section at point P parallel to the normal plane (n, b). The section and deformed shape of the crack are shown in Figure 3.7. The nodes 1, 2 and 3 are at the edge of a collapsed 20 – node brick element. In the undeformed configuration the distance of node 2 to point P is one fourth of that of node 3. Since small displacements are considered in this study, it can be further assumed that $R_2 = R_3 / 4$. Using Equation 3.2, the displacement field on the crack surface $(\theta = \pi)$ can be written as

$$u_b(r,\pi) = \frac{4\left(1 - \left(v^{\text{tip}}\right)^2\right)}{E^{\text{tip}}} \sqrt{\frac{r}{2\pi}} K_I . \tag{3.3}$$

The mode I stress intensity factor can now be expressed as

$$K_I = \frac{\sqrt{2\pi} E^{\text{tip}}}{4\left(1 - \left(v^{\text{tip}}\right)^2\right)} \left[\lim_{r \to 0} \left\{ \frac{u_b(r,\pi)}{\sqrt{r}} \right\} \right]. \tag{3.4}$$
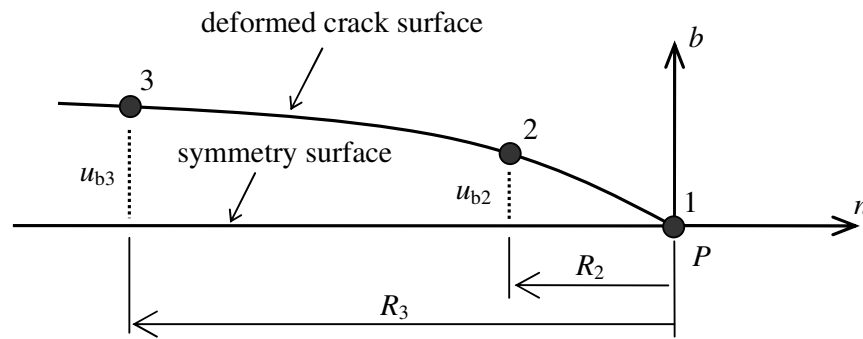
Figure 3.7 Deformed shape of the crack surface and a point P on the crack front.

Using the computed displacements of the nodes 2 and 3 and by using a linear extrapolation to the crack front, the expression for the mode I stress intensity factor is found as follows

38

$$K_I = \frac{\sqrt{2\pi}E^{\text{tip}}}{4\left(1-\left(\nu^{\text{tip}}\right)^2\right)}\left[\frac{R_3^{3/2}u_{b2} - R_2^{3/2}u_{b3}}{\sqrt{R_2}\sqrt{R_3}\left(R_3 - R_2\right)}\right].$$ (3.5)

The mode I stress intensity factors around the crack front can now be calculated for any type of loading provided that the displacement field is solved for using the finite element method.

CHAPTER 4

RESULTS AND DISCUSSION

4.1 Introduction

In this chapter, sample results are presented and discussed. First the finite element model results are compared to the results given by Newman and Raju [19] for various crack dimensions. In these comparisons a homogeneous Aluminum plate is modelled. After checking out the accuracy of the finite element results, same model is used for FGM analysis. In these investigations, the results are computed for different combinations of crack dimensions, mode I loading conditions and FGM coating types.

4.2 Comparisons to Newman and Raju Equation

In this section, the results calculated using the finite element model by considering a homogeneous Aluminum plate are compared to those obtained by using the Newman - Raju equation which is given in Appendix A. These comparisons are made to check out the accuracy of the finite element results. In this analysis a homogeneous surface cracked plate is assumed to be subjected to uniform tension or bending load.

4.2.1 Comparisons for Uniform Tension

In this section, the finite element model is assumed to be subjected to uniform tension σ_t, at the ends $y = \pm l$. The specimen shown in Figure 2.6 is assumed to be homogeneous and made of an Aluminum alloy whose mechanical properties are given in Section 2.3. The stress value is taken as 100 MPa for all the computations.

Normalized mode I stress intensity factors are presented in Figures 4.1-4.5 for various a/h_2 values. In addition sample results for two different crack dimensions are tabulated in Table 4.1.

Table 4.1 Comparisons of the normalized mode I stress intensity factors K_{In} for a homogeneous plate subjected to uniform tension.

$2\phi/\pi$	$a/h_2 = 0.4$			$a/h_2 = 0.8$		
	Present Study	Newman and Raju (1981)	% Diff.	Present Study	Newman and Raju (1981)	% Diff.
1.0000	1.0295	1.0407	1.0780	1.0324	1.0429	1.0080
0.9375	1.0300	1.0407	1.0302	1.0325	1.0429	0.9936
0.8750	1.0307	1.0407	0.9622	1.0332	1.0429	0.9372
0.8125	1.0317	1.0409	0.8831	1.0346	1.0431	0.8124
0.7500	1.0335	1.0413	0.7486	1.0363	1.0435	0.6887
0.6875	1.0359	1.0421	0.5969	1.0386	1.0444	0.5582
0.6250	1.0391	1.0437	0.4372	1.0416	1.0460	0.4165
0.5625	1.0428	1.0461	0.3100	1.0456	1.0485	0.2722
0.5000	1.0477	1.0497	0.1917	1.0507	1.0522	0.1480
0.4375	1.0540	1.0547	0.0724	1.0568	1.0574	0.0569
0.3750	1.0617	1.0614	0.0233	1.0645	1.0644	0.0124
0.3125	1.0713	1.0701	0.1183	1.0744	1.0733	0.1015
0.2500	1.0840	1.0807	0.3031	1.0872	1.0843	0.2622
0.1875	1.1011	1.0936	0.6774	1.1041	1.0977	0.5838
0.1250	1.1208	1.1088	1.0820	1.1245	1.1133	0.9988
0.0000	1.1735	1.1458	2.4136	1.1773	1.1516	2.2308

In Figures 4.1-4.5, the variation of the normalized stress intensity factors are plotted with respect to normalized polar angle ($2\phi/\pi$) and similar trends are observed for each crack dimension. In all of these plots, it can be seen that the minimum and maximum normalized stress intensity factors are obtained at symmetry surface $(\phi = \pi/2)$ and free surface $(\phi = 0)$, respectively. The largest difference is calculated at the free surface for each crack dimension. The percent differences at the free surface are nearly 2.55 % for $a/h_2 = 0.2$, 2.41 % for $a/h_2 = 0.4$, 2.32 % for $a/h_2 = 0.6$, 2.23 % for $a/h_2 = 0.8$ and 2.12 % for $a/h_2 = 1.0$. All of these differences are smaller than 3 %, therefore it can be said

that the accuracy of the finite element model is acceptable. The results obtained by the equation given by Newman and Raju [19], are within $\pm 5\%$ of the finite element analysis results.

It can be seen that the stress intensity factors increase as $\phi \to 0$ in Figures 4.1-4.5. The order of the stress singularity at the free surface $(\phi = 0)$ is in fact different from 1/2. There is a boundary zone near the free surface which affects the stress intensity factors. However, the results of previous detailed analysis (Ayhan and Nied [23]) show that, this effect is confined to a very small region near the free surface. The effect is calculated to be significant for $0° < \phi < 1°$. As a result, the free surface effect is not considered in this study. The results given in Figures 4.1-4.5 for $\phi = 0$ can be used as approximate stress intensity factors at the free surface.

Table 4.2 Comparisons of the normalized mode I stress intensity factors K_{In} for a homogeneous plate subjected to bending load.

$2\phi/\pi$	$a/h_2 = 0.4$			$a/h_2 = 0.8$		
	Present Study	Newman and Raju (1981)	% Diff.	Present Study	Newman and Raju (1981)	% Diff.
1.0000	0.9496	0.9636	1.4524	0.8716	0.8883	1.8772
0.9375	0.9500	0.9639	1.4416	0.8727	0.8889	1.8244
0.8750	0.9519	0.9649	1.3494	0.8753	0.8908	1.7416
0.8125	0.9547	0.9665	1.2275	0.8796	0.8941	1.6129
0.7500	0.9585	0.9690	1.0765	0.8859	0.8987	1.4206
0.6875	0.9637	0.9724	0.8862	0.8940	0.9047	1.1856
0.6250	0.9702	0.9769	0.6826	0.9038	0.9124	0.9401
0.5625	0.9781	0.9827	0.4623	0.9154	0.9218	0.6992
0.5000	0.9873	0.9900	0.2679	0.9289	0.9331	0.4479
0.4375	0.9979	0.9989	0.1079	0.9445	0.9463	0.1913
0.3750	1.0109	1.0098	0.1137	0.9624	0.9617	0.0797
0.3125	1.0258	1.0227	0.3048	0.9828	0.9792	0.3682
0.2500	1.0437	1.0377	0.5831	1.0061	0.9988	0.7321
0.1875	1.0661	1.0548	1.0699	1.0338	1.0206	1.2963
0.1250	1.0913	1.0740	1.6086	1.0645	1.0442	1.9396
0.0000	1.1542	1.1174	3.2965	1.1377	1.0944	3.9556

4.2.2 Comparisons for Bending

In this section, the finite element model is assumed to be subjected to a linearly varying normal stress at $y = \pm l$. The normal stress σ_{yy} is assumed to be equal to σ_b at $x = h_1 + h_2$ and $(-\sigma_b)$ at $x = 0$. There is a linear variation in between. Hence, on the loaded surface the normal stress is equal to 0 at $x = (h_1 + h_2)/2$. In all comparisons the stress on outer fiber is taken as 100 MPa. The normalized stress intensity factors are presented in Figures 4.6-4.10 and Table 4.2.

In Figures 4.6-4.10, the variation of the normalized stress intensity factors are plotted with respect to normalized polar angle and it can be seen that the trends are generally similar to those observed for the uniform tension loading. In these plots, the minimum and maximum stress intensity factors are computed at the symmetry surface and free surface, respectively. When the results are compared to those given by Newman and Raju equation [19], the largest differences are calculated at free surface The percent differences are nearly 2.78 % for $a/h_2 = 0.2$, 3.3 % for $a/h_2 = 0.4$, 3.6 % for $a/h_2 = 0.6$, 3.96 % for $a/h_2 = 0.8$ and 4.32 % for $a/h_2 = 1.0$. All of these differences are smaller than 4.5 %, therefore it can be said that the accuracy of the finite element model is acceptable.

4.3 Mechanical Loading on the FGM Coating and Substrate Structure

In this section, four different mechanical loading types, namely uniform tension, bending, fixed - grip tension and three point bending are considered in the analysis of the surface crack problem in FGM coatings. The normalized mode I stress intensity factors are computed for the homogeneous (H), ceramic - rich (CR), linear (LN) and metal - rich (MR) coatings for various crack dimensions. Finite element analyses are carried out using the material properties of ceramic (ZrO_2) and metal (Ti-6Al-4V) components at $T = 300$ K which are given in Chapter 2.

4.3.1 Uniform Tension

In this section, the FGM coating and substrate system is assumed to be subjected to uniform tension σ_t, at the ends $y = \pm l$ as shown in Figure 2.9. This stress is equal to 100 MPa. Normalized mode I stress intensity factors are presented in Figures 4.11-4.18 for various values of a/h_2. Also, results for some crack dimensions are tabulated in Table 4.3.

In Figures 4.11-4.18, the variation of the normalized stress intensity factors are plotted with respect to normalized polar angle for each FGM coating type. It can be seen that the lowest stress intensity factors are calculated at the symmetry surface. The stress intensity factors continuously increase as $\phi \rightarrow 0$. At the free surface, MR coating gives the largest stress intensity factors for each crack dimension. At the symmetry surface, however MR coating gives the minimum stress intensity factors for all crack dimensions except the case of $a/h_2 = 0.1$ that for which H coating gives the lowest one. In Figures 4.11–4.18, it can be observed that the stress intensity factors for semi – circular cracks in MR and LN coatings are more sensitive to the variations in the crack radius than those for cracks in H and CR coatings. This is due to the fact that material property gradients near the free surface are larger for MR and LN coatings than those of the CR and H coatings. In fact, there is no material property gradient for the H coating.

4.3.2 Bending

In this section, the FGM coating and substrate system is assumed to be subjected to a linearly varying normal stress at $y = \pm l$ as shown in Figure 2.10. The normal stress σ_{yy} is assumed to be equal to σ_b at $x = h_1 + h_2$ and $(-\sigma_b)$ at $x = 0$. There is a linear variation in between. Hence, on the loaded surface the normal stress is equal to 0 at $x = (h_1 + h_2)/2$. This stress on outer fiber is taken as 100 MPa. Crack dimensions are same as those used in Chapter 4.3.1. The normalized stress

intensity factors are presented in Figures 4.19-4.26 and in Table 4.4.

Table 4.3 Normalized mode I stress intensity factors K_{In} for an FGM coating – substrate structure subjected to tension.

$2\phi/\pi$	$a/h_2 = 0.2$				$a/h_2 = 0.4$			
	H	CR	LN	MR	H	CR	LN	MR
1.0000	1.0878	1.0948	1.0970	1.0772	1.0923	1.0979	1.0773	1.0578
0.9375	1.0872	1.0941	1.0964	1.0772	1.0927	1.0983	1.0779	1.0583
0.8750	1.0878	1.0947	1.0973	1.0786	1.0933	1.0990	1.0796	1.0599
0.8125	1.0893	1.0966	1.0998	1.0809	1.0942	1.1000	1.0820	1.0620
0.7500	1.0909	1.0981	1.1021	1.0833	1.0961	1.1019	1.0849	1.0645
0.6875	1.0933	1.1004	1.1049	1.0867	1.0988	1.1047	1.0891	1.0684
0.6250	1.0965	1.1036	1.1096	1.0912	1.1020	1.1079	1.0947	1.0739
0.5625	1.1006	1.1079	1.1154	1.0976	1.1058	1.1117	1.1014	1.0803
0.5000	1.1059	1.1132	1.1224	1.1045	1.1108	1.1166	1.1095	1.0880
0.4375	1.1123	1.1195	1.1300	1.1130	1.1172	1.1233	1.1195	1.0977
0.3750	1.1198	1.1271	1.1402	1.1242	1.1252	1.1313	1.1311	1.1093
0.3125	1.1299	1.1374	1.1524	1.1374	1.1352	1.1414	1.1453	1.1243
0.2500	1.1435	1.1509	1.1686	1.1545	1.1484	1.1547	1.1632	1.1429
0.1875	1.1612	1.1690	1.1884	1.1769	1.1662	1.1725	1.1863	1.1673
0.1250	1.1830	1.1908	1.2135	1.2053	1.1868	1.1934	1.2124	1.1971
0.0000	1.2365	1.2440	1.2756	1.2926	1.2407	1.2478	1.2802	1.2967
$2\phi/\pi$	$a/h_2 = 0.6$				$a/h_2 = 0.8$			
	H	CR	LN	MR	H	CR	LN	MR
1.0000	1.1000	1.0997	1.0587	1.0440	1.1034	1.0995	1.0406	1.0327
0.9375	1.1001	1.1001	1.0592	1.0443	1.1035	1.1002	1.0413	1.0333
0.8750	1.1009	1.1011	1.0610	1.0455	1.1041	1.1023	1.0433	1.0348
0.8125	1.1018	1.1025	1.0638	1.0479	1.1052	1.1053	1.0465	1.0370
0.7500	1.1034	1.1048	1.0676	1.0511	1.1068	1.1090	1.0509	1.0403
0.6875	1.1054	1.1075	1.0726	1.0553	1.1089	1.1131	1.0568	1.0450
0.6250	1.1082	1.1109	1.0791	1.0607	1.1117	1.1175	1.0642	1.0506
0.5625	1.1121	1.1151	1.0873	1.0677	1.1155	1.1224	1.0732	1.0577
0.5000	1.1170	1.1205	1.0967	1.0761	1.1203	1.1278	1.0840	1.0665
0.4375	1.1231	1.1271	1.1077	1.0861	1.1266	1.1342	1.0968	1.0772
0.3750	1.1307	1.1350	1.1213	1.0989	1.1345	1.1422	1.1120	1.0905
0.3125	1.1409	1.1455	1.1379	1.1145	1.1447	1.1524	1.1302	1.1069
0.2500	1.1538	1.1586	1.1574	1.1339	1.1577	1.1652	1.1519	1.1274
0.1875	1.1714	1.1765	1.1826	1.1597	1.1755	1.1831	1.1793	1.1540
0.1250	1.1925	1.1979	1.2118	1.1914	1.1966	1.2044	1.2107	1.1874
0.0000	1.2459	1.2520	1.2850	1.3009	1.2508	1.2590	1.2901	1.3061

Table 4.4 Normalized mode I stress intensity factors K_{In} for an FGM coating – substrate structure subjected to bending.

$2\phi/\pi$	$a/h_2 = 0.2$				$a/h_2 = 0.4$			
	H	CR	LN	MR	H	CR	LN	MR
1.0000	1.0500	1.0555	1.0550	1.0357	1.0107	1.0149	0.9944	0.9760
0.9375	1.0508	1.0561	1.0555	1.0367	1.0111	1.0155	0.9954	0.9770
0.8750	1.0523	1.0576	1.0572	1.0383	1.0130	1.0174	0.9978	0.9793
0.8125	1.0545	1.0597	1.0600	1.0407	1.0161	1.0204	1.0017	0.9828
0.7500	1.0571	1.0623	1.0635	1.0444	1.0203	1.0247	1.0072	0.9880
0.6875	1.0613	1.0667	1.0684	1.0501	1.0259	1.0304	1.0144	0.9949
0.6250	1.0665	1.0720	1.0747	1.0563	1.0328	1.0372	1.0234	1.0033
0.5625	1.0730	1.0784	1.0826	1.0638	1.0413	1.0457	1.0341	1.0137
0.5000	1.0802	1.0857	1.0915	1.0729	1.0512	1.0557	1.0465	1.0258
0.4375	1.0889	1.0944	1.1017	1.0843	1.0626	1.0672	1.0612	1.0403
0.3750	1.1001	1.1057	1.1148	1.0979	1.0765	1.0812	1.0787	1.0574
0.3125	1.1136	1.1191	1.1305	1.1145	1.0925	1.0973	1.0985	1.0774
0.2500	1.1296	1.1351	1.1489	1.1344	1.1116	1.1164	1.1220	1.1015
0.1875	1.1501	1.1558	1.1723	1.1595	1.1355	1.1404	1.1508	1.1317
0.1250	1.1748	1.1808	1.2002	1.1908	1.1626	1.1676	1.1829	1.1668
0.0000	1.2349	1.2411	1.2672	1.2832	1.2283	1.2336	1.2620	1.2771
$2\phi/\pi$	$a/h_2 = 0.6$				$a/h_2 = 0.8$			
	H	CR	LN	MR	H	CR	LN	MR
1.0000	0.9720	0.9720	0.9348	0.9216	0.9309	0.9270	0.8778	0.8713
0.9375	0.9726	0.9727	0.9359	0.9225	0.9319	0.9285	0.8790	0.8724
0.8750	0.9750	0.9753	0.9391	0.9253	0.9346	0.9323	0.8827	0.8756
0.8125	0.9790	0.9797	0.9442	0.9300	0.9393	0.9386	0.8890	0.8810
0.7500	0.9843	0.9855	0.9513	0.9365	0.9460	0.9471	0.8977	0.8888
0.6875	0.9910	0.9927	0.9606	0.9449	0.9545	0.9575	0.9089	0.8988
0.6250	0.9996	1.0018	0.9721	0.9553	0.9649	0.9694	0.9227	0.9110
0.5625	1.0100	1.0126	0.9858	0.9679	0.9773	0.9826	0.9392	0.9256
0.5000	1.0222	1.0251	1.0020	0.9828	0.9919	0.9977	0.9584	0.9428
0.4375	1.0363	1.0395	1.0204	1.0000	1.0086	1.0147	0.9805	0.9629
0.3750	1.0524	1.0558	1.0414	1.0200	1.0280	1.0340	1.0056	0.9860
0.3125	1.0715	1.0751	1.0660	1.0436	1.0498	1.0559	1.0344	1.0127
0.2500	1.0937	1.0975	1.0943	1.0715	1.0751	1.0811	1.0671	1.0439
0.1875	1.1205	1.1246	1.1279	1.1054	1.1048	1.1108	1.1054	1.0815
0.1250	1.1503	1.1547	1.1653	1.1450	1.1380	1.1441	1.1480	1.1252
0.0000	1.2216	1.2265	1.2556	1.2700	1.2158	1.2222	1.2498	1.2633

In Figures 4.19-4.26, the variation of the normalized stress intensity factors are plotted with respect to normalized polar angle for each FGM coating type. It can be seen that the lowest stress intensity factors are calculated at the symmetry

surface. The stress intensity factors continuously increase as $\phi \rightarrow 0$. At the free surface, MR coating gives the largest stress intensity factors for each crack dimension. At the symmetry surface, however, MR coating gives the minimum stress intensity factors. The results computed for bending are observed to be more sensitive to the variations in the crack radius as compared to the results calculated for uniform tension given in Section 4.3.1.

4.3.3 Fixed - Grip Tension

In this section, the FGM coating and substrate system is assumed to be subjected to uniform normal displacement v_0 (displacement in y – direction), at the ends $y = \pm l$ as shown in Figure 2.11. This uniform normal displacement v_0 is taken as 0.5 mm. The normalized stress intensity factors are presented in Figures 4.27-4.34 and given in the tabulated form in Table 4.5.

In Figures 4.27-4.34, the variation of the normalized stress intensity factors are plotted with respect to normalized polar angle for each FGM coating type. It can be observed that the lowest stress intensity factors are calculated at the symmetry surface. The stress intensity factors again continuously increase as $\phi \rightarrow 0$. MR coating gives the largest stress intensity factors for each crack dimension at the free surface. Also this coating type gives the minimum stress intensity factors for each crack radius at the symmetry surface. In this loading case, the stress intensity factors calculated for H and CR coatings are generally very close to each other for each crack radius.

4.3.4 Three Point Bending

In this section, coating-substrate system is loaded by applying a uniform compressive traction of magnitude σ to the surface $x = 0$ as shown in Figure 2.12. The stress, which is taken as 100 MPa, is applied to the rectangular region $-\delta < y < \delta$ and $-b < z < b$ $(\delta \cong 2.11 \, \text{mm})$. The resultant force due to this loading is

$P = 4b\delta\sigma$. The medium is supported by rollers at $y = \pm l$, $x = h_1 + h_2$. The computed results are presented in Figures 4.35-4.42 and tabulated in Table 4.6.

Table 4.5 Normalized mode I stress intensity factors K_{In} for an FGM coating – substrate structure subjected to fixed – grip tension.

$2\phi/\pi$	$a/h_2 = 0.2$				$a/h_2 = 0.4$			
	H	CR	LN	MR	H	CR	LN	MR
1.0000	1.0371	1.0369	1.0203	0.9933	1.0375	1.0387	1.0023	0.9761
0.9375	1.0372	1.0374	1.0214	0.9946	1.0376	1.0387	1.0024	0.9759
0.8750	1.0370	1.0377	1.0219	0.9957	1.0383	1.0395	1.0034	0.9770
0.8125	1.0377	1.0378	1.0223	0.9963	1.0396	1.0407	1.0057	0.9790
0.7500	1.0399	1.0405	1.0254	0.9994	1.0415	1.0424	1.0091	0.9821
0.6875	1.0430	1.0440	1.0296	1.0036	1.0437	1.0446	1.0129	0.9858
0.6250	1.0458	1.0468	1.0332	1.0077	1.0469	1.0480	1.0179	0.9902
0.5625	1.0493	1.0499	1.0375	1.0122	1.0506	1.0518	1.0240	0.9961
0.5000	1.0543	1.0544	1.0441	1.0186	1.0556	1.0565	1.0316	1.0032
0.4375	1.0609	1.0609	1.0522	1.0273	1.0620	1.0630	1.0411	1.0124
0.3750	1.0682	1.0692	1.0617	1.0376	1.0697	1.0708	1.0522	1.0236
0.3125	1.0778	1.0789	1.0732	1.0498	1.0797	1.0808	1.0660	1.0374
0.2500	1.0909	1.0911	1.0875	1.0651	1.0924	1.0935	1.0823	1.0543
0.1875	1.1076	1.1078	1.1065	1.0863	1.1087	1.1098	1.1028	1.0764
0.1250	1.1271	1.1282	1.1295	1.1121	1.1296	1.1307	1.1288	1.1048
0.0000	1.1787	1.1787	1.1857	1.1916	1.1815	1.1830	1.1925	1.1977
$2\phi/\pi$	$a/h_2 = 0.6$				$a/h_2 = 0.8$			
	H	CR	LN	MR	H	CR	LN	MR
1.0000	1.0421	1.0385	0.9833	0.9617	1.0444	1.0368	0.9651	0.9503
0.9375	1.0426	1.0391	0.9843	0.9628	1.0443	1.0371	0.9653	0.9503
0.8750	1.0430	1.0399	0.9856	0.9636	1.0450	1.0391	0.9672	0.9518
0.8125	1.0439	1.0414	0.9878	0.9652	1.0464	1.0424	0.9707	0.9546
0.7500	1.0457	1.0436	0.9920	0.9688	1.0480	1.0459	0.9746	0.9572
0.6875	1.0481	1.0466	0.9971	0.9732	1.0500	1.0498	0.9800	0.9611
0.6250	1.0508	1.0498	1.0027	0.9778	1.0531	1.0544	0.9870	0.9666
0.5625	1.0544	1.0541	1.0100	0.9837	1.0569	1.0592	0.9958	0.9737
0.5000	1.0591	1.0592	1.0191	0.9918	1.0616	1.0643	1.0058	0.9816
0.4375	1.0655	1.0658	1.0300	1.0018	1.0678	1.0707	1.0175	0.9912
0.3750	1.0730	1.0736	1.0425	1.0130	1.0760	1.0788	1.0320	1.0038
0.3125	1.0827	1.0835	1.0577	1.0274	1.0861	1.0888	1.0493	1.0193
0.2500	1.0956	1.0964	1.0765	1.0460	1.0986	1.1012	1.0696	1.0380
0.1875	1.1124	1.1135	1.0998	1.0696	1.1156	1.1181	1.0950	1.0627
0.1250	1.1327	1.1340	1.1270	1.0985	1.1366	1.1391	1.1248	1.0935
0.0000	1.1845	1.1862	1.1958	1.2003	1.1886	1.1914	1.1989	1.2024

Table 4.6 Normalized mode I stress intensity factors K_{In} for an FGM coating – substrate structure subjected to three point bending.

	$a/h_2 = 0.2$				$a/h_2 = 0.4$			
$2\phi/\pi$	H	CR	LN	MR	H	CR	LN	MR
1.0000	0.9270	0.9313	0.9301	0.9122	1.7601	1.7672	1.7300	1.6969
0.9375	0.9274	0.9315	0.9306	0.9132	1.7610	1.7681	1.7310	1.6980
0.8750	0.9287	0.9329	0.9320	0.9147	1.7644	1.7713	1.7356	1.7022
0.8125	0.9308	0.9350	0.9349	0.9173	1.7708	1.7778	1.7435	1.7094
0.7500	0.9339	0.9381	0.9386	0.9208	1.7793	1.7864	1.7541	1.7195
0.6875	0.9377	0.9420	0.9433	0.9258	1.7901	1.7971	1.7680	1.7326
0.6250	0.9427	0.9469	0.9492	0.9320	1.8036	1.8106	1.7850	1.7489
0.5625	0.9489	0.9530	0.9561	0.9393	1.8200	1.8272	1.8056	1.7688
0.5000	0.9560	0.9603	0.9648	0.9482	1.8399	1.8472	1.8297	1.7921
0.4375	0.9650	0.9692	0.9753	0.9589	1.8625	1.8699	1.8579	1.8197
0.3750	0.9753	0.9797	0.9874	0.9717	1.8888	1.8963	1.8909	1.8526
0.3125	0.9876	0.9920	1.0019	0.9873	1.9201	1.9277	1.9291	1.8908
0.2500	1.0029	1.0074	1.0194	1.0060	1.9570	1.9649	1.9735	1.9361
0.1875	1.0221	1.0267	1.0411	1.0294	2.0019	2.0099	2.0272	1.9920
0.1250	1.0444	1.0490	1.0656	1.0569	2.0530	2.0611	2.0879	2.0580
0.0000	1.0991	1.1037	1.1274	1.1412	2.1751	2.1838	2.2337	2.2601
	$a/h_2 = 0.6$				$a/h_2 = 0.8$			
$2\phi/\pi$	H	CR	LN	MR	H	CR	LN	MR
1.0000	2.5038	2.5038	2.4046	2.3691	3.1520	3.1373	2.9658	2.9434
0.9375	2.5061	2.5064	2.4073	2.3723	3.1550	3.1418	2.9702	2.9473
0.8750	2.5129	2.5137	2.4162	2.3801	3.1656	3.1566	2.9840	2.9593
0.8125	2.5240	2.5259	2.4307	2.3931	3.1842	3.1807	3.0072	2.9797
0.7500	2.5395	2.5428	2.4511	2.4117	3.2091	3.2119	3.0391	3.0082
0.6875	2.5597	2.5642	2.4776	2.4358	3.2414	3.2501	3.0804	3.0453
0.6250	2.5853	2.5909	2.5103	2.4656	3.2814	3.2950	3.1319	3.0908
0.5625	2.6153	2.6222	2.5494	2.5015	3.3293	3.3463	3.1932	3.1457
0.5000	2.6505	2.6581	2.5946	2.5436	3.3849	3.4037	3.2646	3.2104
0.4375	2.6919	2.7000	2.6472	2.5931	3.4492	3.4688	3.3471	3.2854
0.3750	2.7398	2.7486	2.7084	2.6506	3.5228	3.5427	3.4413	3.3720
0.3125	2.7948	2.8041	2.7777	2.7176	3.6073	3.6270	3.5489	3.4725
0.2500	2.8585	2.8686	2.8575	2.7963	3.7038	3.7233	3.6714	3.5893
0.1875	2.9346	2.9452	2.9518	2.8913	3.8168	3.8365	3.8147	3.7292
0.1250	3.0198	3.0312	3.0577	3.0022	3.9430	3.9631	3.9730	3.8917
0.0000	3.2215	3.2344	3.3101	3.3468	4.2352	4.2564	4.3504	4.3961

In Figures 4.35-4.42, the variation of the normalized stress intensity factors are plotted with respect to normalized polar angle for each FGM coating type. The lowest stress intensity factors are computed at the symmetry surface. MR coating

gives the minimum stress intensity factors for all crack dimensions at the symmetry surface. The trends are generally similar to those observed for the other loading cases.

4.4 Transient Thermal Loading

In this section, thermal fracture analysis of the FGM coatings is carried out. The composite medium is initially assumed to be at a high processing temperature of 1273 K. Then, the coating – substrate system is left in an environment whose temperature is $T_0 = 300$ K. It is assumed that at all the surfaces except the surface at $x = h_1 + h_2$, there is free convection with a convection coefficient of $h = 5$ W/(m^2 K). At the surface, $x = h_1 + h_2$, there is forced convection and the convection coefficient is $h = 10000$ W/(m^2 K). The thermal boundary conditions are shown in Figure 2.13. In the analysis, the material properties computed at the mid temperature $T_m = 786.5$ K are used. These thermomechanical parameters are given in Chapter 2. The results are presented in Figures 4.43-4.58 and in Tables 4.7-4.8.

In Figures 4.43, 4.47, 4.51 and 4.55, the temperature of the deepest point on the crack front $(\phi = \pi/2)$ is plotted with respect to normalized time for $a/h_2 = 0.2$, $a/h_2 = 0.3$, $a/h_2 = 0.4$ and $a/h_2 = 0.6$, respectively. Double scales are used in these figures in order to clearly present the temperature variations for short times. As expected the temperature decreases from the initial value 1273 K to 300 K and reaches to its steady – state value at about $\tau = 50$ for each crack radius. The temperature decrease starts with a sudden drop for each crack dimension and as expected the amount of this drop is less for larger crack radius.

In the computations it is observed that the semi – circular crack remains fully open only for a short time interval as the composite system starts cooling. The variation of the normalized stress intensity factors at the deepest point with respect to normalized time is shown in Figure 4.44 for $a/h_2 = 0.2$. Again, a double time

scale is used in this figure. The stress intensity factors are zero initially. Then, they increase and go through a maximum in a short time period. These maximum values are about 0.6, 0.57, 0.36 and 0.37 for H, CR, LN and MR coatings, respectively. After reaching these maximum values, the stress intensity factors start to decrease. Crack closure is found to begin at the deepest point for H, CR and LN coatings at $\tau \cong 8.9,\ 6.6$ and 1.37, respectively and at the free surface for MR coating at $\tau \cong 1.15$. It can be seen in Figure 4.44 that the stress intensity factors of LN and MR coatings are close to each other. It is also found that crack contact occurrence time for MR and LN coatings is shorter than those of H and CR coatings. The curves given for the coatings in Figure 4.44 are valid only up to the point of closure. During the relatively short time interval when the crack is fully open, maximum stress intensity factor is calculated as 0.6 for H coating at $\tau \cong 0.43$. As a result, it can be concluded that material gradation causes a decrease in the amplitude of the transient stress intensity factors. Minimum peak occurs for LN coating.

Figure 4.48 shows the transient stress intensity factors for $a/h_2 = 0.3$. Crack closure in this case begins at the deepest point for H, CR and LN coatings at $\tau \cong 8.0,\ 5.7$ and 1.37, respectively and at the free surface for MR coating at $\tau \cong 1.2$. If these crack closure times are compared with the ones computed for $a/h_2 = 0.2$, it can be seen that crack closure times decrease for H and CR coatings, does not change for LN coating and increases a little for the MR coating. The peak values for the stress intensity factors are about 0.53, 0.49, 0.29 and 0.32 for H, CR, LN and MR coatings, respectively. After reaching these maximum values, the stress intensity factors start to decrease and approach to their steady state value at $\tau \cong 50$. Again, the curves given for the coatings in Figure 4.48 are valid only up to the point of closure.

The stress intensity factors for $a/h_2 = 0.4$ are given in Figure 4.52. Crack closure begins at the deepest point for H, CR and LN coatings at $\tau \cong 7.0,\ 4.8$ and 1.37, respectively and at the free surface for MR coating at

$\tau \cong 1.25$. The peak values are about $0.45, 0.4, 0.24$ and 0.28 for H, CR, LN and MR coatings, respectively. After reaching these maximum values, the stress intensity factors again start to decrease and approach to their steady state value at $\tau \cong 50$.

The results for $a/h_2 = 0.6$ are given in Figure 4.56. In this case, crack closure begins at the deepest point for H, CR and LN coatings at $\tau \cong 5.1, 3.0$ and 1.56, respectively and at the free surface for MR coating at $\tau \cong 1.33$. The shortest crack closure times for H and CR coatings are found for this crack dimension. The maximum values are calculated as $0.32, 0.25, 0.18$ and 0.23 for H, CR, LN and MR coatings, respectively. For this crack radius, we also observe that material property gradation causes a decrease in the amplitude of the stress intensity factors.

The distribution of the stress intensity factors at two given points in time are depicted in Figures 4.45-4.46 for $a/h_2 = 0.2$, Figures 4.49-4.50 for $a/h_2 = 0.3$, Figures 4.53-4.54 for $a/h_2 = 0.4$ and Figures 4.57-4.58 for $a/h_2 = 0.6$. Also, results related to these figures are tabulated in Tables 4.7 and 4.8. It can be observed that the semi circular crack is fully open at $\tau = 0.67$ in all coatings and stress intensity factors are larger in H coating for each crack dimension. There is crack closure at steady state $(\tau = 67)$ in Figures 4.46, 4.50, 4.54 and 4.58. Hence, the results given in these figure are not valid and the problem has to be remodeled by taking into account the crack closure. However, these results can still be useful if they are used to obtain the solution for given arbitrary loads by using the principle of superposition provided that the resultant stress intensity factor is positive.

Table 4.7 Normalized mode I stress intensity factors K_{In} for an FGM plate subjected to transient thermal load at $\tau = 0.67$.

$2\phi/\pi$	$a/h_2 = 0.3$				$a/h_2 = 0.6$			
	H	CR	LN	MR	H	CR	LN	MR
1.0000	0.4891	0.4292	0.1695	0.1976	0.2997	0.2094	0.1268	0.1742
0.9375	0.4901	0.4303	0.1699	0.1977	0.3014	0.2112	0.1271	0.1745
0.8750	0.4930	0.4335	0.1709	0.1981	0.3065	0.2167	0.1279	0.1754
0.8125	0.4977	0.4389	0.1726	0.1988	0.3149	0.2259	0.1294	0.1769
0.7500	0.5044	0.4463	0.1750	0.1997	0.3267	0.2388	0.1316	0.1789
0.6875	0.5128	0.4558	0.1782	0.2009	0.3417	0.2555	0.1345	0.1814
0.6250	0.5231	0.4672	0.1823	0.2023	0.3600	0.2760	0.1382	0.1846
0.5625	0.5351	0.4806	0.1872	0.2039	0.3813	0.3001	0.1430	0.1882
0.5000	0.5489	0.4958	0.1932	0.2057	0.4057	0.3278	0.1488	0.1923
0.4375	0.5643	0.5129	0.2004	0.2076	0.4329	0.3587	0.1560	0.1968
0.3750	0.5816	0.5317	0.2089	0.2097	0.4628	0.3926	0.1647	0.2017
0.3125	0.6007	0.5525	0.2190	0.2120	0.4951	0.4290	0.1755	0.2070
0.2500	0.6219	0.5754	0.2311	0.2143	0.5298	0.4677	0.1887	0.2125
0.1875	0.6461	0.6011	0.2456	0.2167	0.5671	0.5088	0.2053	0.2182
0.1250	0.6724	0.6288	0.2626	0.2188	0.6059	0.5513	0.2258	0.2237
0.0000	0.7331	0.6920	0.3080	0.2292	0.6919	0.6438	0.2885	0.2452

Table 4.8 Normalized mode I stress intensity factors K_{In} for an FGM plate subjected to transient thermal load at $\tau = 67$.

$2\phi/\pi$	$a/h_2 = 0.3$				$a/h_2 = 0.6$			
	H	CR	LN	MR	H	CR	LN	MR
1.0000	-0.3875	-0.4295	-0.4030	-0.2854	-0.4260	-0.4321	-0.2451	-0.1537
0.9375	-0.3875	-0.4296	-0.4038	-0.2861	-0.4258	-0.4324	-0.2465	-0.1547
0.8750	-0.3876	-0.4296	-0.4062	-0.2885	-0.4252	-0.4332	-0.2506	-0.1576
0.8125	-0.3877	-0.4298	-0.4102	-0.2923	-0.4243	-0.4343	-0.2575	-0.1625
0.7500	-0.3879	-0.4301	-0.4158	-0.2978	-0.4230	-0.4356	-0.2671	-0.1694
0.6875	-0.3882	-0.4305	-0.4229	-0.3050	-0.4217	-0.4370	-0.2794	-0.1784
0.6250	-0.3887	-0.4310	-0.4316	-0.3139	-0.4204	-0.4383	-0.2942	-0.1895
0.5625	-0.3893	-0.4318	-0.4418	-0.3246	-0.4193	-0.4395	-0.3117	-0.2029
0.5000	-0.3902	-0.4329	-0.4536	-0.3374	-0.4184	-0.4406	-0.3317	-0.2188
0.4375	-0.3915	-0.4344	-0.4670	-0.3523	-0.4180	-0.4419	-0.3541	-0.2374
0.3750	-0.3933	-0.4365	-0.4821	-0.3697	-0.4182	-0.4435	-0.3789	-0.2590
0.3125	-0.3958	-0.4394	-0.4989	-0.3901	-0.4193	-0.4456	-0.4062	-0.2841
0.2500	-0.3993	-0.4433	-0.5176	-0.4139	-0.4215	-0.4487	-0.4359	-0.3133
0.1875	-0.4043	-0.4489	-0.5389	-0.4424	-0.4255	-0.4535	-0.4685	-0.3480
0.1250	-0.4104	-0.4558	-0.5620	-0.4760	-0.4308	-0.4594	-0.5030	-0.3890
0.0000	-0.4267	-0.4741	-0.6121	-0.5651	-0.4461	-0.4758	-0.5742	-0.4977

4.5 Figures
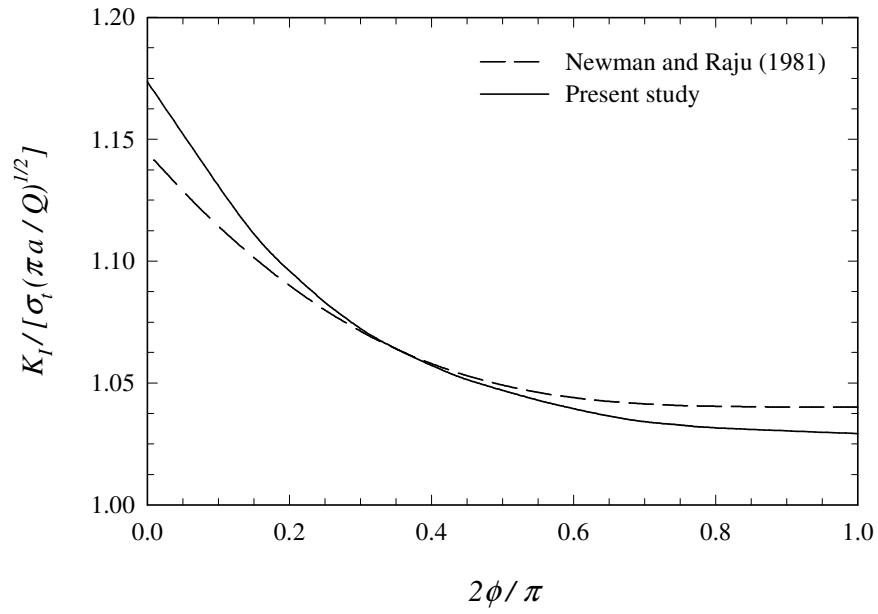
Figure 4.1 Comparisons to Newman and Raju equation for uniform tension, $a/h_2 = 0.2$
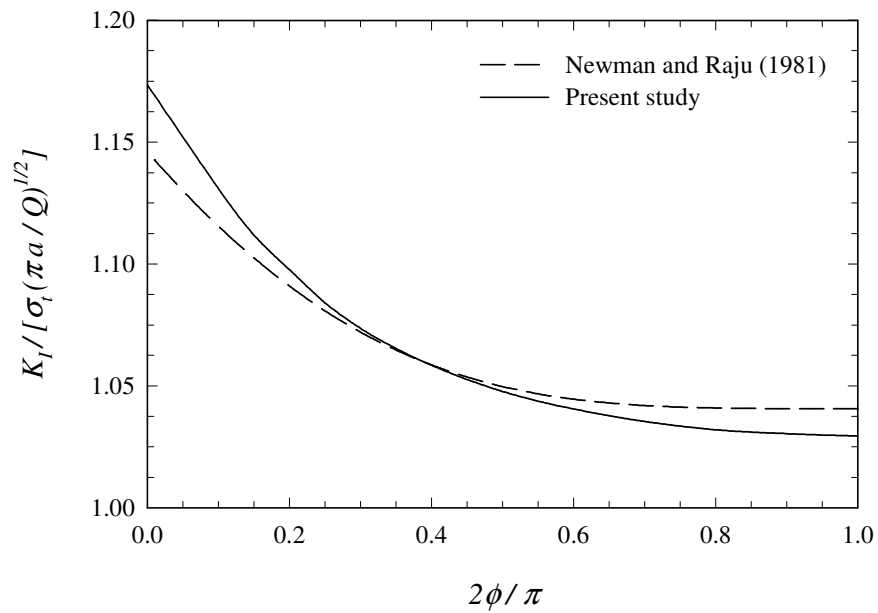
Figure 4.2 Comparisons to Newman and Raju equation for uniform tension, $a/h_2 = 0.4$
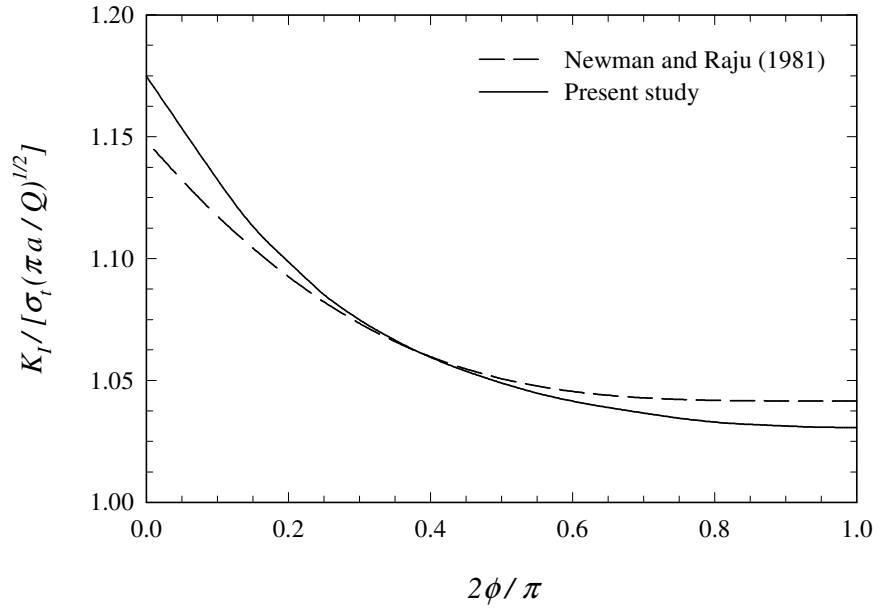
Figure 4.3 Comparisons to Newman and Raju equation for uniform tension, $a/h_2 = 0.6$
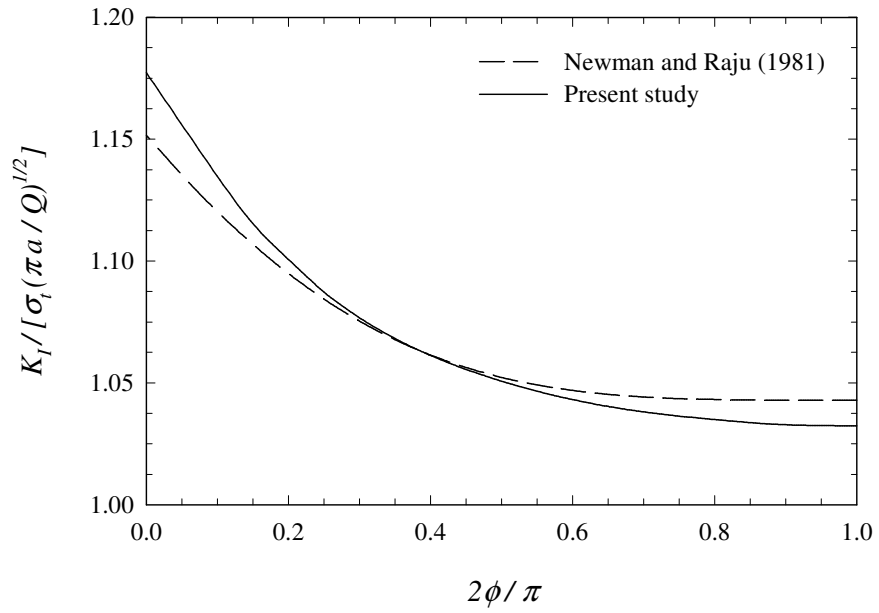
Figure 4.4 Comparisons to Newman and Raju equation for uniform tension, $a/h_2 = 0.8$
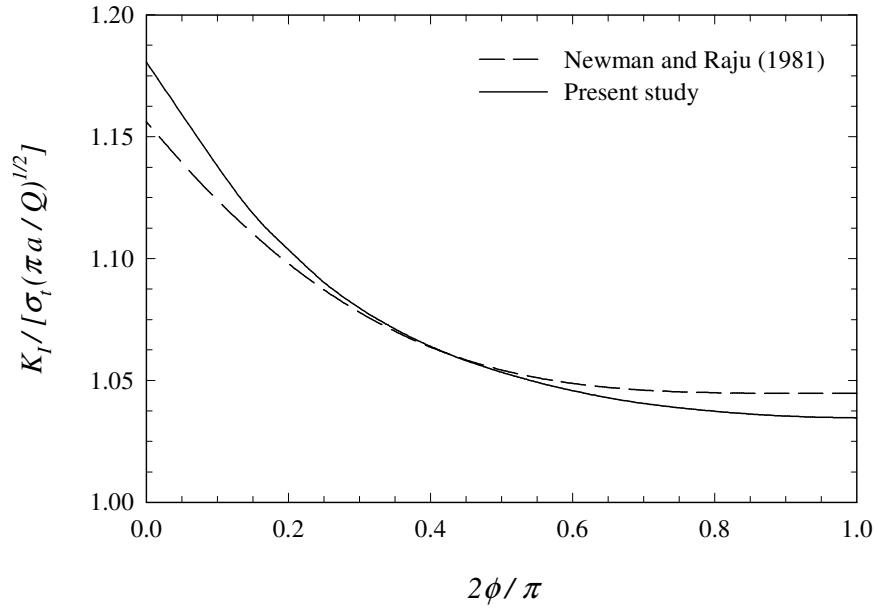
Figure 4.5 Comparisons to Newman and Raju equation for uniform tension, $a/h_2 = 1.0$
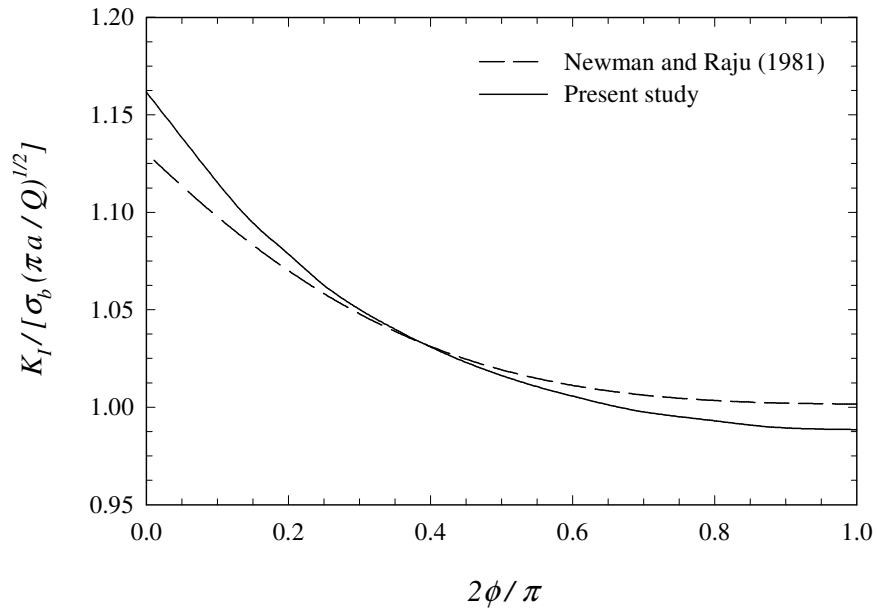
Figure 4.6 Comparisons to Newman and Raju equation for bending, $a/h_2 = 0.2$
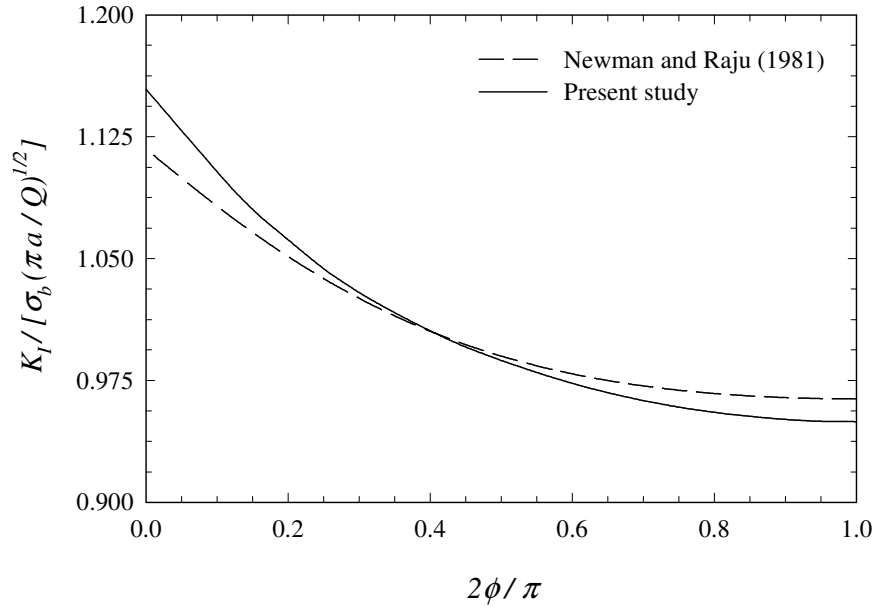
Figure 4.7 Comparisons to Newman and Raju equation for bending, $a/h_2 = 0.4$
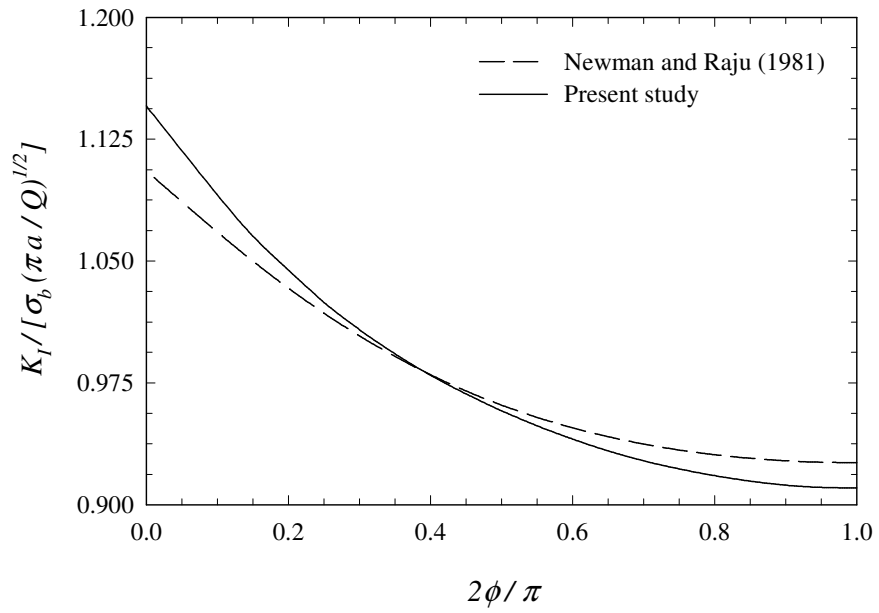
Figure 4.8 Comparisons to Newman and Raju equation for bending, $a/h_2 = 0.6$
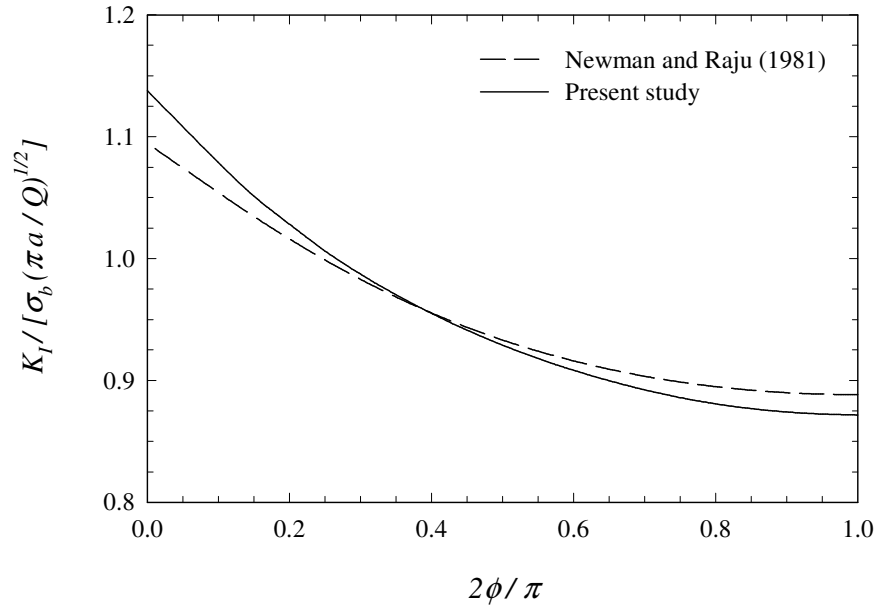
Figure 4.9 Comparisons to Newman and Raju equation for bending, $a/h_2 = 0.8$
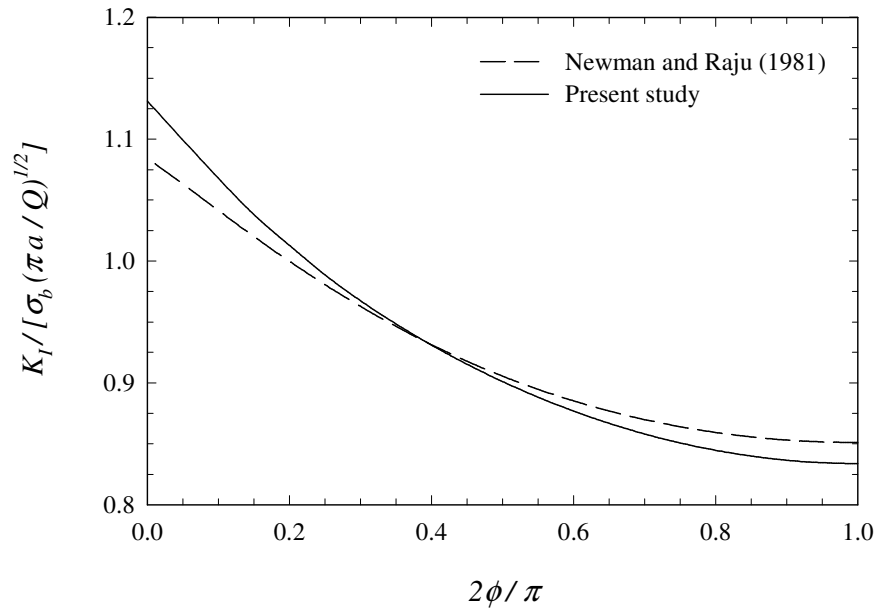
Figure 4.10 Comparisons to Newman and Raju equation for bending, $a/h_2 = 1.0$
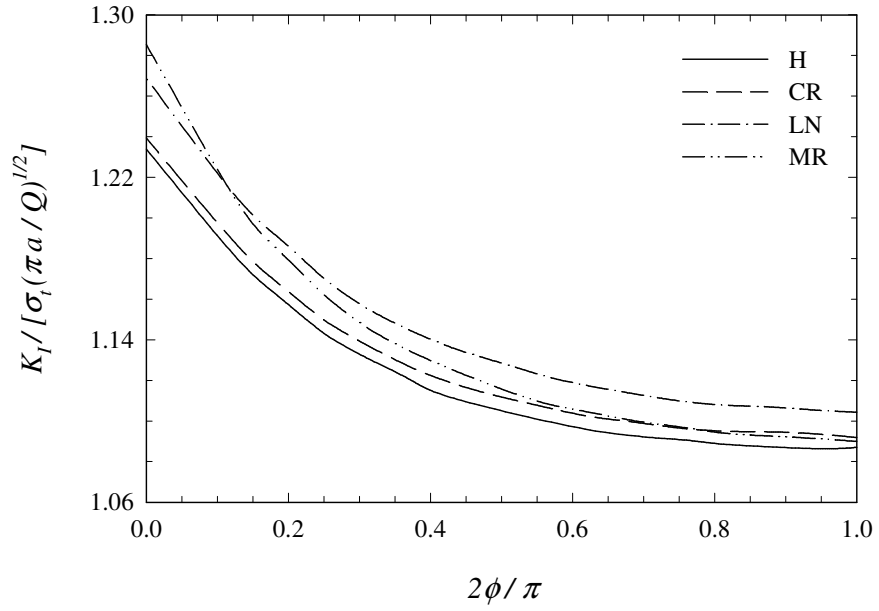
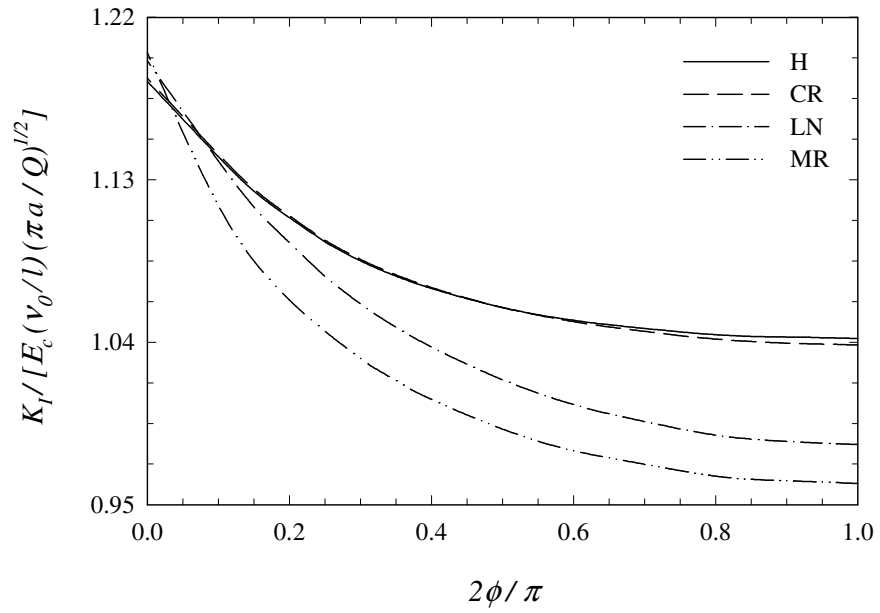Figure 4.11 Normalized mode I stress intensity factors for uniform tension, $a/h_2 = 0.1$
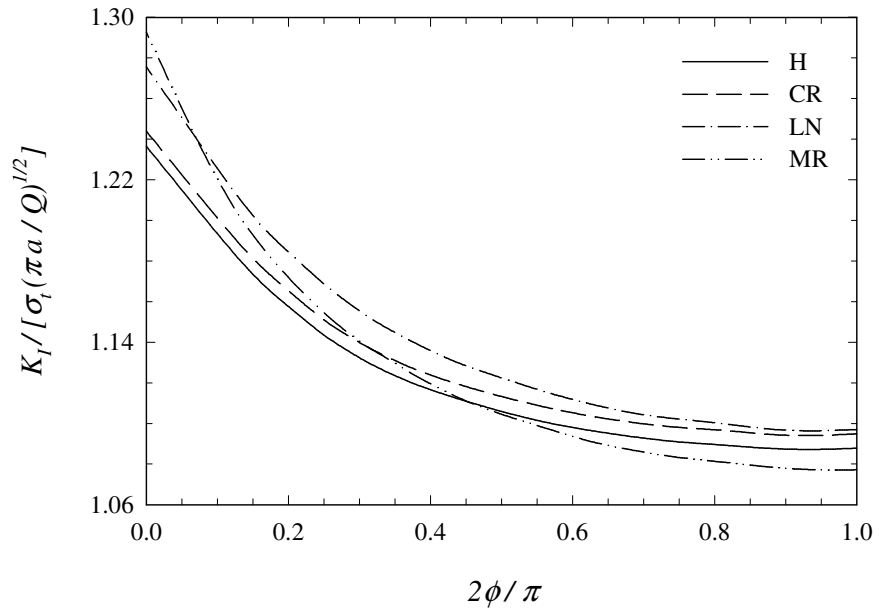
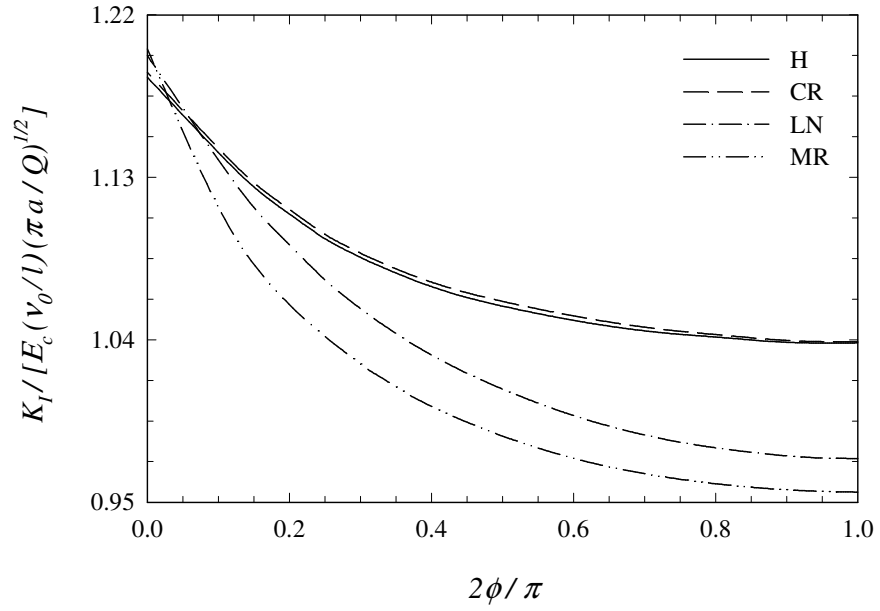Figure 4.12 Normalized mode I stress intensity factors for uniform tension, $a/h_2 = 0.2$
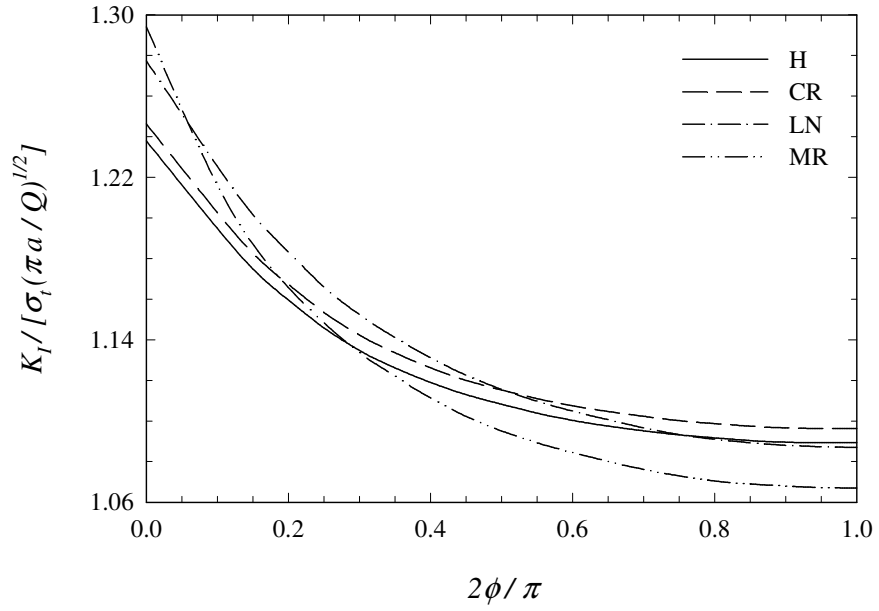
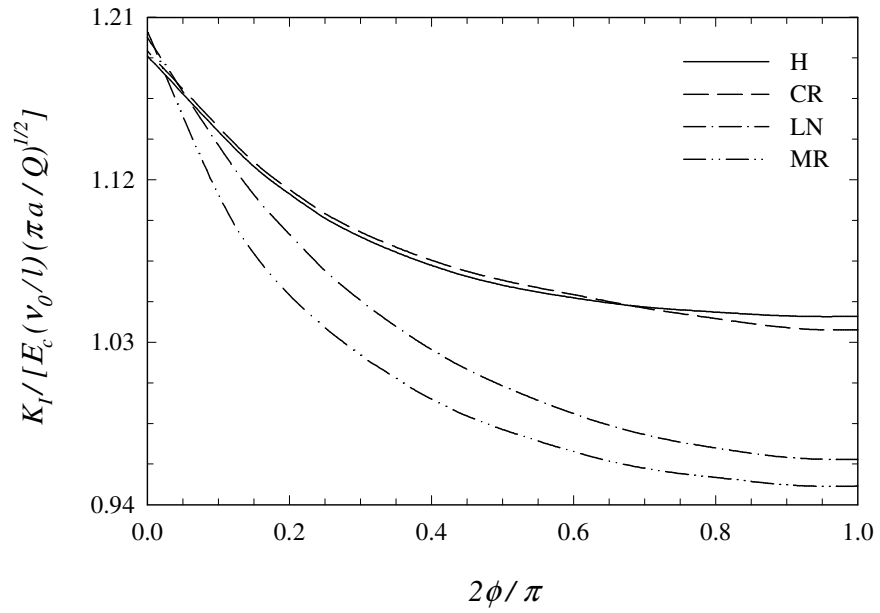Figure 4.13 Normalized mode I stress intensity factors for uniform tension, $a/h_2 = 0.3$
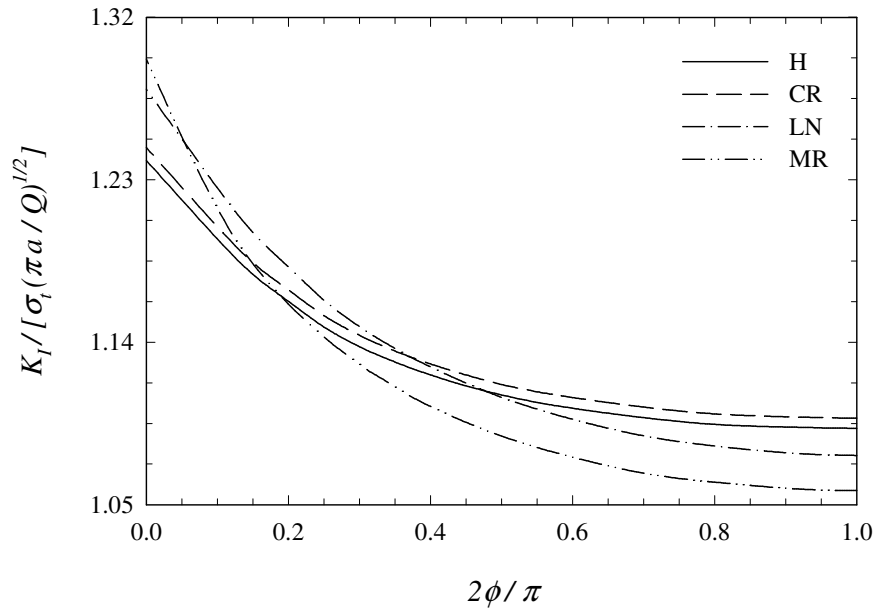
Figure 4.14 Normalized mode I stress intensity factors for uniform tension, $a/h_2 = 0.4$
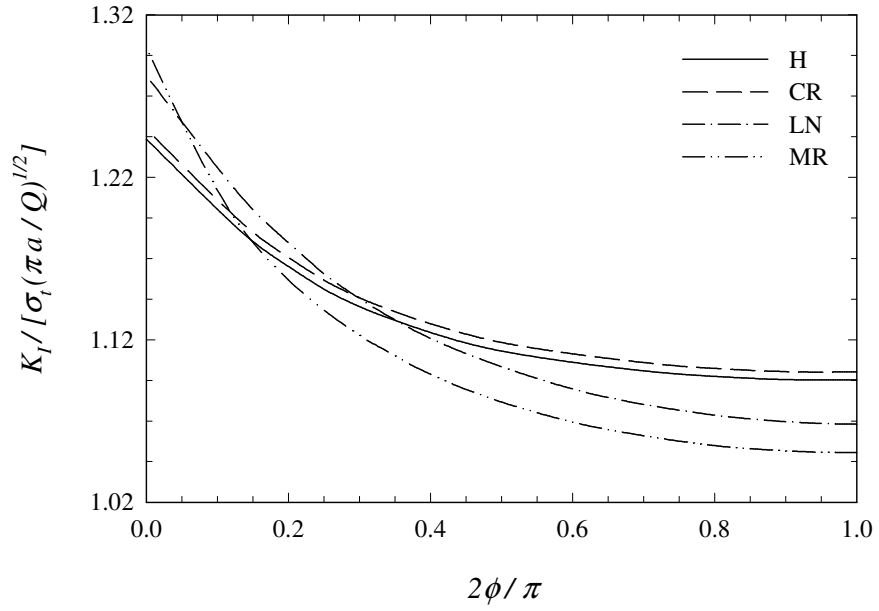
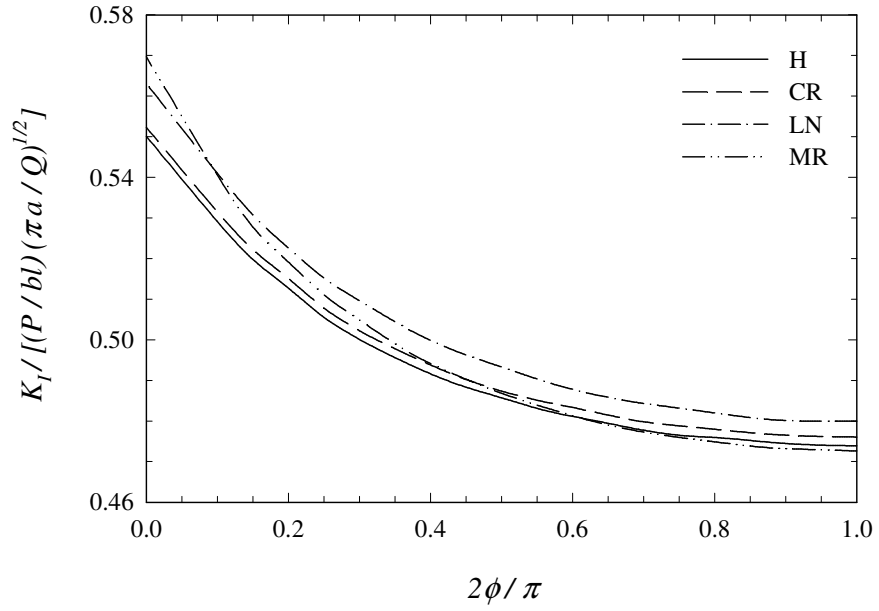Figure 4.15 Normalized mode I stress intensity factors for uniform tension, $a/h_2 = 0.5$
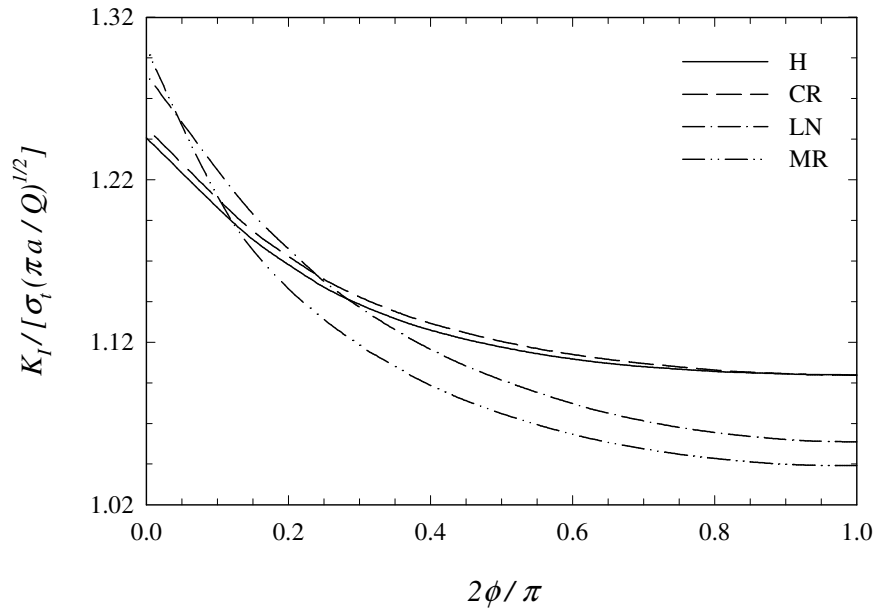
Figure 4.16 Normalized mode I stress intensity factors for uniform tension, $a/h_2 = 0.6$
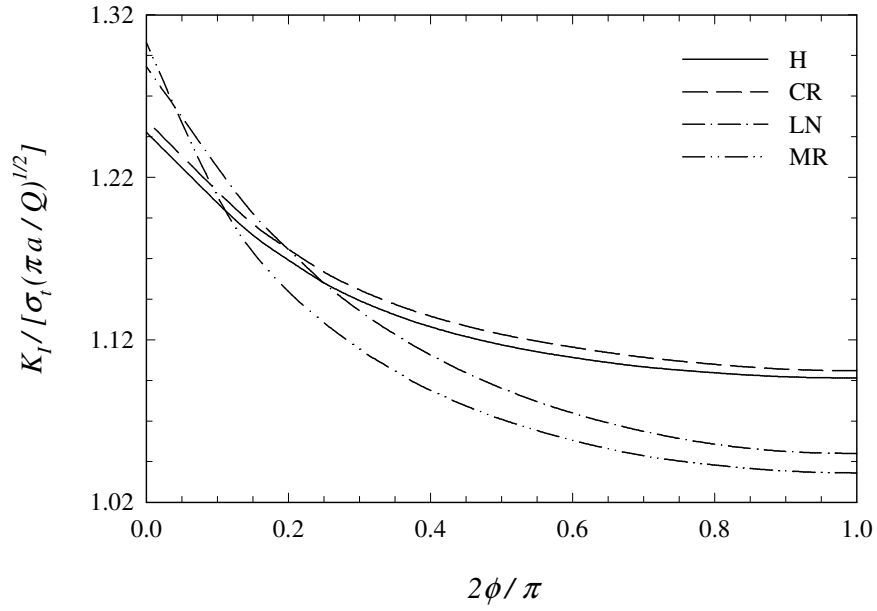
Figure 4.17 Normalized mode I stress intensity factors for uniform tension, $a/h_2 = 0.7$
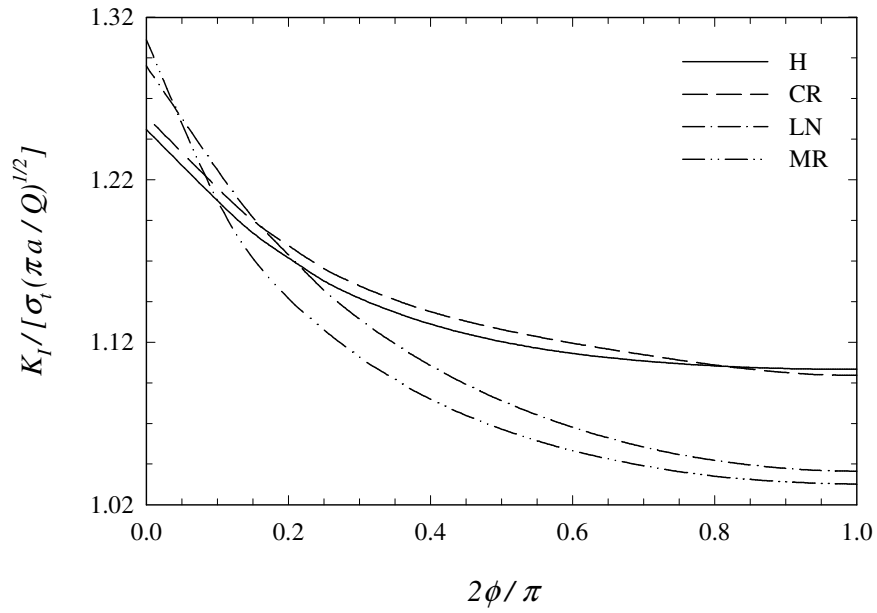
Figure 4.18 Normalized mode I stress intensity factors for uniform tension, $a/h_2 = 0.8$
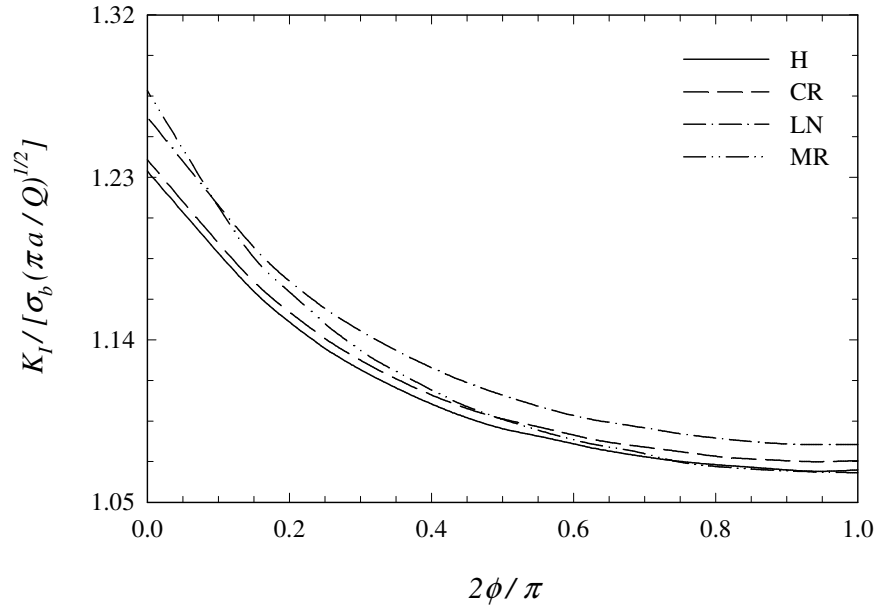
Figure 4.19 Normalized mode I stress intensity factors for bending, $a/h_2 = 0.1$
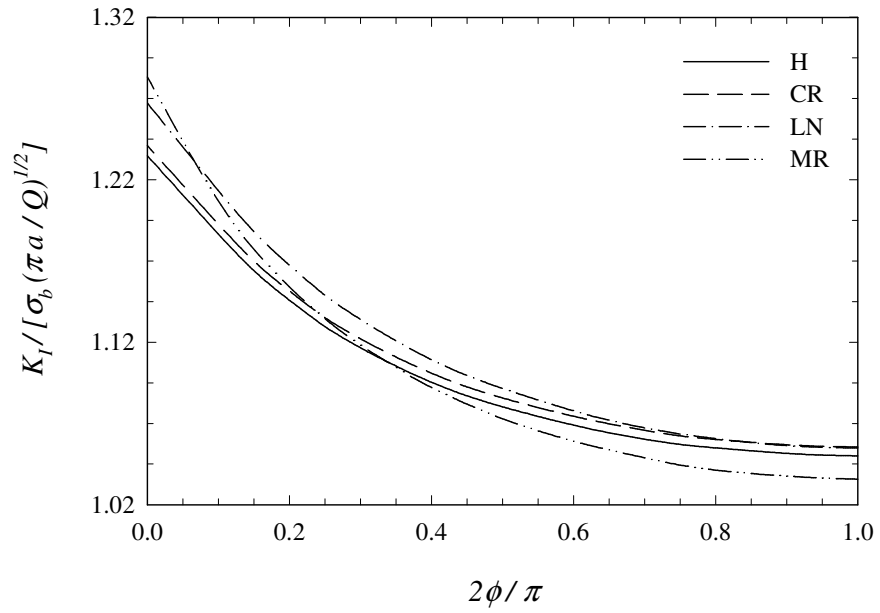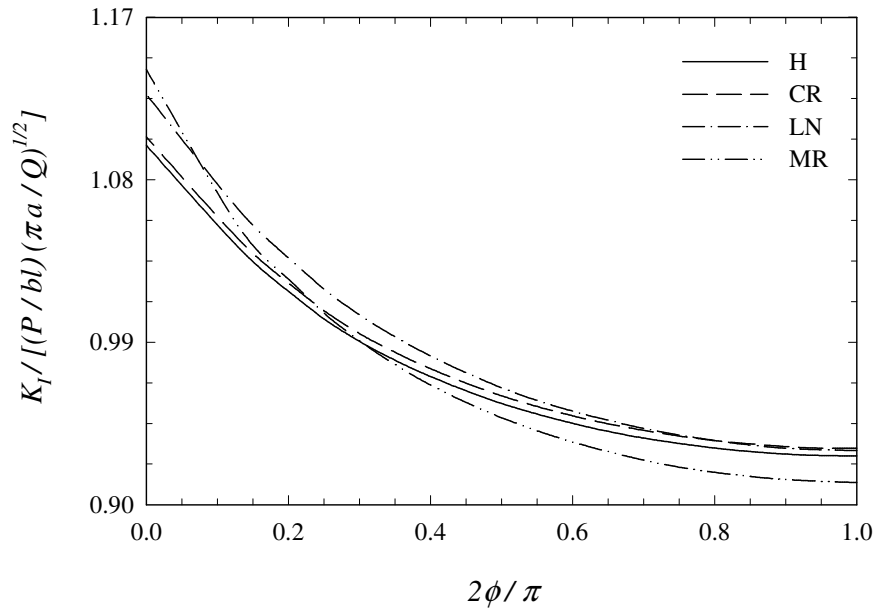

Figure 4.20 Normalized mode I stress intensity factors for bending, $a/h_2 = 0.2$
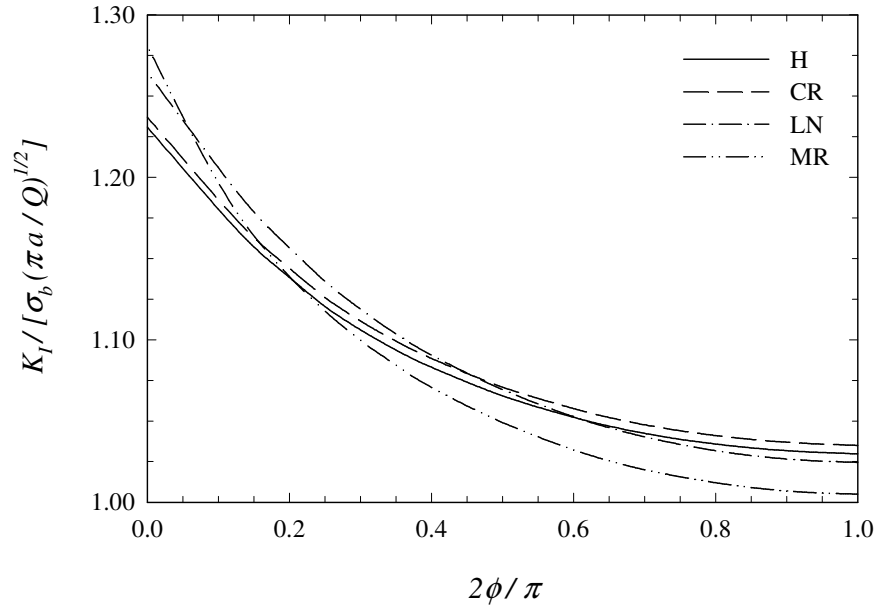
Figure 4.21 Normalized mode I stress intensity factors for bending, $a/h_2 = 0.3$
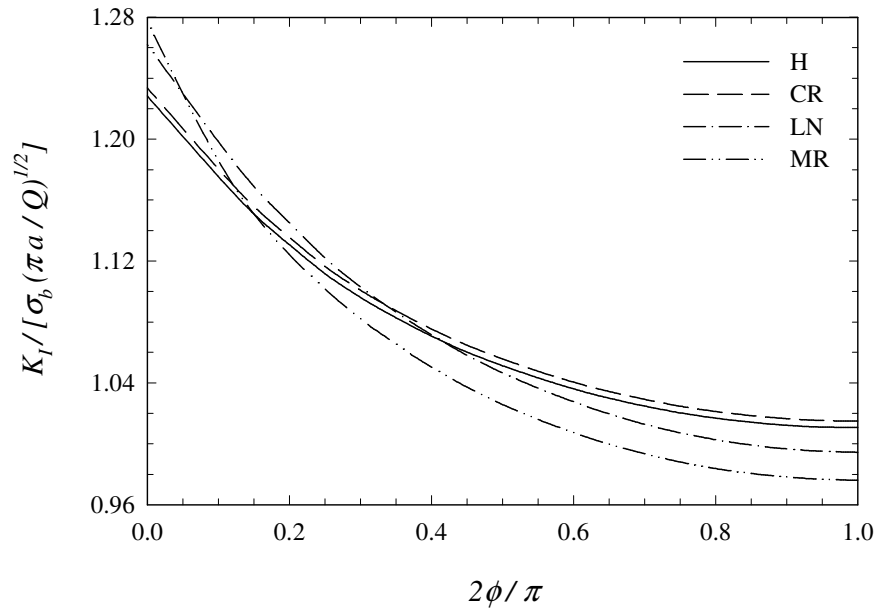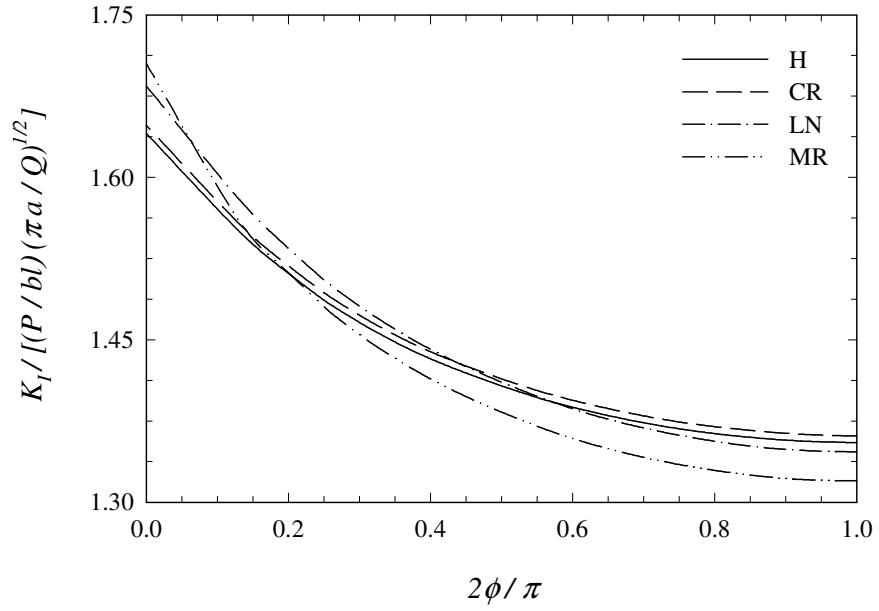

Figure 4.22 Normalized mode I stress intensity factors for bending, $a/h_2 = 0.4$
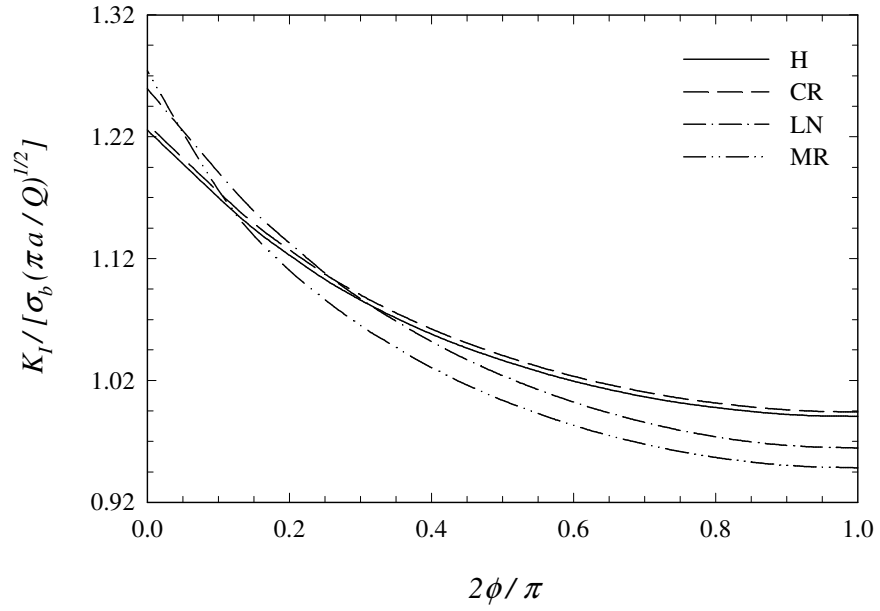
Figure 4.23 Normalized mode I stress intensity factors for bending, $a/h_2 = 0.5$
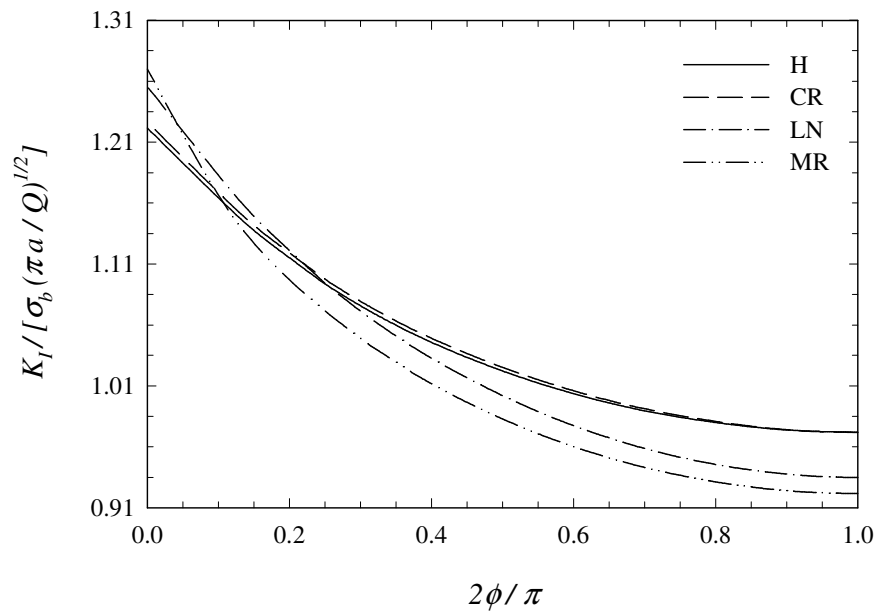
Figure 4.24 Normalized mode I stress intensity factors for bending, $a/h_2 = 0.6$
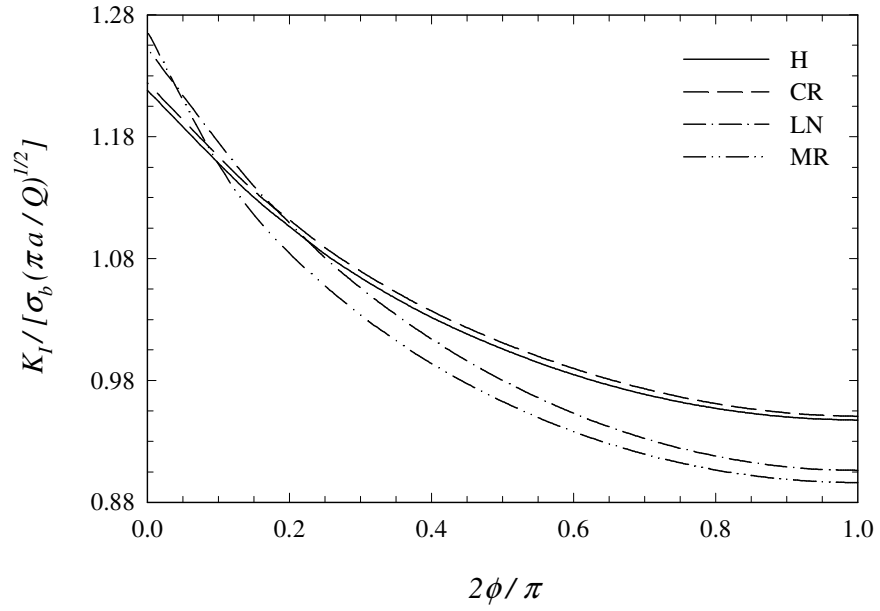
Figure 4.25 Normalized mode I stress intensity factors for bending, $a/h_2 = 0.7$
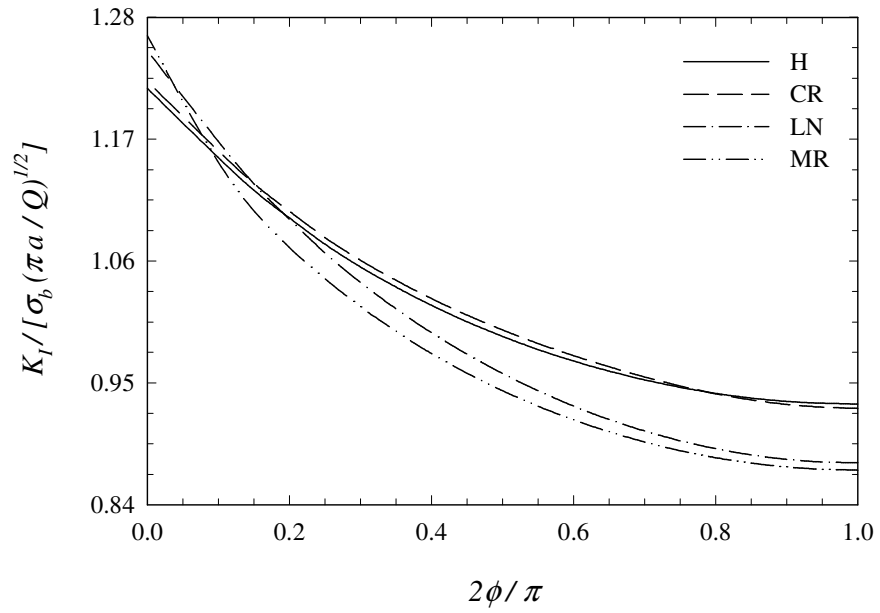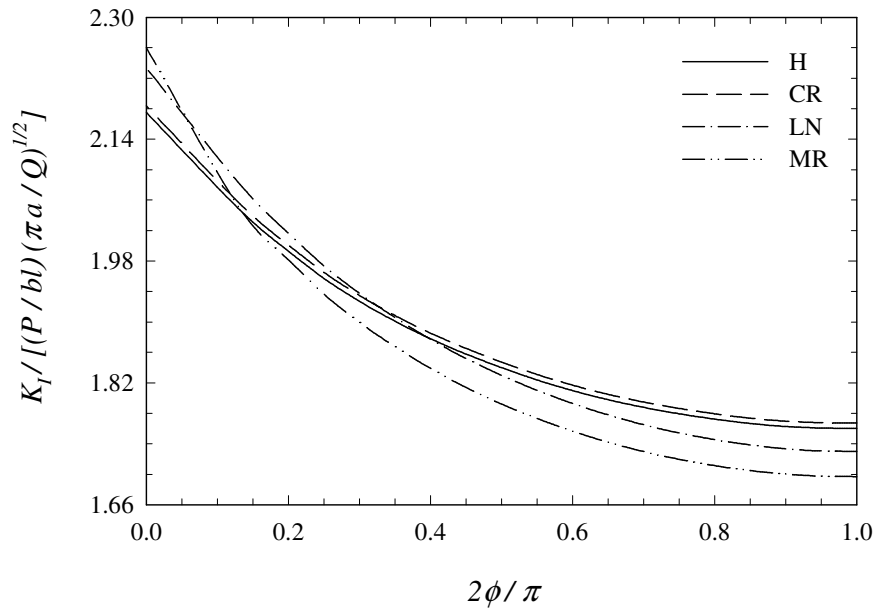

Figure 4.26 Normalized mode I stress intensity factors for bending, $a/h_2 = 0.8$
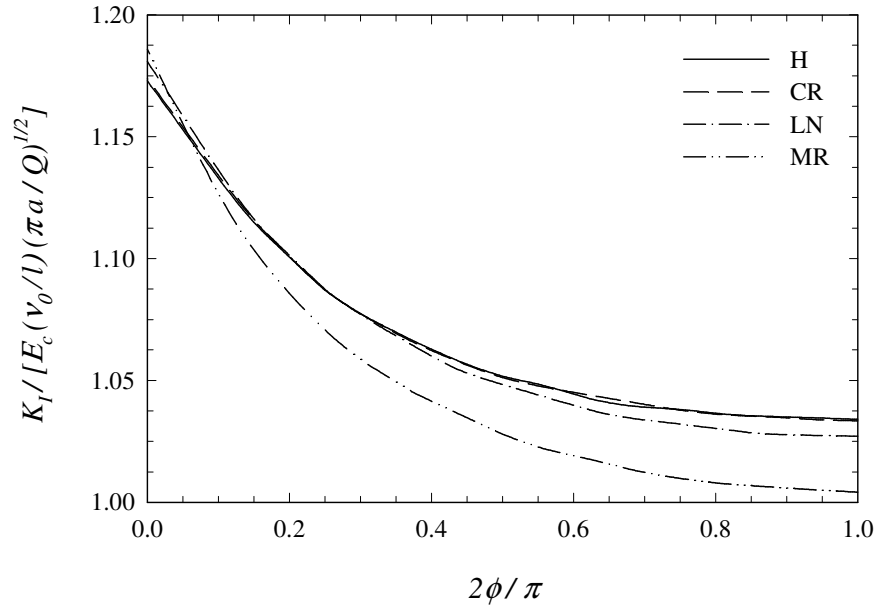
Figure 4.27 Normalized mode I stress intensity factors for fixed - grip tension, $a/h_2 = 0.1$
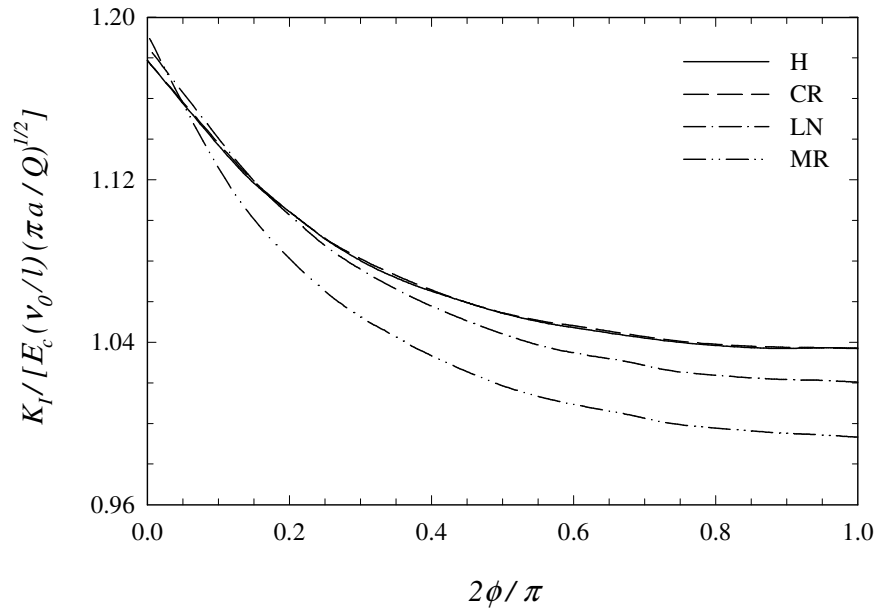
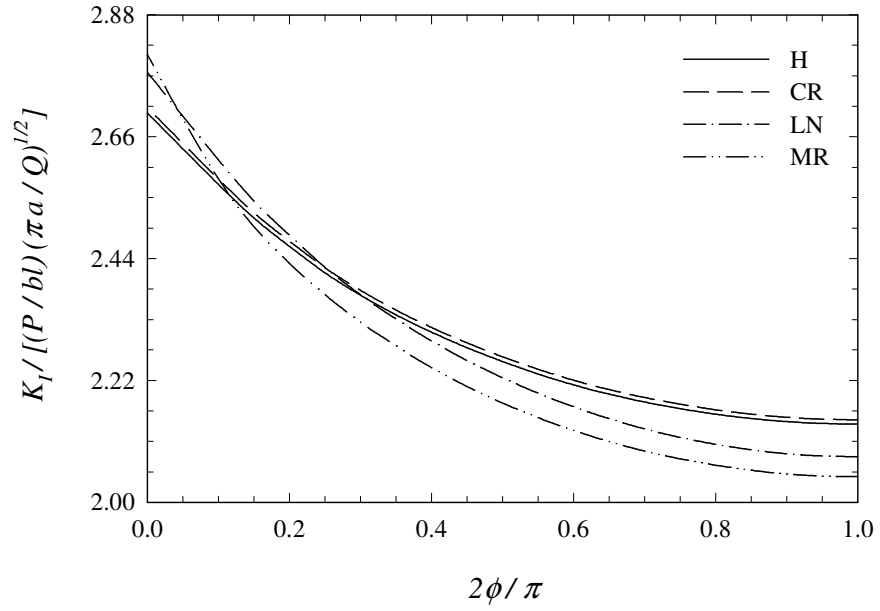Figure 4.28 Normalized mode I stress intensity factors for fixed - grip tension, $a/h_2 = 0.2$
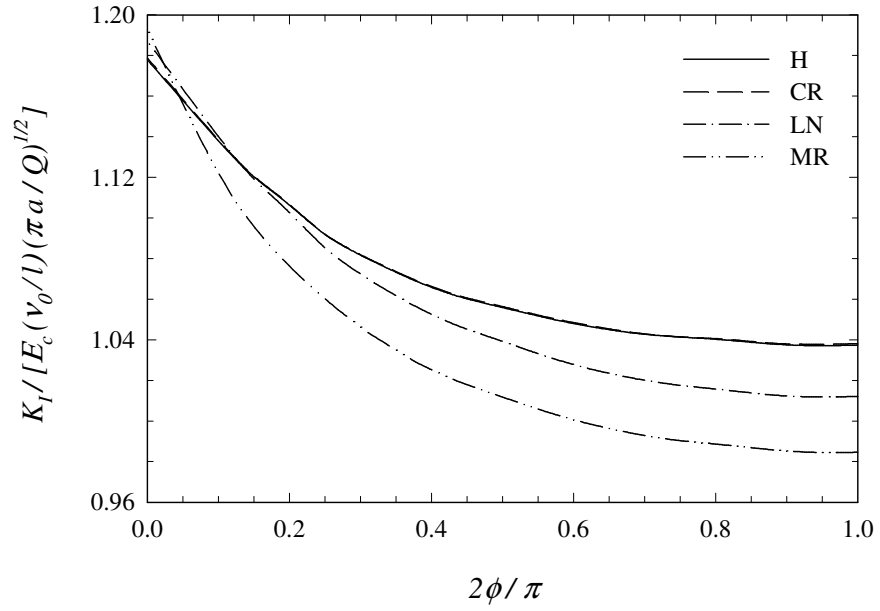
Figure 4.29 Normalized mode I stress intensity factors for fixed - grip tension, $a/h_2 = 0.3$
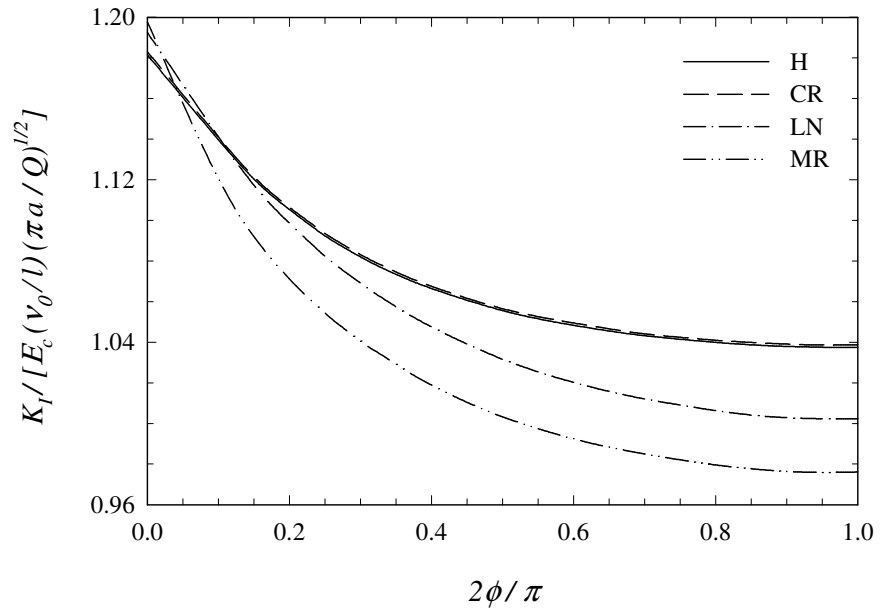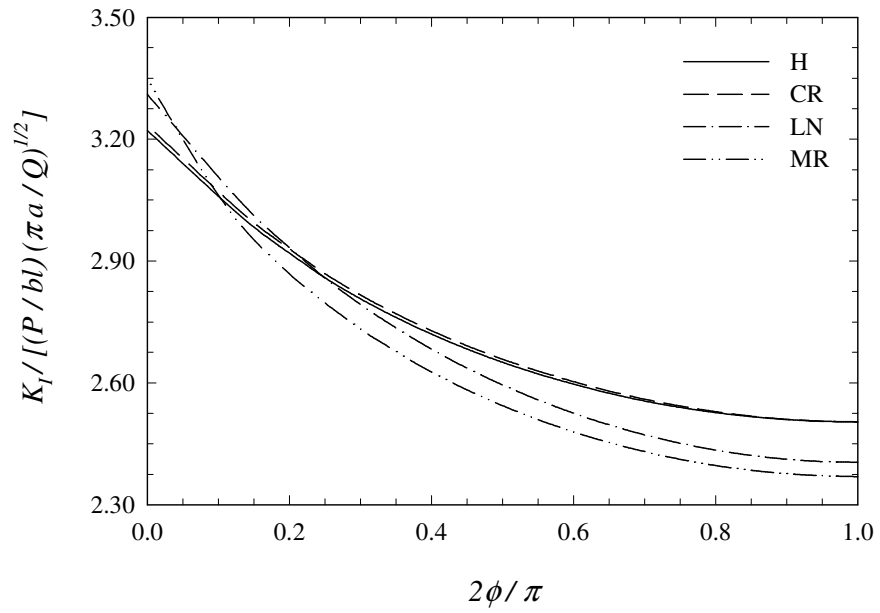

Figure 4.30 Normalized mode I stress intensity factors for fixed - grip tension, $a/h_2 = 0.4$
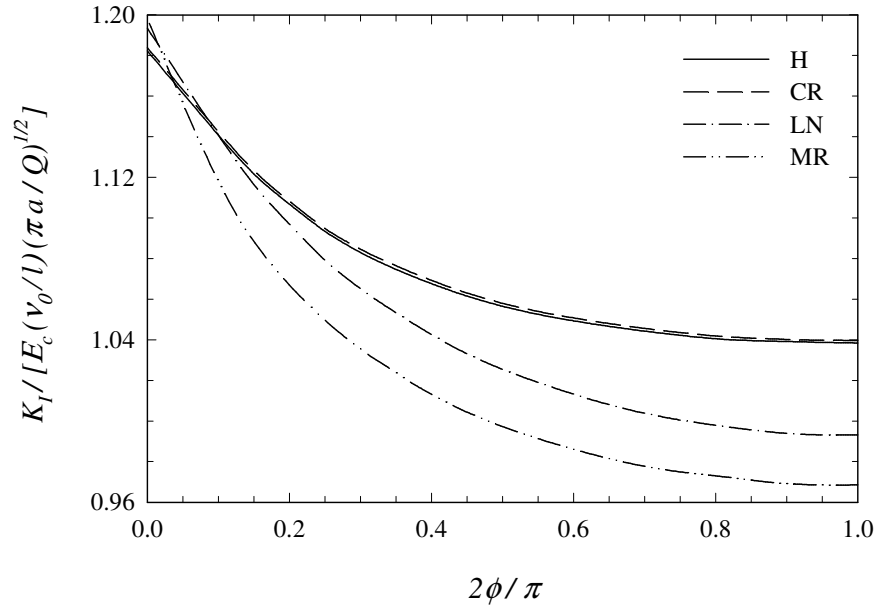
Figure 4.31 Normalized mode I stress intensity factors for fixed - grip tension, $a/h_2 = 0.5$

Figure 4.32 Normalized mode I stress intensity factors for fixed - grip tension, $a/h_2 = 0.6$

Figure 4.33 Normalized mode I stress intensity factors for fixed - grip tension, $a/h_2 = 0.7$

Figure 4.34 Normalized mode I stress intensity factors for fixed - grip tension, $a/h_2 = 0.8$

Figure 4.35 Normalized mode I stress intensity factors for three point bending, $a/h_2 = 0.1$

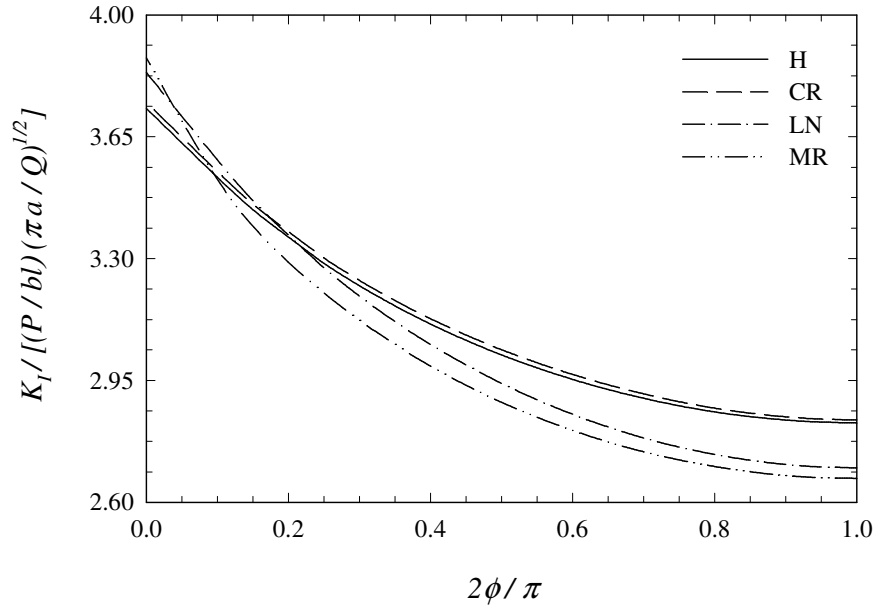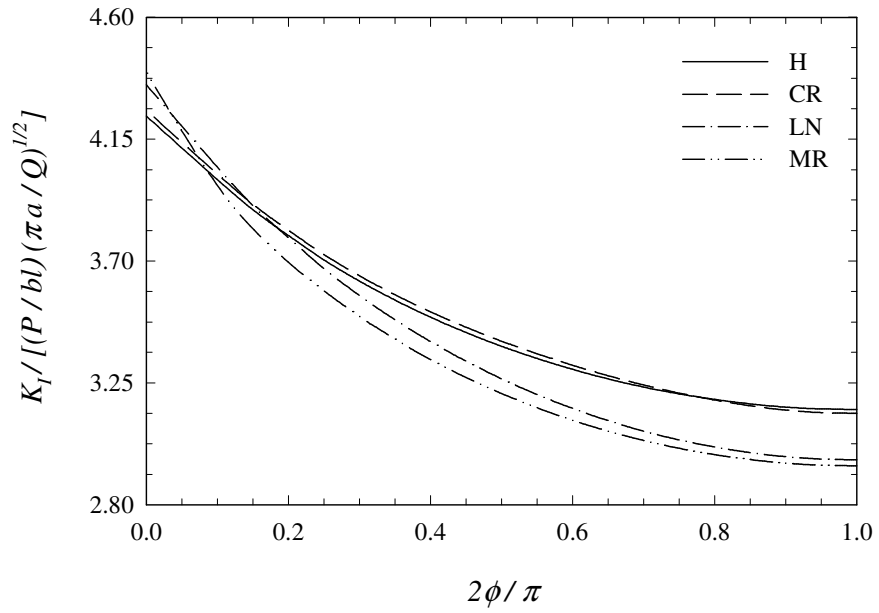Figure 4.36 Normalized mode I stress intensity factors for three point bending, $a/h_2 = 0.2$
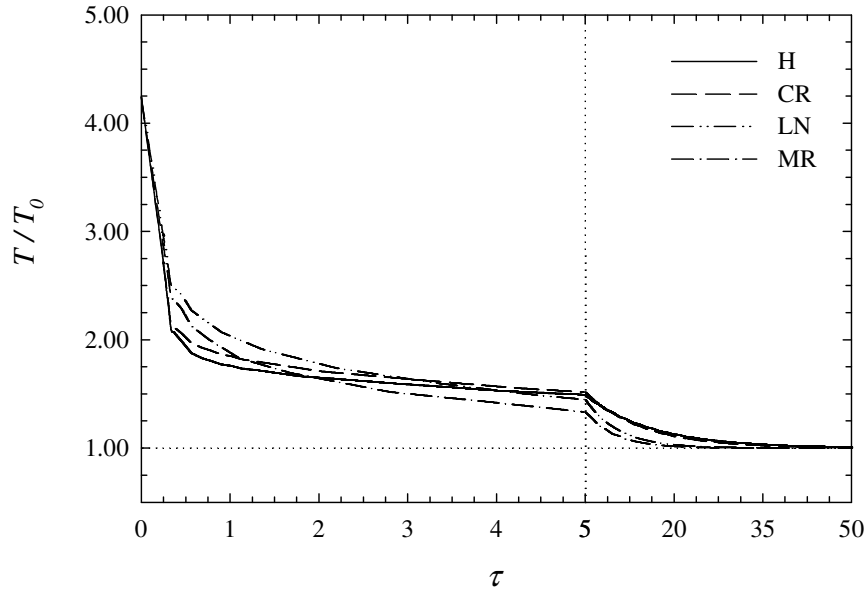
Figure 4.37 Normalized mode I stress intensity factors for three point bending, $a/h_2 = 0.3$

Figure 4.38 Normalized mode I stress intensity factors for three point bending, $a/h_2 = 0.4$

Figure 4.39 Normalized mode I stress intensity factors for three point bending, $a/h_2 = 0.5$

Figure 4.40 Normalized mode I stress intensity factors for three point bending, $a/h_2 = 0.6$

Figure 4.41 Normalized mode I stress intensity factors for three point bending, $a/h_2 = 0.7$

Figure 4.42 Normalized mode I stress intensity factors for three point bending, $a/h_2 = 0.8$

Figure 4.43 Temperature of the deepest point ($\phi = \pi/2$) with respect to normalized time, $a/h_2 = 0.2$
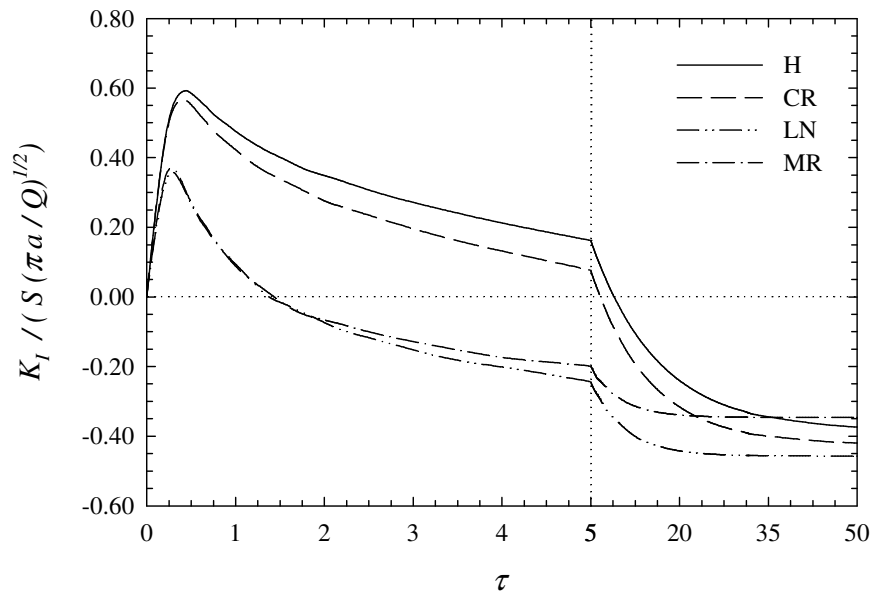

Figure 4.44 Normalized stress intensity factors at the deepest point ($\phi = \pi/2$) with respect to normalized time, $a/h_2 = 0.2$
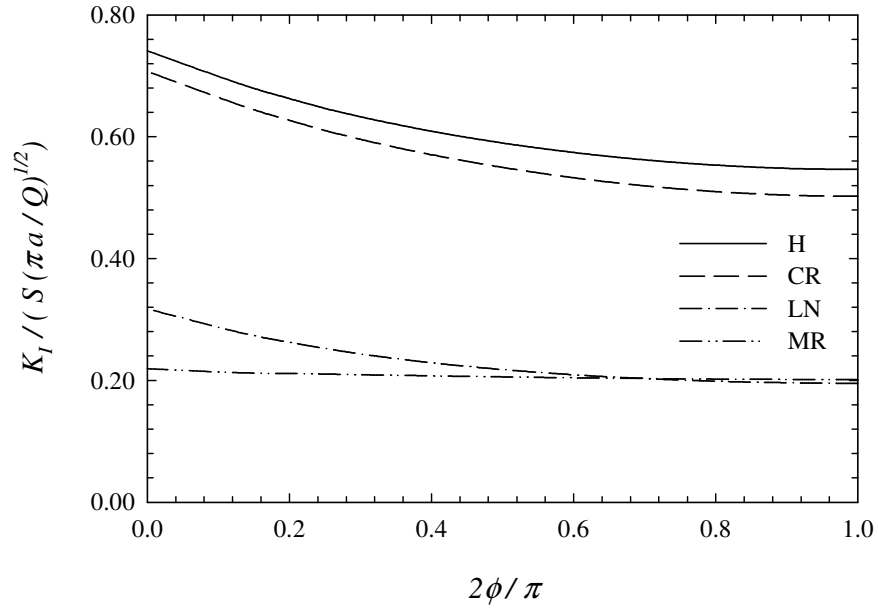
Figure 4.45 The distribution of the stress intensity factors around the crack front at $\tau = 0.67$, $a/h_2 = 0.2$
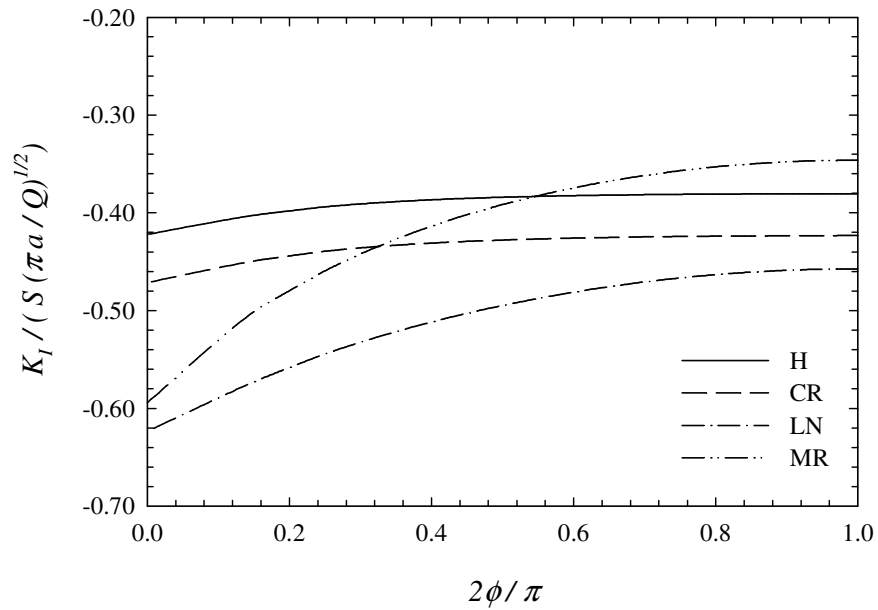

Figure 4.46 The distribution of the stress intensity factors around the crack front at $\tau = 67$, $a/h_2 = 0.2$
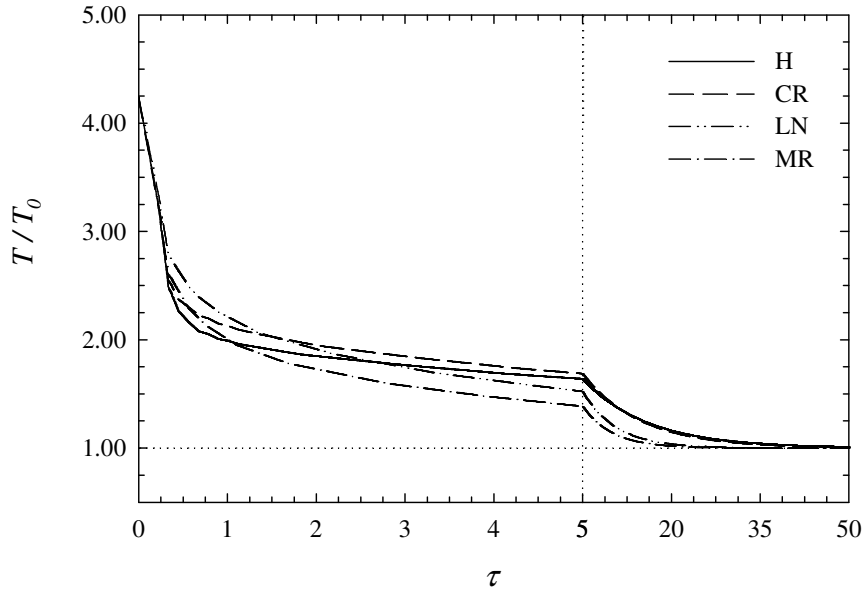
Figure 4.47 Temperature of the deepest point ($\phi = \pi/2$) with respect to normalized time, $a/h_2 = 0.3$
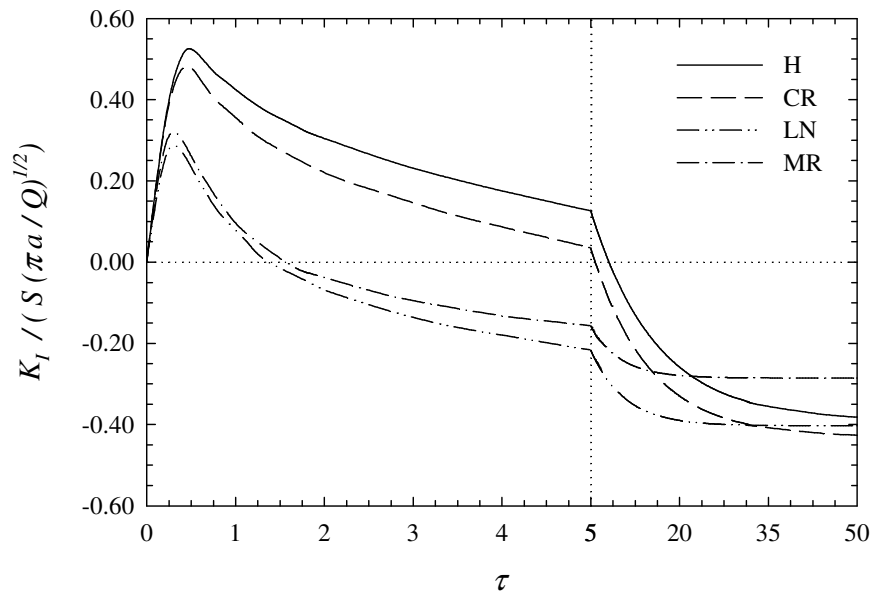

Figure 4.48 Normalized stress intensity factors at the deepest point ($\phi = \pi/2$) with respect to normalized time, $a/h_2 = 0.3$

Figure 4.49 The distribution of the stress intensity factors around the crack front at $\tau = 0.67$, $a/h_2 = 0.3$

Figure 4.50 The distribution of the stress intensity factors around the crack front at $\tau = 67$, $a/h_2 = 0.3$

Figure 4.51 Temperature of the deepest point ($\phi = \pi/2$) with respect to normalized time, $a/h_2 = 0.4$

Figure 4.52 Normalized stress intensity factors at the deepest point ($\phi = \pi/2$) with respect to normalized time, $a/h_2 = 0.4$
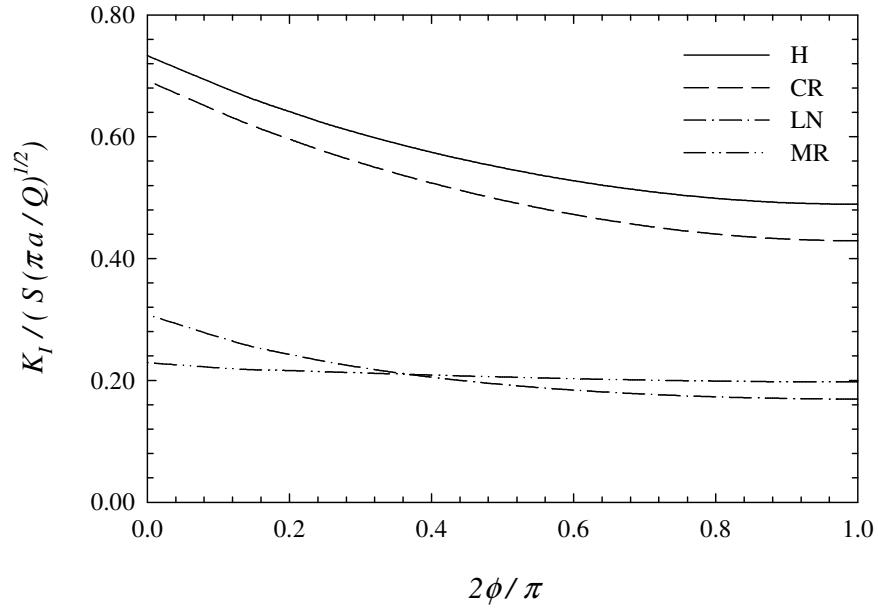
Figure 4.53 The distribution of the stress intensity factors around the crack front at $\tau = 0.67$, $a/h_2 = 0.4$
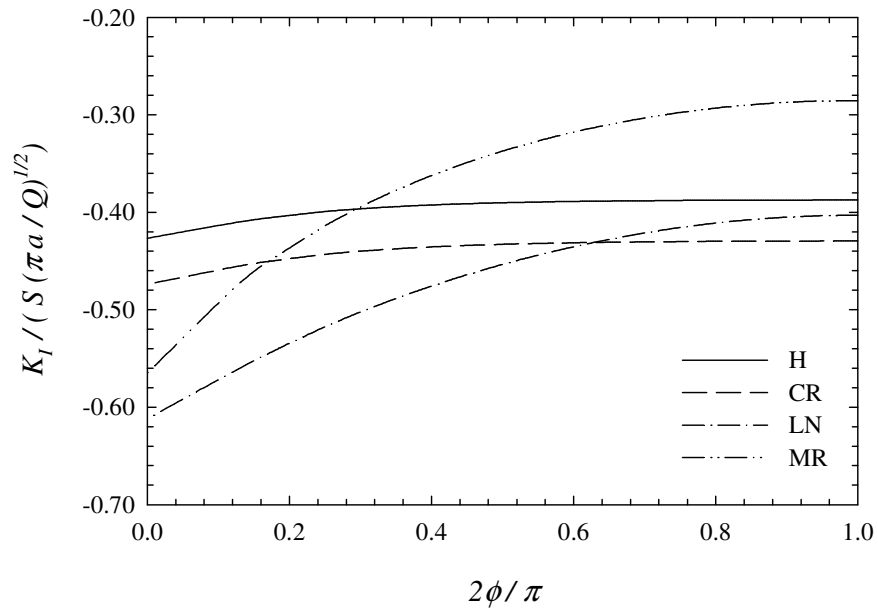

Figure 4.54 The distribution of the stress intensity factors around the crack front at $\tau = 67$, $a/h_2 = 0.4$
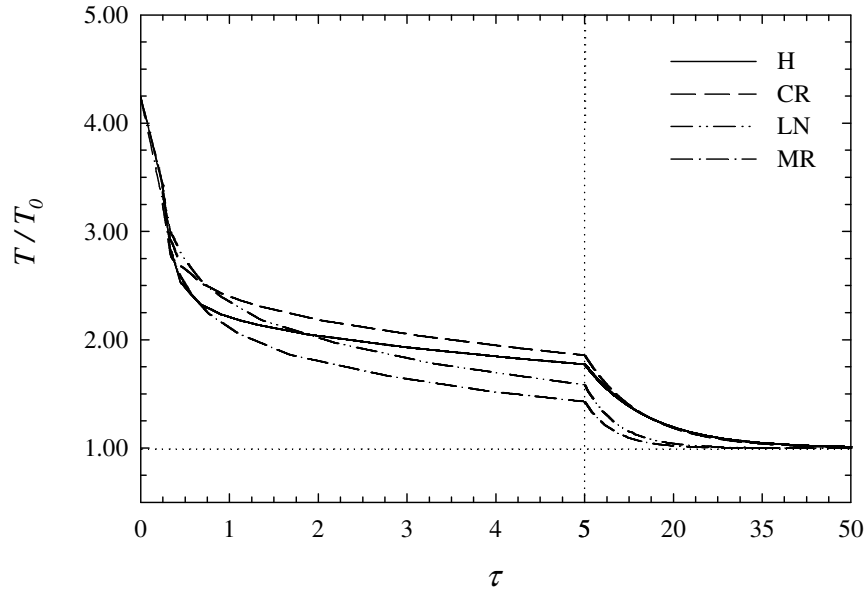
Figure 4.55 Temperature of the deepest point ($\phi = \pi/2$) with respect to normalized time, $a/h_2 = 0.6$
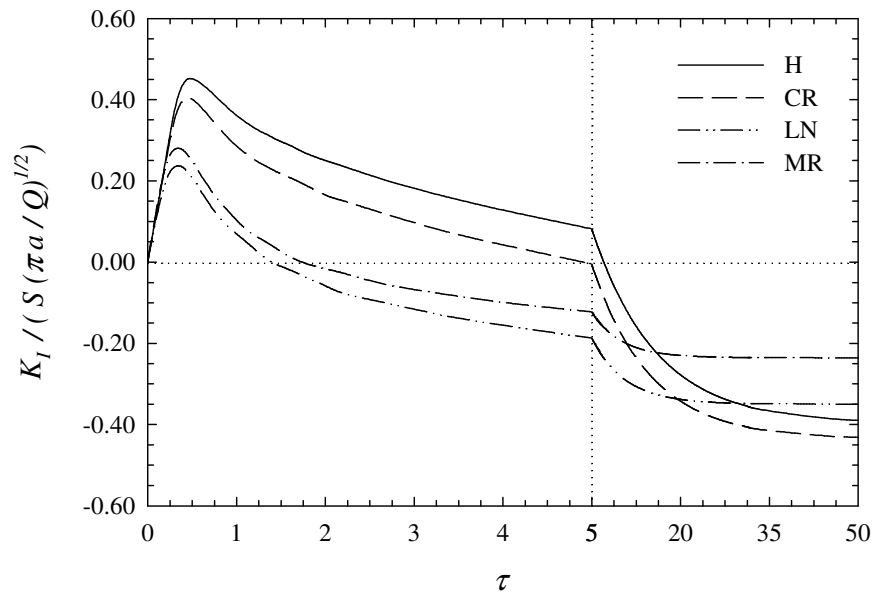

Figure 4.56 Normalized stress intensity factors at the deepest point ($\phi = \pi/2$) with respect to normalized time, $a/h_2 = 0.6$
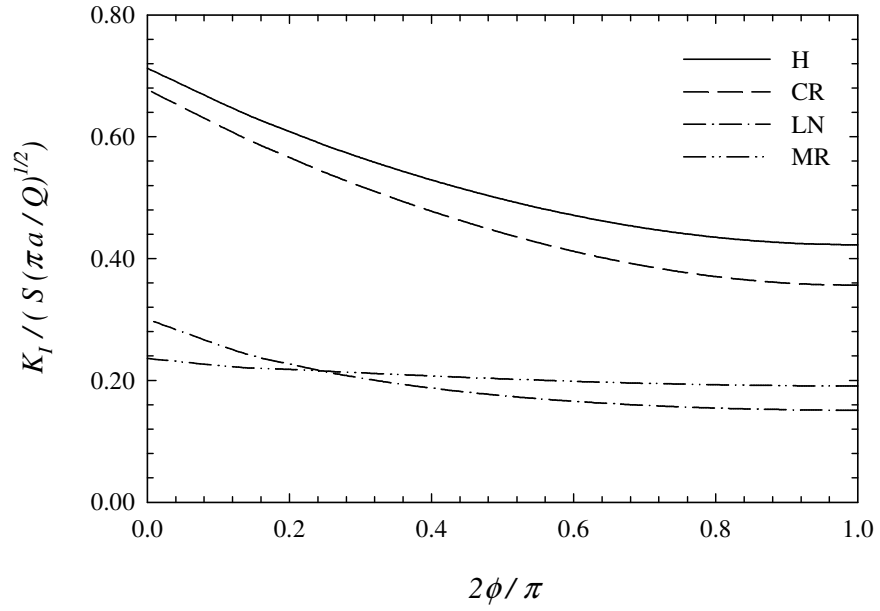
81

Figure 4.57 The distribution of the stress intensity factors around the crack front at $\tau = 0.67$, $a/h_2 = 0.6$
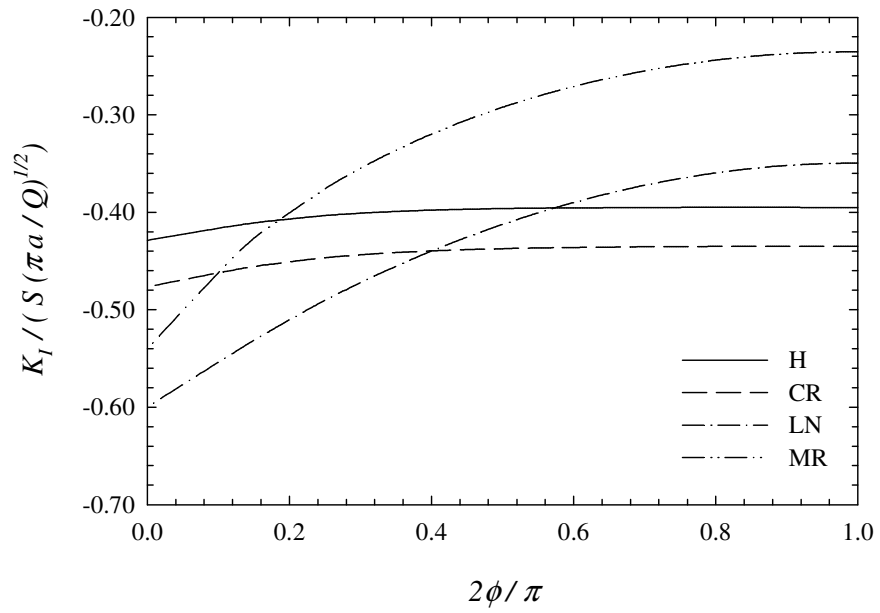

Figure 4.58 The distribution of the stress intensity factors around the crack front at $\tau = 67$, $a/h_2 = 0.6$
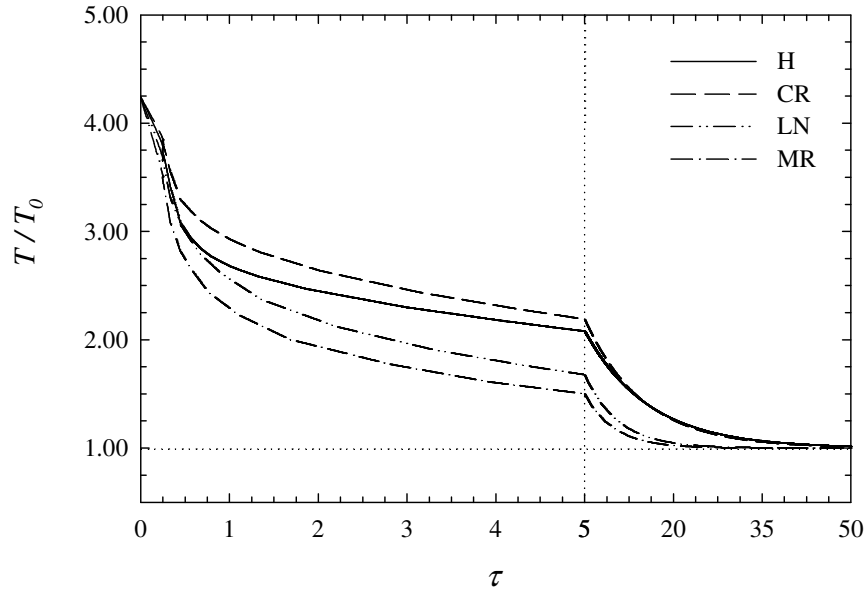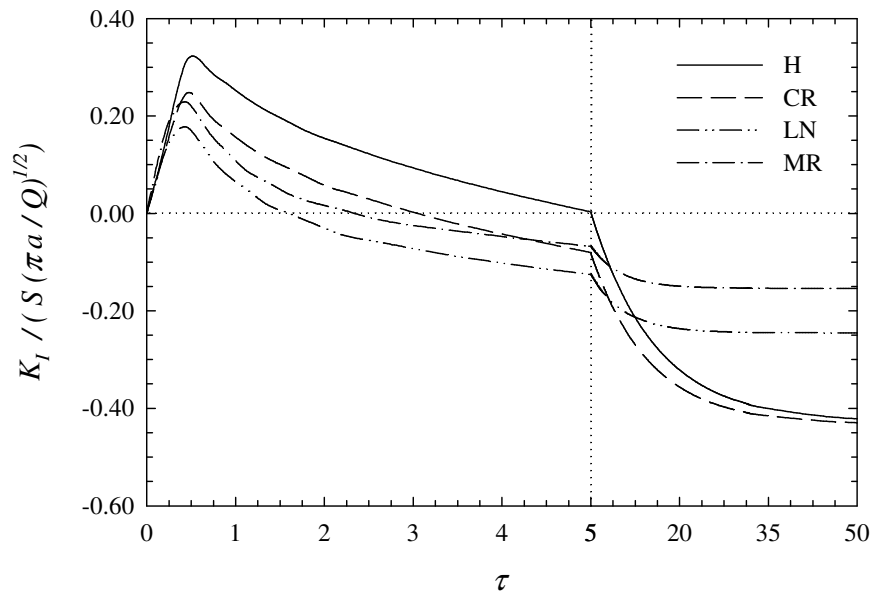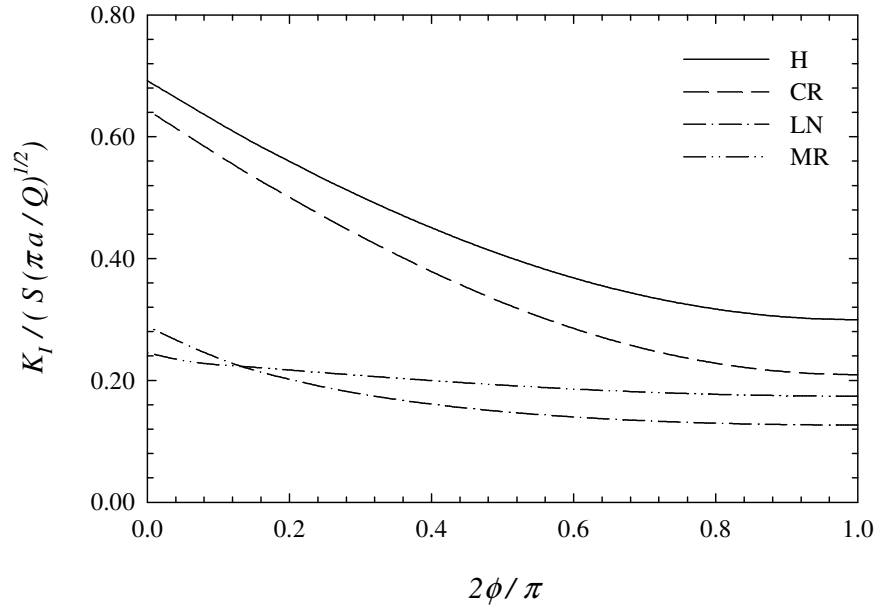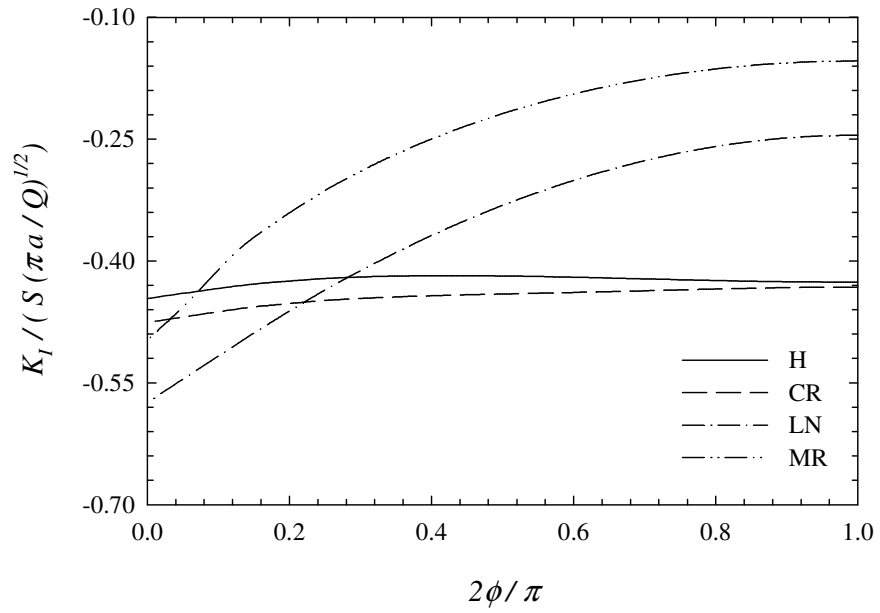
CHAPTER 5

CONCLUDING REMARKS

In this study, in order to calculate the stress intensity factors around a semi-circular crack front for a surface crack in an FGM coating, finite element models are developed. 3-D finite element models are generated using the finite element analysis software ANSYS 7.0 and several case studies containing various loading conditions, FGM variations and crack radii are performed. The stress intensity factors around the circular crack front are calculated using the displacement correlation technique in which the varying material properties on the crack front nodes are required for the FGM analysis. Hence, the stress intensity factors are not calculated directly using the default stress intensity factor calculation command (KCALC) in ANSYS and additional APDL programming is performed.

In order to check out the accuracy of the displacement correlation technique first homogeneous material properties are used for two mechanical loading conditions, namely uniform tension and bending. Then, the results are compared to those given by Newman and Raju [19]. In these comparisons the maximum percent differences are found to be smaller than 5 % for all crack dimensions used in these computations. So, it can be concluded that the results of the finite element model are sufficiently accurate.

It is important to note that the stress intensity factor at the free surface can not be determined correctly using this method, since the order of the stress singularity is different from 1/2 here. There is a boundary zone near the free surface which affects the stress intensity factors. This effect is not considered in this study. However, free surface results can still be used as approximate stress intensity factors.

In the FGM analysis, four different material profiles, namely homogeneous (H), ceramic-rich (CR), metal-rich (MR) and linear (LN) variation coatings are used. In this case coating-substrate system containing a surface crack in the FGM coating is investigated under different loading conditions which are uniform tension, bending, fixed - grip tension, three point bending and transient thermal loading.

In all the computations carried out for mechanical loading cases, it is observed that normalized mode I stress intensity factors monotonically increase as ϕ decreases from symmetry plane to surface. For all coating types and crack radii considered, maximum mode I stress intensity factors are calculated at the free surface. This leads to the conclusion that under cyclic loading, the semi – circular crack will tend to propagate slower in the thickness direction. It is also interesting to note that for all mechanical loading cases and crack radii considered (except for uniform tension and $a/h_2 = 0.1$), the minimum stress intensity factors at the symmetry surface are calculated for the MR coating. It is also seen that, the stress intensity factors are more sensitive to the variations in the crack length when the medium is under bending or three point bending rather than uniform tension or fixed – grip tension.

In transient thermal loading, as expected, the temperature at the symmetry surface first drops rapidly and afterwards reaches to a steady - state value. When the crack radius is increased, the rate of the sudden drop decreases due to the increase in the distance between the deepest crack tip node and loaded (force convected) surface. For all cases the crack remains fully open only for a short time interval as the composite system starts cooling. The crack closure begins at the symmetry surface for H, CR and LN coatings, and at free surface for MR coating. During transient period, maximum and minimum peaks for the transient stress intensity factors at the deepest point are computed for H and LN coatings, respectively. As a result, it can be concluded that material gradation causes a decrease in the amplitude of the transient stress intensity factors. Due to the crack closure at steady-

state the results are not valid and the problem has to be remodeled by taking into account the crack closure. However, these results can still be useful if they are used to obtain the solution for given arbitrary loads by using the principle of superposition provided that the resultant stress intensity factor is positive.

An immediate extension of the present study can be the modelling of the semi – elliptical surface cracks with arbitrary aspect ratio in FGM coatings subjected to thermomechanical loading. Another problem that is of particular interest is the three dimensional fracture analysis of FGM coatings under mixed – mode loading conditions. This requires the modelling of inclined surface cracks in functionally graded materials. After developing reliable models to compute the three dimensional stress intensity factors in functionally graded materials under mixed – mode loading, the next step would be the computation of the crack front morphology under cyclic loading. This will allow the life estimation of the FGM coatings and layers under repeated loads.

REFERENCES

[1] Book of Abstracts of the Eighth International Symposium on Multifunctional and Functionally Graded Materials (FGM2004), 2004, Leuven, Belgium.

[2] Dağ, S., 2001, Crack and Contact Problems in Graded Materials, Ph.D. Dissertation, Department of Mechanical Engineering and Mechanics, Lehigh University, Bethlehem, Pennsylvania, USA.

[3] İnan, Ö., Dağ, S. and Erdoğan, F., 2004, "Three Dimensional Fracture Analysis of FGM Coatings," Proceedings of the Eighth International Symposium on Multifunctional and Functionally Graded Materials (FGM2004), *Materials Science Forum*, in press.

[4] Erdoğan, F. and Wu, B.H., 1997, "The Surface Crack Problem for a Plate with Functionally Graded Properties", *Transactions of the ASME Journal of Applied Mechanics*, Vol. 64, pp. 449-456.

[5] Kadıoğlu, S., Dağ, S. and Yahşi, O.S., 1998, "Crack Problem for a Functionally Graded Layer on an Elastic Foundation", *International Journal of Fracture*, Vol. 94, pp. 63-77.

[6] Jin, Z.-H. and Paulino, G.H., 2001, "Transient Thermal Stress Analysis of an Edge Crack in a Functionally Graded Material", *International Journal of Fracture*, Vol. 107, pp. 73-98.

[7] Dağ, S., Kadıoğlu, S. and Yahşi, O.S., 1999, "Circumferential Crack Problem for an FGM Cylinder Under Thermal Stresses", *Journal of Thermal Stresses*, Vol. 22, pp. 659-687.

[8] Dağ, S. and Erdoğan, F., 2002, "A Surface Crack in a Graded Medium Under General Loading Conditions", *Transactions of the ASME Journal of Applied Mechanics*, Vol. 69, pp. 580-588.

[9] Dağ, S. and Erdoğan, F., 2002, "A Surface Crack in a Graded Medium Loaded by a Sliding Rigid Stamp", *Engineering Fracture Mechanics*, Vol. 69, pp. 1729-1751.

[10] Wang, B.L., Mai, Y.-W. and Noda, N., 2002, "Fracture Mechanics Analysis Model for Functionally Graded Materials with Arbitrarily Distributed Properties", *International Journal of Fracture*, Vol. 116, pp. 161-177.

[11] Wang, B.L., Mai, Y.-W. and Noda, N., 2004, "Fracture Mechanics Analysis Model for Functionally Graded Materials with Arbitrarily Distributed Properties (Mode II and Mode III Problems)", *International Journal of Fracture*, Vol. 0, pp. 1-14.

[12] Guo, L.-C., Wu, L.-Z., Zeng, T. and Ma, L., 2004, "Mode I Crack Problem for a Functionally Graded Orthotropic Strip", *European Journal of Mechanics A/Solids*, Vol. 23, pp. 219-234.

[13] Guo, L.-C., Wu, L.-Z., Ma, L. and Zeng, T., 2004, "Fracture Analysis of a Functionally Graded Coating - Substrate Structure with a Crack Perpendicular to the Interface – Part I: Static Problem", *International Journal of Fracture*, Vol. 0, pp. 1-18.

[14] Guo, L.-C., Wu, L.-Z., Zeng, T. and Ma, L., 2004, "Fracture Analysis of a Functionally Graded Coating-Substrate Structure with a Crack Perpendicular to the Interface – Part II: Transient Problem", *International Journal of Fracture*, Vol. 0, pp. 1-22.

[15] Chi, S.-H. and Chung, Y.-L., 2003, "Cracking in Coating - Substrate Composites with Multi - Layered and FGM Coatings", *Engineering Fracture Mechanics*, Vol. 70, pp. 1227-1243.

[16] Jin, Z.-H., 2003, "Effect of Thermal Property Gradients on the Edge Cracking in a Functionally Graded Coating", *Surface and Coatings Technology*, Vol. 179, pp. 210-214.

[17] Lee, Y.-D. and Erdoğan, F., 1998, "Interface Cracking of FGM Coatings Under Steady – State Heat Flow", *Engineering Fracture Mechanics*, Vol. 59, No. 3, pp. 361-380.

[18] ANSYS Users Manual (Elements/Commands/Procedures/Theory), 2003, Revision 7.0, Swanson Analysis Systems, Pennsylvania, USA.

[19] Newman, J.C. and Raju, I.S., 1981, "An Empirical Stress – Intensity Factor Equation for the Surface Crack", *Engineering Fracture Mechanics*, Vol. 15, pp. 185-192.

[20] Cisilino, A., 2000, "Linear and Nonlinear Crack Growth using Boundary Elements", *WIT Press*, Southhampton, UK.

[21] Ootao, Y., Tanigawa, Y. and Nakamura, T., 1999, "Optimization of Material Composition of FGM Hollow Circular Cylinder Under Thermal Loading: A Neural Network Approach", *Composites: Part B,* Vol. 30, pp. 415-422.

[22] Koers, R.W.J., 1989, "Use of Modified Standard 20-Node Isoparametric Brick Elements for Representing Stress/Strain Fields at a Crack Tip for Elastic and Perfectly Plastic Material", *International Journal of Fracture*, Vol. 40, pp. 79-110.

[23]   Ayhan, A.O. and Nied, H.F., 2002, "Stress Intensity Factors for Three-Dimensional Surface Cracks Using Enriched Finite Elements", *International Journal for Numerical Methods in Engineering,* Vol. 54, pp. 899-921.

[24]   Eischen, J.W., 1987, "Fracture of Non-Homogeneous Materials", *International Journal of Fracture*, Vol. 34, pp. 3-22.

APPENDIX A

NEWMAN AND RAJU EQUATION

This section presents a stress-intensity factor equation [19] for a semi - elliptical surface crack as a function of parametric angle, crack depth, crack length, plate thickness and plate width for tension and bending loads.
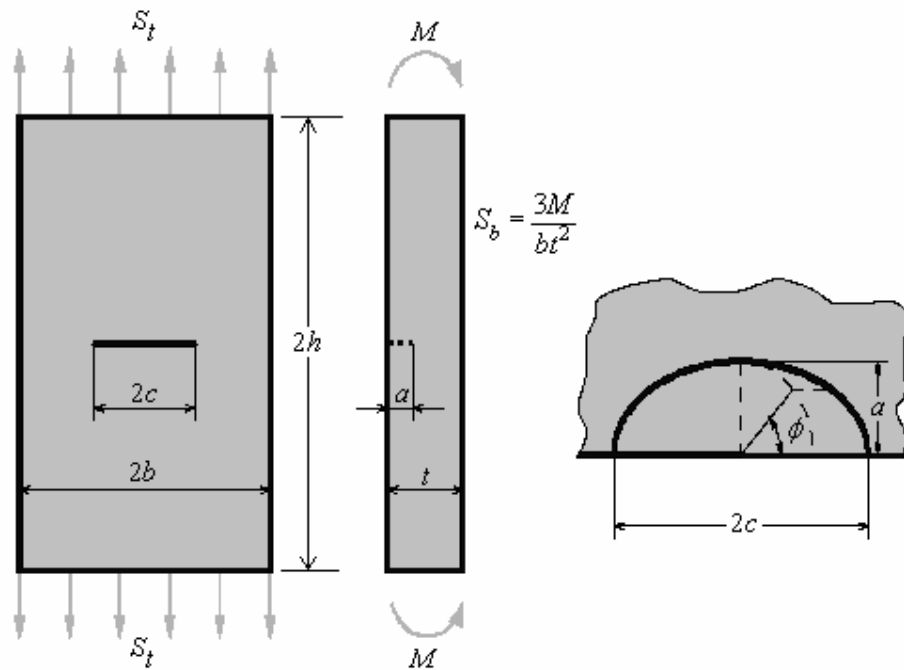

Figure A.1 Surface-cracked plate subjected to tension or bending loads.

A.1 Notation

a   depth of surface crack, mm

b   half - width of cracked plate, mm

c   half - length of surface crack, mm

h half - length of cracked plate, mm

F stress - intensity boundary - correction factor

K_I mode I stress - intensity factor, kN/m$^{3/2}$

M   applied bending moment, N.m

Q shape factor for elliptical crack

S_b remote bending stress on outer fiber, 3M/bt^2, Pa

S_t remote uniform - tension stress, Pa

t plate thickness, mm

ϕ parametric angle of the ellipse, deg.

A.2 Stress Intensity Factor Equation for the Semi - Elliptical Surface Crack

The stress-intensity factor equation for combined tension and bending loads is

$$K_I = \left(S_t + HS_b\right)\sqrt{\pi\frac{a}{Q}}F\left(\frac{a}{t},\frac{a}{c},\frac{c}{b},\phi\right) \qquad (A1)$$

for $0 < a/c \leq 1.0$, $0 \leq a/t < 1.0$, $c/b \leq 0.5$ and $0 \leq \phi \leq \pi$. Q is given as

$$Q = 1 + 1.464\left(\frac{a}{c}\right)^{1.65} \qquad \left(\frac{a}{c} \leq 1\right). \qquad (A2)$$

The functions F and H are defined so that the boundary-correction factor for tension is equal to F and the boundary-correction for bending is equal to the product of H and F. The function F is obtained from a systematic curve-fitting procedure to FEA results by using double-series polynomials in terms of *a/c, a/t*, and angular functions of ϕ. The choice of functions was based on engineering judgment. The function F was taken to be

$$F = \left[M_1 + M_2\left(\frac{a}{t}\right)^2 + M_3\left(\frac{a}{t}\right)^4\right]f_\phi g f_w \qquad (A3)$$

where

$$M_1 = 1.13 - 0.09\left(\frac{a}{c}\right) \qquad (A4)$$

$$M_2 = -0.54 + \frac{0.89}{0.2 + (a/c)} \qquad (A5)$$

$$M_3 = 0.5 - \frac{1.0}{0.65 + (a/c)} + 14\left(1.0 - \frac{a}{c}\right)^{24} \qquad (A6)$$

$$g = 1 + \left[0.1 + 0.35\left(\frac{a}{t}\right)^2\right](1 - \sin\phi)^2. \qquad (A7)$$

The function f_ϕ is

$$f_\phi = \left[\left(\frac{a}{c}\right)^2 \cos^2\phi + \sin^2\phi\right]^{1/4}. \qquad (A8)$$

The function f_w is

$$f_w = \left[\sec\left(\frac{\pi c}{2b}\sqrt{\frac{a}{t}}\right)\right]^{1/2}. \qquad (A9)$$

The function H is developed also by curve fitting and engineering judgment, and has the form

$$H = H_1 + (H_2 - H_1)\sin^p\phi \qquad (A10)$$

where

$$p = 0.2 + \frac{a}{c} + 0.6\frac{a}{t} \tag{A11}$$

$$H_1 = 1 - 0.34\frac{a}{t} - 0.11\frac{a}{c}\left(\frac{a}{t}\right) \tag{A12}$$

$$H_2 = 1 + G_1\left(\frac{a}{t}\right) + G_2\left(\frac{a}{t}\right)^2. \tag{A13}$$

G_1 and G_2 are given as,

$$G_1 = -1.22 - 0.12\frac{a}{c} \tag{A14}$$

$$G_2 = 0.55 - 1.05\left(\frac{a}{c}\right)^{0.75} + 0.47\left(\frac{a}{c}\right)^{1.5}. \tag{A15}$$